EXPERIMENTAL INVESTIGATION OF LOCAL SCOUR AROUND BRIDGE PIER GROUPS

A THESIS SUBMITTED TO
THE GRADUATE SCHOOL OF NATURAL AND APPLIED SCIENCES
OF
MIDDLE EAST TECHNICAL UNIVERSITY

BY

MURAT CAN ÖZALP

IN PARTIAL FULFILLMENT OF THE REQUIREMENTS
FOR
THE DEGREE OF THE MASTER OF SCIENCE
IN
CIVIL ENGINEERING

JANUARY 2013

Approval of the thesis:

EXPERIMENTAL INVESTIGATION OF LOCAL SCOUR AROUND BRIDGE PIER GROUPS

submitted by **MURAT CAN ÖZALP** in partial fulfillment of the requirements for the degree of **Master of Science in Civil Engineering Department, Middle East Technical University** by,

Prof. Dr. Canan Özgen
Dean, Graduate School of **Natural and Applied Science** _____

Prof. Dr. Ahmet Cevdet Yalçıner
Head of Department, **Civil Engineering** _____

Assoc. Prof. Dr. Zafer Bozkuş
Supervisor, **Civil Engineering** _____

Examining Committee Members:

Prof. Dr. Melih Yanmaz
Civil Engineering Dept., METU _____

Assoc. Prof. Dr. Zafer Bozkuş
Civil Engineering Dept., METU _____

Assoc. Prof. Dr. Elçin Kentel
Civil Engineering Dept., METU _____

Inst. Dr. Onur Pekcan
Civil Engineering Dept., METU _____

Assoc. Prof.Dr. Mehmet Ali Kökpınar
State Hydraulic Works _____

Date: _____

I hereby declare that all information in this document has been obtained and presented in accordance with academic rules and ethical conduct. I also declare that, as required by these rules and conduct, I have fully cited and referenced all material and results that are not original to this work.

Name, Last name : Murat Can Özalp

Signature :

ABSTRACT

EXPERIMENTAL INVESTIGATION OF LOCAL SCOUR AROUND BRIDGE PIER GROUPS

Özalp, Murat Can
M.Sc., Department of Civil Engineering
Supervisor: Assoc. Prof. Dr. Zafer Bozkuş

January 2013, 134 pages

It is an important task that design engineers in practice predict the local scour around bridge piers as accurately as possible because excessive local scour around bridge piers unbalance and demolish the bridges. Many equations have been proposed previously by various researchers, based on their experimental findings, but no general method has been developed so far due to the complexity of the topic. In the present study two new bridge pier groups were employed to investigate the inclination effect of the most upstream and downstream piers on the local scours around all piers. Total of 72 experiments have been conducted with 3 inclination angles, one of which representing the vertical case, each experiment lasting 6 hours, under uniform flow and clear-water conditions for a range of water depths and flow velocities on the uniform bed material. It is clearly observed and measured that the amount of local scour reduces substantially by the effect of inclination in the group piers, especially the reduction in the scour around the most upstream pier is found notable. Based on the experimental data, regression analyses are made and an empirical scour depth equation is developed for each individual pier in the pier groups studied. Comparisons with the similar studies performed by other researchers have been made and the results discussed.

Keywords: Local scour, inclined bridge piers, clear-water condition.

ÖZ

KÖPRÜ AYAK GRUPLARI ETRAFINDA OLUŞAN YEREL OYULMALARIN DENEYSEL ARAŞTIRILMASI

Özalp, Murat Can
Yüksek Lisans, İnşaat Mühendisliği Bölümü
Tez Yöneticisi: Doç. Dr. Zafer Bozkuş

Ocak 2013, 134 sayfa

Köprü ayakları etrafındaki aşırı yerel oyulmalar köprülerin dengesini bozup yıkabileceğinden, pratikteki tasarım mühendislerinin köprü ayakları etrafındaki yerel oyulmayı mümkün olduğunca doğru tahmin etmeleri önemli bir iştir. Geçmişte bu konuda çalışan araştırmacılar tarafından deneysel bulgulara dayanarak bir çok denklem önerilmiştir, fakat konunun karmaşıklığından dolayı halen genel bir yöntem geliştirilememiştir. Bu çalışmada köprü ayak gruplarının menbasında ve mansabında yer alan ayakların eğikliğinin yerel oyulmalara olan etkisini incelemek için iki yeni grup konfigürasyonu kullanılmıştır. Bir tanesi düşey konumu temsil eden 3 farklı eğiklik açısı kullanılarak, her biri 6 saat süren, toplamda 72 deney yapılmış olup, üniform akım ve temiz su koşullarında farklı akım derinlikleri ve hızları için üniform yatak malzemesi üzerinde çalışılmıştır. Eğiklik etkisiyle yerel oyulmaların büyük miktarda azaldığı gözlemlenmiş ve ölçülmüş olup, özellikle membadaki köprü ayağı etrafındaki oyulmadaki azalma dikkat çekici bulunmuştur. Deneysel verilere dayanılarak, iki konfigürasyon içinde bulunan her bir köprü ayağı etrafındaki yerel oyulma için regresyon analizi yardımı ile bir denklem geliştirilmiştir. Başka araştırmacılarca yürütülen benzer çalışmalarla kıyaslamalar yapılmış ve sonuçlar tartışılmıştır.

Anahtar Kelimeler: Yerel oyulma, eğik köprü ayakları, temiz su koşulları.

To My Mother

ACKNOWLEDGEMENTS

The most enjoyable part of preparing this thesis is surely extending appreciation to those who helped in its completion. The author wishes to express his deepest gratitude to his supervisor Associate Professor Dr. Zafer Bozkuş, for his valuable guidance and support throughout the conduction of experiments and preparation of this thesis.

Also special thanks to my thesis jury members for their valuable comments for the improvement of the quality of this thesis.

The assistance and support of all the members of the METU Civil Engineering Department of Hydromechanics Laboratory throughout the construction and maintenance of test channel and throughout the conduction of the experiments, is also gratefully acknowledged.

Many thanks go to Ali Ersin Dinçer, Cüneyt Yavuz, Emir Alimoğlu and Pınar Berberoğlu who are my classmates and friends in the Hydromechanics Division. I truly appreciate that they always took the time to understand my work.

I am also grateful to my friends Ali Taşkın, Damla Işnel, Taylan Özgür Elma and Aysen Arslankurt for their help during different phases of this study.

Many others deserve thanks for their hospitality and making the time here enjoyable including Görkem Çağlar Sayan, Mehmet Tiker, Osman Küçükşen and Hüseyin Alpay Özendi. Additional gratitude go to Akın Family, Doğru Family and Özgür Family for their continuos encouragement and moral support in many ways.

I appreciate my friends and my partners from Vogapps; Volkan Demircin, Gökhan Çağatay and Berkay Dönmez for their patience that allows me to complete my experimental work.

Most importantly, my special thanks go to a wonderful girl, Pınar Başkesik. Without her constant support and love, the completion of this thesis would be impossible.

Finally, words cannot express my appreciation for Mehmet Selçuk and my mother Şengül Çelik whose lifelong support and encouragement have kept me going.

I believe that my father, whom we lost him years ago, sees this moment and he is so proud of me.

To all these, and to the many other friends and family who have helped me, I can only say, “Thank you very, very much!”

TABLE OF CONTENTS

LIST OF TABLES

TABLES

LIST OF FIGURES

FIGURES

LIST OF SYMBOLS

d_s	Scour Depth
d_{se}	Equilibrium Scour Depth
d_0	Flow Depth
d_{50}	Median Sediment Size
$d_{\max}$	Maximum Sediment Size
C	Cohesion
Fr	Froude Number
g	Gravitational Acceleration
h	Deposition Height
a	Spacing Between Piers
D	Pier Diameter
b	Pier Width
H	Head on Sharp Crested Weir
C_d	Discharge Coefficient
K_d	Sediment Size Factor
K_s	Shape Factor of Pier
K_r	Surface Roughness Factor of Pier
K_α	Flume Alignment Factor
K_a	Roughness Effect of Sidewalls
K_{yb}	Correction Factor for Approach Flow Depth
K_β	Factor Showing the Effect of Vertical Angle of Attack
K_σ	Factor Indicating the Gradation Effect of the Sediment
K_g	Factor Indicating the Group Effect of the Piers
K_1	Flow Intensity Factor
K_t	Time Factor
L	Length of the Pier
m	Mass
P	Pressure
Q	Discharge
R	Hydraulic Radius
Re	Reynolds Number
r	Correlation Coefficient
r_1	Radius of the Pier
S_0	Flume Bed Slope
B	Flume Width
t	Time
t_e	Equilibrium Time of the Experiment
u_r	Radial Component of Velocity
u_θ	Tangential Component of Velocity
V	Velocity
V_*	Shear Velocity
V_c	Critical Velocity
V_{*c}	Critical Shear Velocity
W	Height of the Sharp Crested Weir

W_1	Width at the Uncontracted Section
W_2	Width at the Contracted Section
X_1	Variable of Multiple Regression Analysis
X_2	Variable of Multiple Regression Analysis
X_3	Variable of Multiple Regression Analysis
Y	Variable of Multiple Regression Analysis
z	Elevation From the Reference Point
β	Vertical Angle of Attack With the Pier Axis
α	Angle of Attack of Approach Flow with the Pier Axis
γ	Specific Weight of the Water
γ_s	Specific Weight of the Sediment
ρ_w	Density of Water
ρ_s	Density of the Sediment
σ_g	Geometric Standard Deviation of Sediment Grading
τ_0	Shear Stress at the Bed Level
τ_c	Critical Shear Stress
υ	Kinematic Viscosity of the Fluid

CHAPTER 1

INTRODUCTION

1.1 Problem Statement

The flow of water in rivers and streams excavates and moves material from bed and banks of streams and from around the bridge piers and abutments. Correspondingly, foundations of the structures are undermined by this erosive action of the flowing water, which is named as *scour*. Past observations show that scouring is a noteworthy problem in bridge hydraulics topic. When hydraulic and structural interaction is not evaluated accurately, during the high floods scour can give rise to destruction of structure, loss of life and property.

Statistical studies over the last decades show that the reasons of the damage for most of the harmed river bridges are based on hydraulic factors. Shirhole and Holt (1991) put forth that, since 1950 in United States, 60% of 823 bridges have been damaged or collapsed as a result of channel-bed scour and channel instability. According to this study, the U.S. Federal Highway Association reported that every year about 50 bridges fail in the USA. In another study, involving 383 bridge failures (Brice and Blodgett, 1978), local scour was stated as the main cause of 50% of these failures. In the light of this research, FHWA notes that damage to bridges and highway cost US$100 million per year. Miller (2003) reported that the failures of the bridges at New York and Tennessee resulted in the loss of 18 lives in 1987 and 1989 respectively and also 2 people have lost their lives due to the collapse of spans of a bridge in the Great Miami River in 1989. In addition to them, as a result of the collapse of the bridges over Arrayo Pasajero, 7 people were killed in 1995. According to Richardson and Davis (2001), the storm Alberto in Georgia brought on a cost of $130 million to repair and reconstruct more than 100 bridges. In the past years, many river bridges have collapsed or have been damaged due to the flooding incidents in Turkey. Some of them took place in 1990, Trabzon; 1991, Malatya; 1998, Bartin; 2001, Hatay (Yanmaz, 2002).

In addition to the loss of life and property, the damaged bridges lose their functions; therefore, lead to interrupted traffic and add extra costs. In Turkey, river bridges have become a current issue only after excessive floods (Yanmaz, 2002). On the other hand, New Zealand and USA show national importance to the topic and support the research projects regarding the issue. In the USA, the condition of the river bridges has been observed since 1991. It is determined that 66000 of them are sensitive and 17000 of them are critical to the scouring problem. These bridges are monitored and repairing works are carried on continuously (Lagasse et al., 1998). In New Zealand, many studies have been undertaken since 70's and parallel with these studies monitoring instruments are installed in many bridges (Melville and Coleman, 2000).

1.2 Types of Scour

There are 3 main components of total scour:

1. General scour of the river bed
2. Contraction scour at the bridge cross section
3. Local scour around bridge piers and abutments

The addition of these components presents the total scour. The types of scour that can occur at a bridge are illustrated in Figure 1.1. It is assumed that each of them occurs independently.

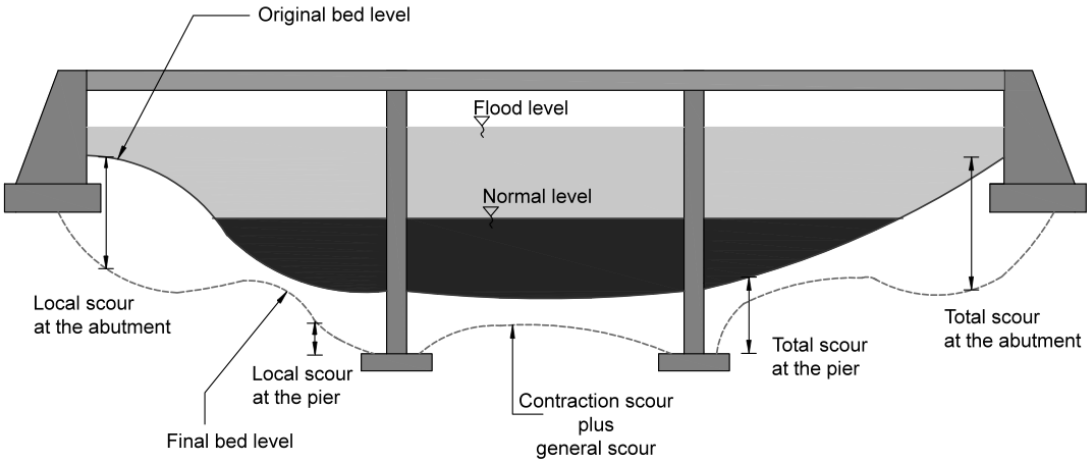

Figure 1.1: The types of scour that can occur at a bridge (Melville and Coleman, 2000)

1.2.1 General Scour

General scour forms as a result of natural processes whether there is a bridge or not at the cross section. It can be referred as bed aggradation/degradation and categorized as short-term scour and long-term scour according to the time it takes to reach the scour. Short-term general scour occurs during single or sequential floods (daily, weekly, monthly or seasonally). Scour at channel confluences, scour at bends, scour arising from a shift in the channel thalweg and bed-form migration are included in short-term general scour (Coleman and Melville, 2001). Because of the fact that formation of contraction scour and local scour dominate over that of short-term scour, it is very hard to anticipate it at structure, hence short-term scour is not included in the design computations. Long-term general scour forms naturally or develops with some modifications at watershed and stream and undoubtedly occurs over the years and has a relatively longer time scale. Human causes of long-term general scour are channel alterations, streambed mining and dam/reservoir construction. In addition; channel straightening, tectonic activities, fire and climate change develop long-term scour naturally. The engineer has to specify the present condition of stream and watershed and estimate the future streambed changes (Melville and Coleman, 2000).

1.2.2 Contraction Scour

The reduction in flow area of a stream either by a natural contraction (or by a bridge) causes scour at the loose bed (Figures 1.2a and 1.2.b). Similarly, roadway embankments cause contraction scour by repulsing the overbank flow to the channel. As a rule, average velocity and bed shear stress increase when flow area reduces. For this reason, increase in erosive forces leads to more bed material removed from the contracted section than transported to the section (Richardson and Davis, 2001). This process continues until the equilibrium is reached. Bed elevation is lowered, average velocity and bed stress decrease at the reach and the amount of bed material removed from the reach becomes equal to that of bed material transported to the reach.

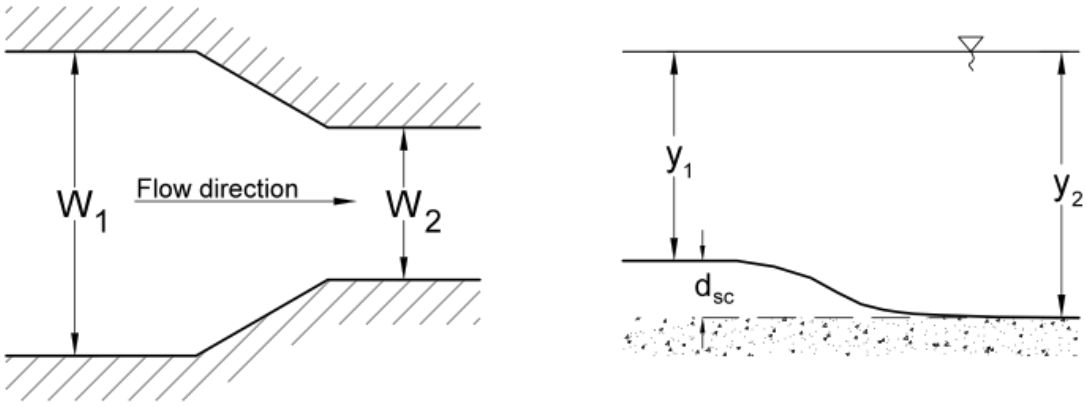

a) b)

Figure 1.2: Contraction scour a) Plan view b) Profile (Yanmaz, 2002)

1.2.3 Local Scour

River structures such as piers, abutments, and guide banks are often required in riverbanks in conjunction with river training or road construction works. Interference of the man made structures with the flow causes scour holes around the bridge piers and abutments. When flow strikes to the obstacle, vortexes are formed and flow is accelerated, sediment particles are removed around the obstacles. Local scour profile is displayed in Figure 1.3. Local scour around bridge pier groups, factors and parameters affecting the local scour will be explained extensively in the following chapters.

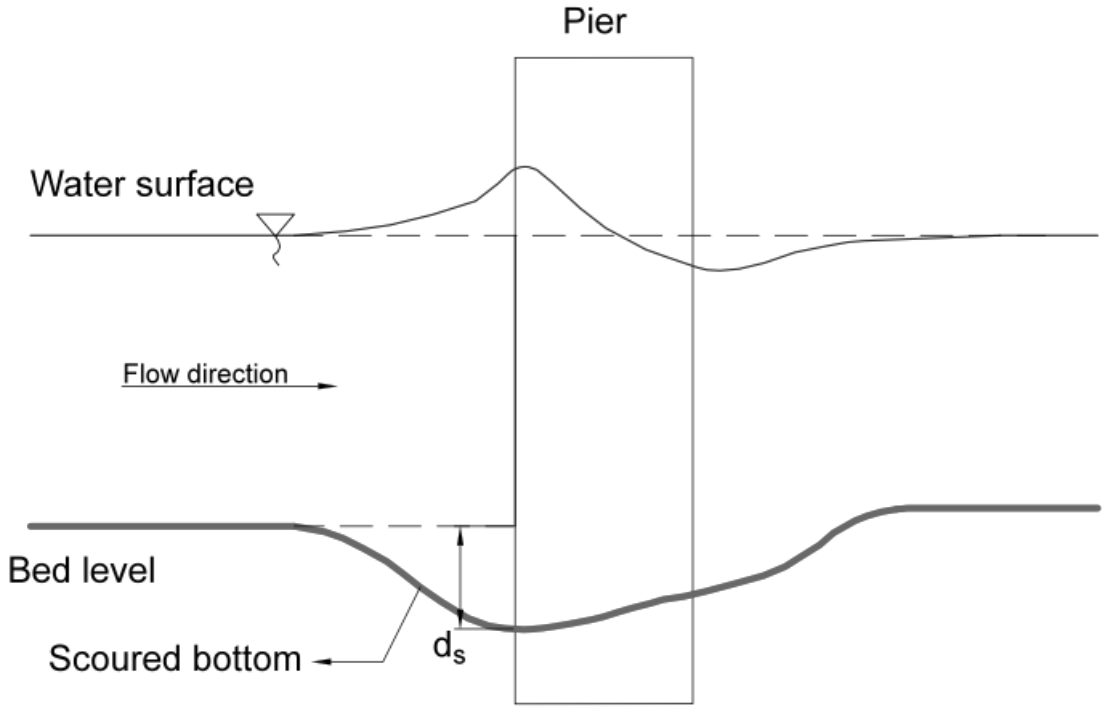

Figure 1.3: Local scour profile (Cesme, 2005)

1.3 Scour in Different Conditions of Transport

In bridge hydraulics, bed material transportation is a great concern because it affects the foundation design of the river structures. Local scour is divided into two according to the conditions of transport: Clear-water scour and live-bed scour, which will be explained in following sections. The formation of scour hole in time and the relationship between scour depth and approach flow velocity depend on the conditions of transport. Thereupon, the local scour equations derived by the researchers are categorized according to the conditions that they are based on. Figure 1.4 shows the comparison of clear water and live bed conditions according to the scour depth as a function of time.

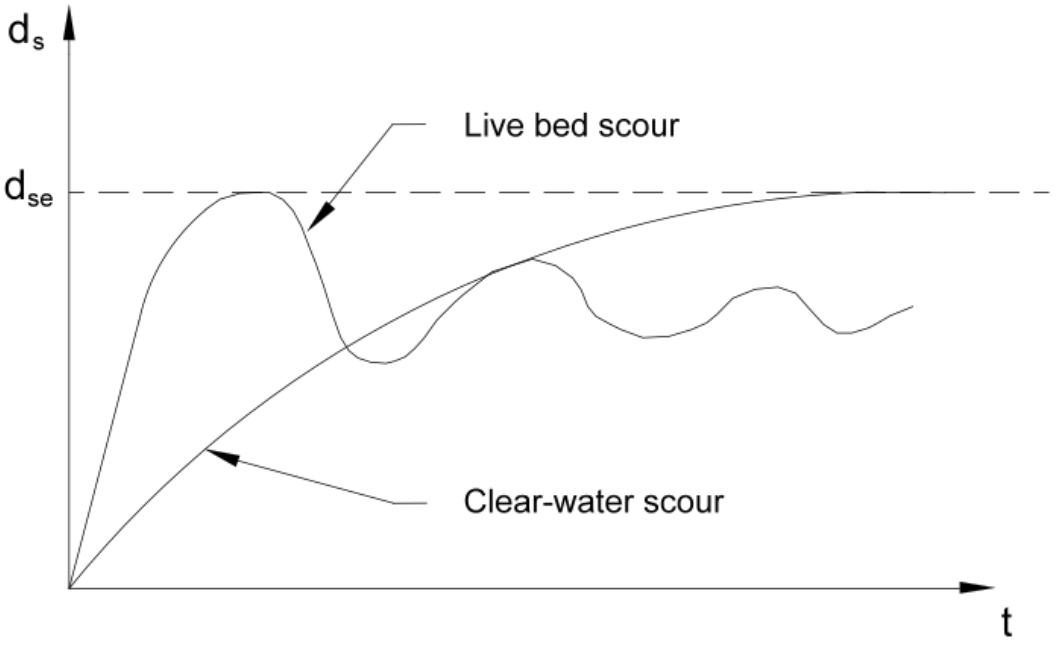

Figure 1.4: Variation of scour depth under clear-water scour and live bed scour conditions (Yanmaz, 2002)

1.3.1 Clear-Water Scour

Clear-water scour occurs when the bed material at the upstream of the bridge structure has no motion. In this condition, the shear stresses, which are created by the flow of water, at the bed should be smaller than the critical shear stress $(\tau_0 < \tau_c)$. Likewise, if the mean approach velocity of the flow is less than the critical velocity, then no bed load transport occurs $(V_0 < V_c)$. The degree of scour depends on the flow properties in scour hole and the flow properties in scour hole are affected by pier geometry and inertia of flow (Yanmaz 2002). Under clear-water conditions, pier foundation is eroded rapidly at the early stages, but subsequently scour hole development reaches equilibrium as the magnitude of the shear stresses is reduced due to the flow alteration caused by the generation of scour hole. At the equilibrium time, sediment is not transported to or carried away from the hole. Variation of depth of scour with time is shown in Figure 1.4, where d_{se} is the equilibrium scour depth

around the pier. Yanmaz (2002) states that, about half of the equilibrium depth of scour takes place in almost 10-20% of equilibrium time of scour.

Past researchers have studied the hydraulic conditions necessary for the start of clear-water scour. Shen et al. (1969) recommends that clear-water scour starts when the mean approach velocity (V_0) reaches half of the critical shear velocity value (V_{*c}). Raudkivi (1986) proposes a different relationship, which tells that the clear-water scour begins when mean flow velocity (V) approaches 50% of mean critical velocity (V_c). Additionally, Chiew (1995) states that shear velocity (V_*) has to be at least 30% of the critical shear velocity (V_{*c}) to initiate the clear-water scour.

1.3.2 Live Bed Scour

Scour with the bed material sediment transport (live bed scour) takes place when flow initiates the general sediment transport by the river. When flow intensity increases until bed shear stresses at the upstream exceed the critical shear stress $(\tau_0 > \tau_c)$, bed load transport in the flow direction is developed. This motion is combined with the flow in the scour hole; thus, development of the scour hole depends on the flow in scour hole and flow conditions in the upstream together. Scour hole development rate rapidly increases at first, then decreases in time. As resistance changes in time according to the bed forms at the upstream, bed load transport in scour hole depends on additional shear stress that is generated in upstream (Yanmaz, 2002). The equilibrium condition is reached when the rate of sediment entering the scour hole becomes equal to the rate being taken out. In this case, depth of scour fluctuates in time about equilibrium scour depth according to the change of location of sediment particles (Figure 1.4). Fluctuation is not observed when there is no bed load transport from the upstream.

Different from the clear-water conditions, under live bed conditions, an average equilibrium scour depth, an average maximum scour depth and an average minimum equilibrium scour depth are defined (Raudkivi 1991). Variation of scour depths with mean approach velocity for clear-water and live bed conditions is illustrated in Figure 1.5.

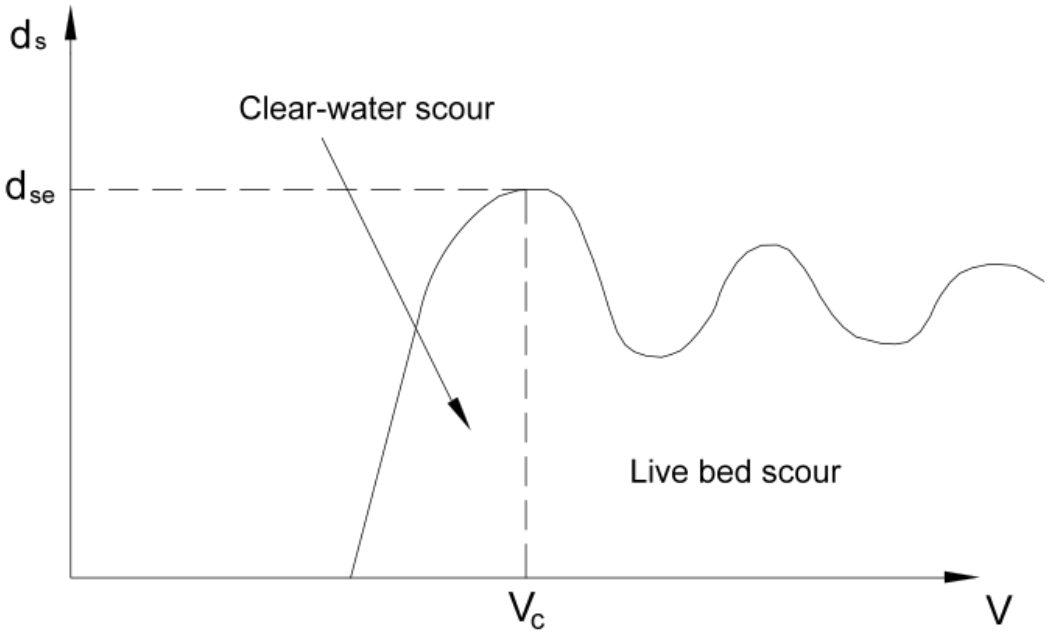

Figure 1.5: Variation of scour depth with approach flow velocity (Yanmaz, 2002)

1.4 Scope and Objective of The Study

From past observations and experiences, it is recognized that local scour around bridge piers is one of the most serious causes of bridge failures. Many studies have been conducted since 1950's and researchers have adopted different approaches and particular conditions to develop design criteria. As the nature of the problem is very complex and it is very difficult to collect meaningful data, a general equation could not be derived for all conditions. Most researchers have developed local scour equations based on laboratory experiments; however, these findings can give utterly different results in any special condition.

The primary objective of this study is to investigate the local scour around bridge pier groups at various inclination angles of piers and also to develop local scour depth equations for bridge pier groups by multiple regression analysis. Furthermore, variations of depth of scour (d_s) with pier diameter (D) and depth of flow (d_0) (i.e. blockage ratio, d_0 / D) are examined based on experimental results. Pier spacing (a / D), flume dimensions and sediment characteristics are kept constant throughout the experiments. Local scour evolution in time, approach velocity and flow depth with particular sediment size and grading are examined.

The following parameters and conditions are covered in this study:

- Bridge pier configurations:
  - Bridge pier groups with 3 piers
  - Bridge pier groups with 4 piers

- Hydraulic conditions:
  - Uniform flow
  - Clear-water scour

- Bed material:
  - Uniform
  - Cohesionless

- Variables affecting the local scour:
  - Pier diameter
  - Depth of flow
  - Inclination angle (β) of piers

- Measurements done:
  - Discharge
  - Flow depth
  - Flow velocity
  - Depth of scour hole
  - Height/depth of aggradation/degradation of bed material between piers.

In some way, this is a follow up study of previous research that have been made by Bozkus and Yildiz (2004) and Bozkus and Cesme (2010). Bozkus and Yildiz (2004) have investigated the effect of inclination of a single circular pier (Figure 1.6). On the other hand, Bozkus and Cesme (2010) have performed series of experiments on inclined dual circular bridge piers (Figure 1.7). They both carried out experiments with various depths of flow (d_0), inclination angle (β) and Froude number values. By this way, they developed curves and equations showing the effect of inclination of circular bridge piers on scour depths. Bridge pier groups with 3 piers and 4 piers are examined in this study and compared with previous researches. Figure 1.8 and 1.9 give descriptive sketches of vertically inclined bridge pier groups; where β is the inclination angle, D is the pier diameter and d_0 is the approach flow depth.

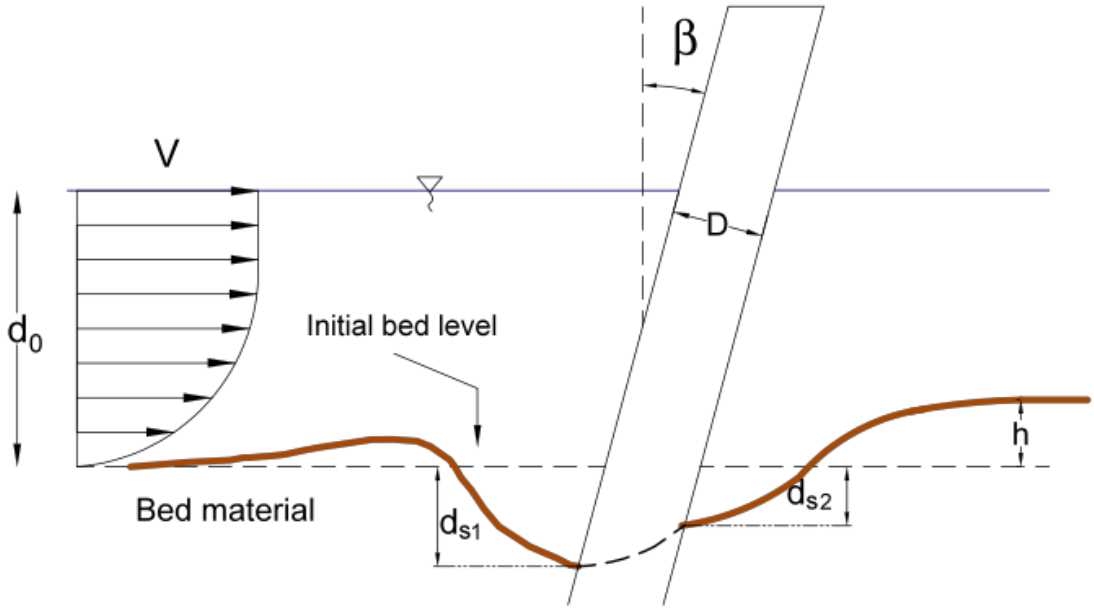

Figure 1.6: Definition sketch for a single inclined pier (Bozkus and Yildiz, 2004)

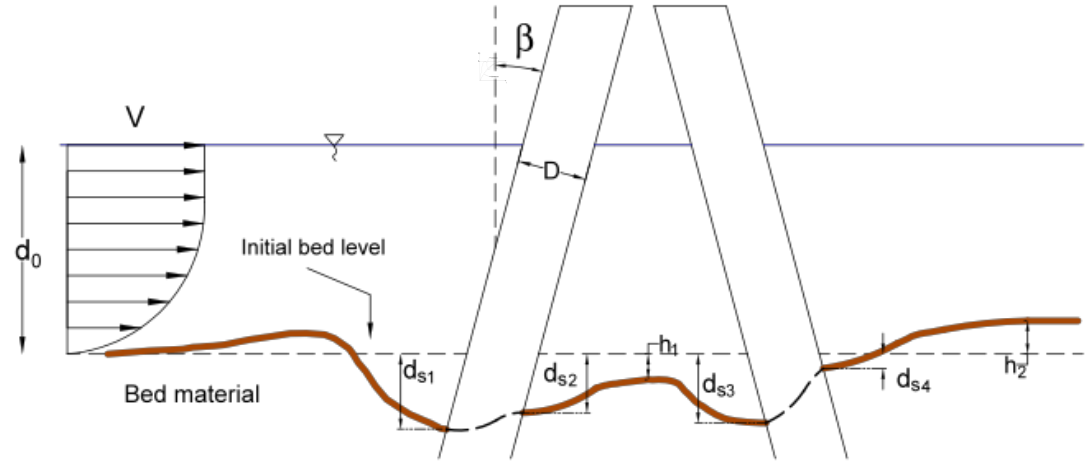

Figure 1.7: Definition sketch for the scour measurements around the two inclined piers (Bozkus and Cesme, 2010)

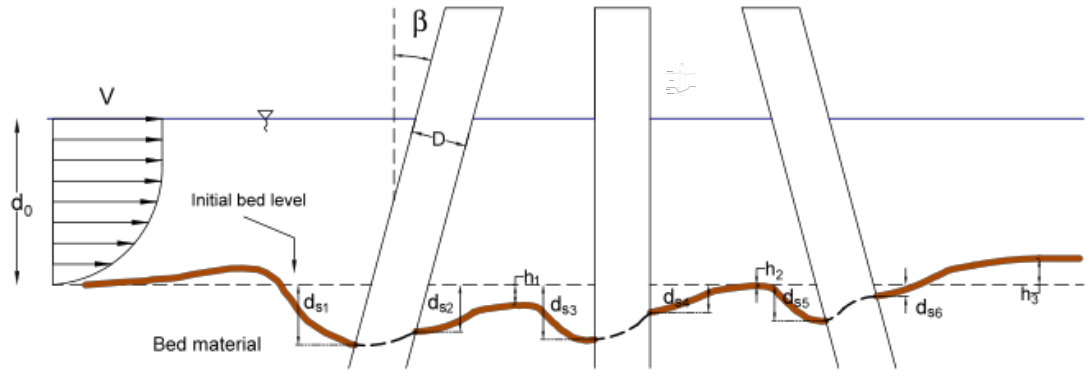

Figure 1.8: Illustration of the scour measurements around 3 piers

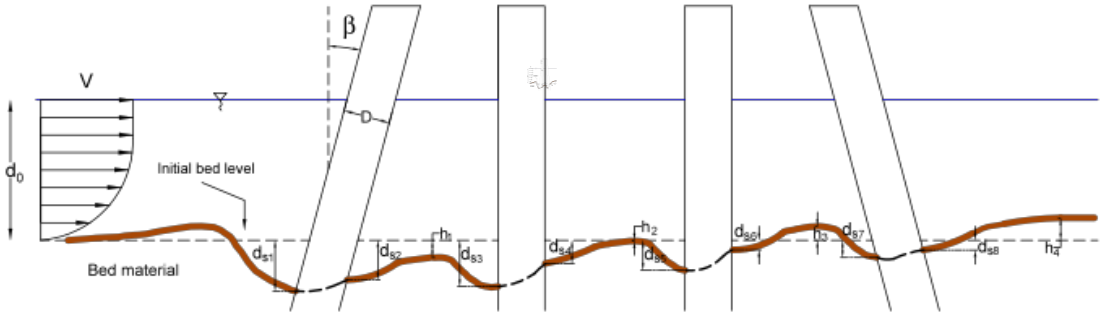

Figure 1.9: Illustration of the scour measurements around 4 piers

CHAPTER 2

LOCAL SCOUR MECHANISM AROUND BRIDGE PIERS

2.1 General Information

Local scour is the erosive action of accelerated flow due to the presence of an obstacle (pier) in rivers and streams. As the flow passes the pier, mean flow velocity increases and vortices are formed at piers face. The formation of this flow pattern adjacent to a cylinder causes the scour.

2.2 Velocity and Pressure Expressions Around Bridge Piers

This experimental study follows the *potential flow theory*. The velocity components are seen in Figure 2.1, where u_r is the radial velocity component, u_θ is the tangential velocity component, u is the total velocity at any point (r, θ) and V_m is the mean velocity at the upstream.

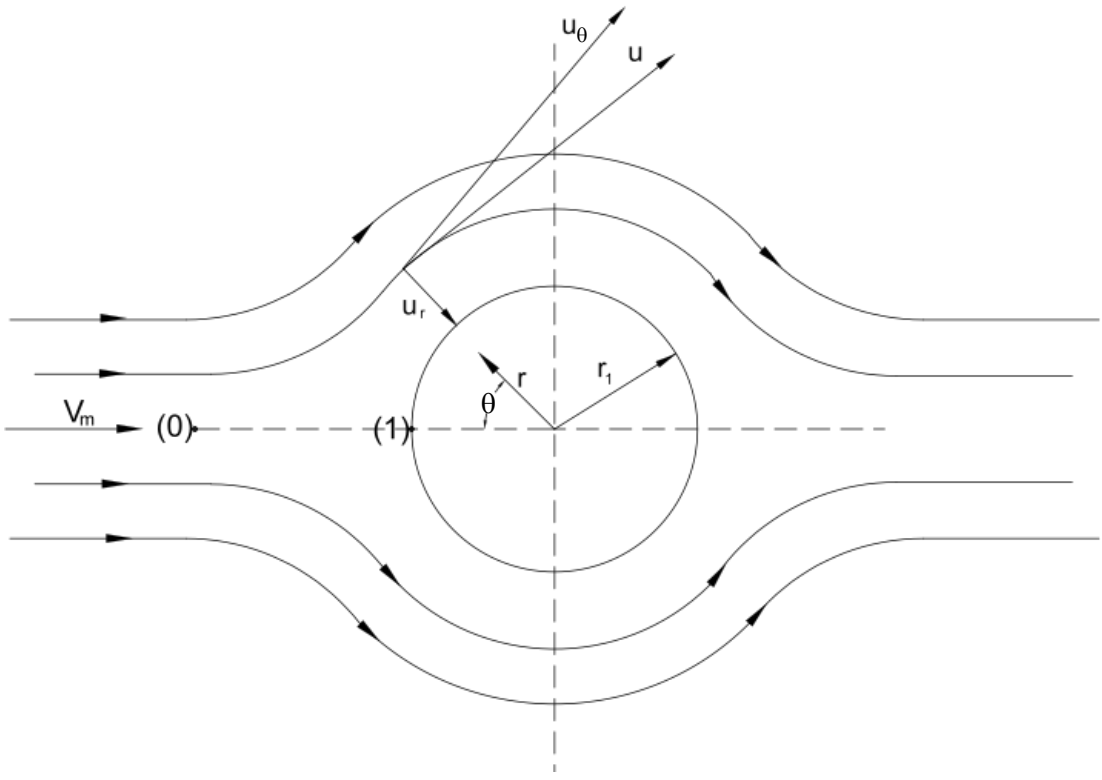

Figure 2.1: Potential flow definition sketch

According to the potential flow theory, radial and angular components of velocity can be written as (Yanmaz, 2002):

$$u_r = -u_0\left(1-\left(\frac{r_1}{r}\right)^2\right)\cos\theta \tag{2.1}$$

$$u_\theta = u_0\left(1+\left(\frac{r_1}{r}\right)^2\right)\sin\theta \tag{2.2}$$

$$u_1 = \sqrt{u_r^2 + u_\theta^2} \tag{2.3}$$

In these equations r_1 is the radius of the cylinder, r is the radial coordinate and θ refers to the angular coordinate. If Eqs. (2.1) and (2.2) are put into Eq. (2.3), where it defines the total velocity, the below expression is obtained after necessary simplifications:

$$u_1 = u_0\left[1-2\left(\frac{r_1}{r}\right)^2\cos 2\theta+\left(\frac{r_1}{r}\right)^4\right]^{1/2} \tag{2.4}$$

Ignoring the head losses between sections (0) and (1) and assuming that the bed elevations of both sections are equal in Figure 2.1, energy equation can be written as:

$$\frac{P_0}{\gamma}+\frac{u_0^2}{2g}=\frac{P_1}{\gamma}+\frac{u_1^2}{2g} \tag{2.5}$$

Considering $r = r_1$ and $\theta = 0^\circ$ at the face of pier, u_r and u_θ are found to be "0" and "$2u_0\sin\theta$" respectively. Thus, Eq. (2.5) is transformed into following form (Yanmaz, 2002):

$$P_1 = P_0 + \frac{\rho u_0^2}{2} \tag{2.6}$$

The pressure at the upstream face of the pier (stagnation pressure) is greater than the pressure at section (0), as it is recognized from Eq. (2.6). Here the term $\rho u_0^2/2$, which is the difference between sections (0) and (1), is called dynamic pressure.

2.3 Flow Pattern Around Cylindrical Piers

The flow pattern past a cylindrical bridge pier is a very complex problem. To gain better understanding of the scour problem, several investigators made detailed studies of these flow patterns. Depending on the study carried out by Melville; Hjorth (1972, 1975), Melville (1975), Melville and Raukivi (1977) have reported the results of flow pattern (Raudkivi, 1991). The flow pattern is divided into 4 components to give a better understanding of the topic:

- Downflow in front of pier
- Horseshoe vortex
- Wake vortices
- Bow wave

Vortex formation at the base of a cylindrical bridge pier is the fundamental reason of generation of scour hole. Figure 2.2 presents schema of a flow field around a bridge pier.

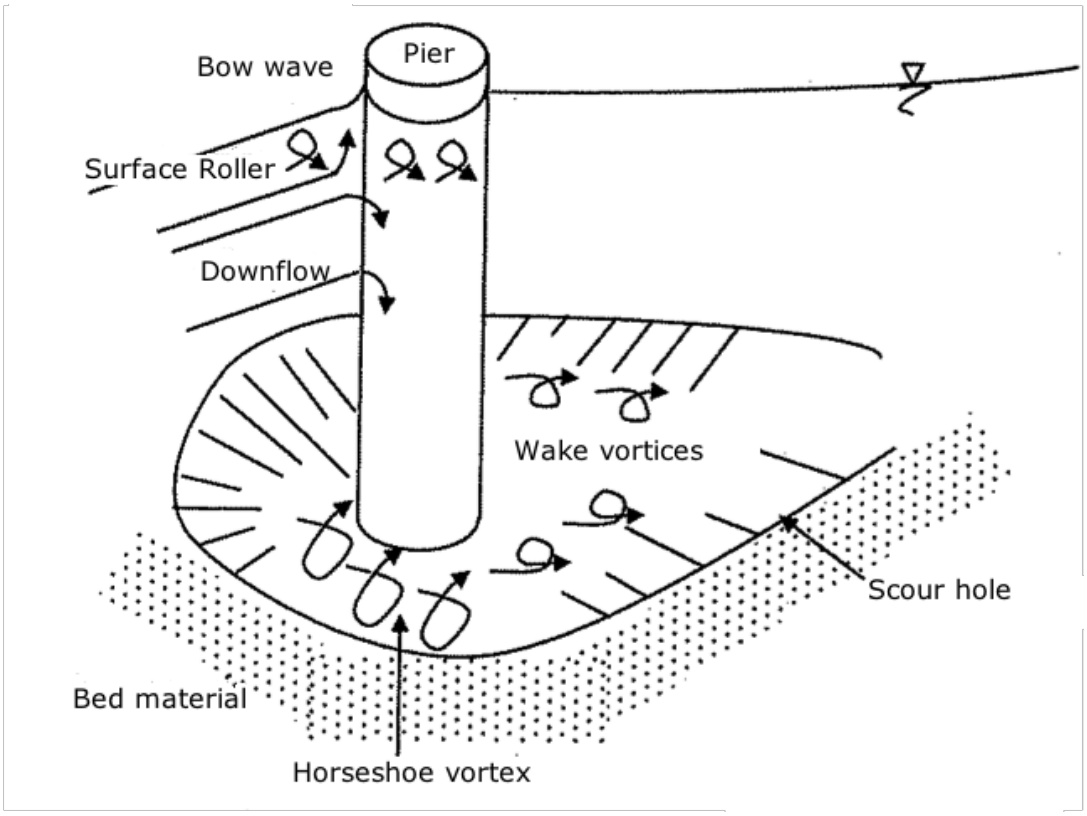

Figure 2.2: Illustration of the flow and scour patterns at a circular pier (Reproduced from Yanmaz, 2002)

2.3.1 Downflow in Front of Pier

When the flow hits the pier face, depth of flow increase and a stagnation plane is formed at the face. Thus, it results a pressure difference between the upstream and stagnation point, which is equal to $\rho u_0^2 / 2$ (see Eq. (2.6)). Yanmaz (2002) states that, increase in flow depth depends on approach flow velocity and pier shape. Since velocity decreases gradually from water surface to the bed level, stagnation pressure also decreases downwards as it depends on approach velocity. That means there exists a high pressure at the water surface and downward pressure gradient to the bed. In the presence of a scour hole, the strength of downflow at the face of the pier gets through to its utmost value just beneath the bed level. According to Raudkivi (1991), the ultimate velocity of the downflow presents itself at a distance of 0.05 to 0.02 pier diameters upstream of it at any level, being closer to the pier taken down. Furthermore, downflow reaches its maximum velocity value in the scour hole approximately one-pier diameter (D) below the bed level and can reach up to 80% of the mean approach velocity.

2.3.2 Horseshoe Vortex

As a result of the interaction of approach flow and downflow, vortices are formed at the upstream side of the pier. These vortices are called *horseshoe vortex* because of the shape they generate at the scour hole. To take the point, it is of note to express that horseshoe vortex is developed after the scour hole generation. As it is formed as a consequence of a scour, horseshoe vortex takes an important role in transporting material away from the scour hole. Horseshoe vortex loses its strength and becomes a part of general turbulence after extending downwards for a few pier diameters (Raudkivi, 1991).

The intensity of the horseshoe vortex directly depends on the degree of the turbulent flow and pier geometry (Yanmaz, 2002). As it is out of question to change the flow conditions, appropriate pier geometry should be chosen to reduce the effects of horseshoe vortex.

2.3.3 Wake Vortices

Downflow and horseshoe vortex play a major role in scour process. Due to the shear stress gradients at the upstream side of the pier, the wake vortices originate from flow separation at the sides of the pier. With the effect of downflow, wake vortices are transferred downstream by the approach flow and behave like vacuum cleaners picking up and carrying the sediment entrained by the downflow and horseshoe vortex (Melville and Coleman, 2000).

The strength of wake vortices decreases very quickly as the distance downstream of the pier increases. When compared to horseshoe vortex, the intensity of wake vortices is weaker. Thus, maximum scour depth occurs at upstream face of the pier.

2.3.4 Bow Wave

Bow wave, which rotates in counter direction of the horseshoe vortex, is generated at the upstream side of the pier on the water surface, results in the increase of water depth as the flow approaches the pier. Bow wave has an influence on horseshoe vortex. As long as depth of flow decreases, bow wave affects the horseshoe vortex to become weaker, so local scour depth is reduced for shallow flow (Richardson and Davis, 2001).

CHAPTER 3

EFFECTS OF SPECIFIC PARAMETERS ON LOCAL SCOUR DEPTH

Past researches show that local scour around bridge piers is mainly influenced by bed material characteristics, bed configuration, flow characteristics, fluid properties, the geometry of the pier and time. Most of the parameters are interrelated. This means that an effect of a particular parameter on development of local scour may surpass other parameters. The interaction of the parameters brings complexity to the issue. Preventive precautions can be taken, if importance of these parameters is known in detail.

3.1 Effect of Flow Intensity

As mentioned before in Chapter 1, local scour can be developed in two different conditions of transport: 1) Live bed scour 2) Clear-water scour. Melville and Coleman (2000) state that, when flow intensity $V / V_c < 1$ for uniform sediments and $[V - (V_a - V_c)] / V_c < 1$ for nonuniform sediments, clear water scour conditions are present, where V_a is the mean approach velocity at the armor peak. In the case of live bed scour for uniform sediments, critical velocity is lower than the mean approach velocity $(V / V_c > 1)$. Armoring process takes place on the riverbed and in the scour hole for nonuniform sediments, where the ratio V / V_a indicates the flow intensity (Raudkivi, 1986; and Melville and Sutherland, 1988). It has to be said that armoring within the scour hole reduces the local scour depth. As a general rule, if $V / V_a > 1$, live bed scour conditions occur; however in the situation of $V / V_a < 1$ clear-water conditions pertain. The determinations of threshold velocity and armor peak velocity are given in below equations (Melville and Coleman, 2000):

Threshold Velocity, V_{*c}:

$$0.1mm < d_{50} < 1mm, \qquad V_{*c} = 0.0115 + 0.0125 d_{50}^{1.4} \tag{3.1}$$

$$1mm < d_{50} < 100mm, \qquad V_{*c} = 0.0305 d_{50}^{0.5} - 0.0065 d_{50}^{-1} \tag{3.2}$$

where V_{*c} for a given d_{50} can be also found from the Shield's diagram (see Figure 3.1). One should take d_{50} in mm to obtain V_{*c} in m/s. Mean critical velocity is obtained from Eq. 3.3.

$$\frac{V_c}{V_{*c}} = 5.75 \log\left(5.53 \frac{d_0}{d_{50}} \right) \tag{3.3}$$

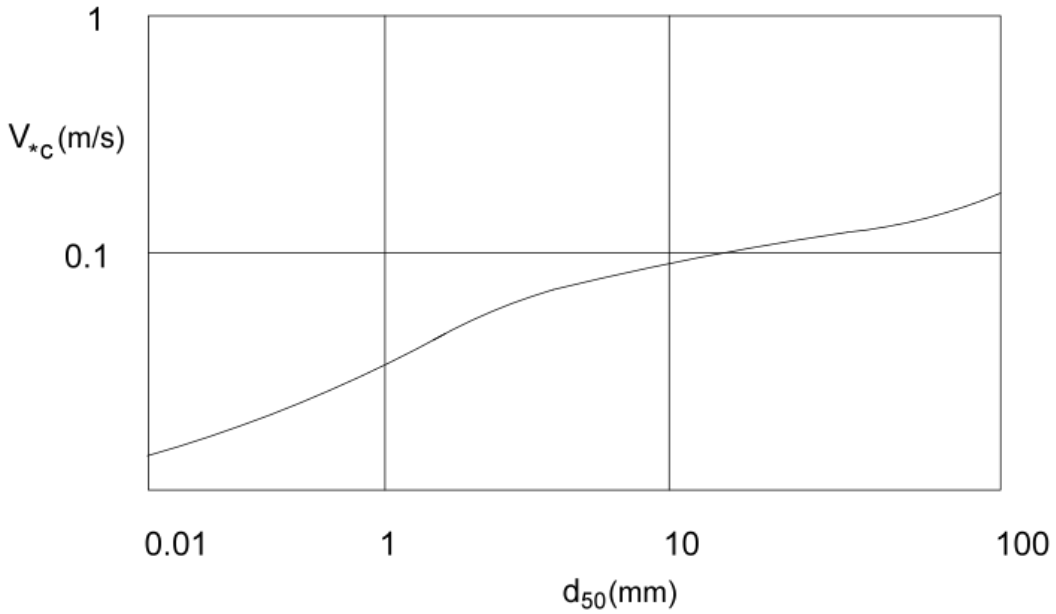

Figure 3.1: Determination of the critical shear velocity as a function of median sediment diameter (Reproduced from Melville and Sutherland, 1988)

Armor Peak Velocity, V_a:

Armor peak velocity is valid only for σ_g>1.3 (nonuniform sediments). Critical shear velocities in armored beds are obtained from Equations 3.4 and 3.5 (Melville and Coleman, 2000).

$$0.1mm < d_{50a} < 1mm, \qquad V_{*c} = 0.0115 + 0.0125 d_{50a}^{1.4} \tag{3.4}$$

$$1mm < d_{50a} < 100mm, \qquad V_{*c} = 0.0305 d_{50a}^{0.5} - 0.0065 d_{50a}^{-1} \tag{3.5}$$

where $d_{50a} = \dfrac{d_{\max}}{1.8}$ (3.6)

Mean critical velocity in armored bed is:

$$\frac{V_c}{V_{*ca}} = 5.75 \log\left(5.53 \frac{d_0}{d_{50a}} \right) \tag{3.7}$$

Finally, $V_a = 0.8 V_{ca}$ (3.8)

Figure 3.2 presents the variation of local scour depth with flow intensity (Melville and Coleman, 2000). As velocity increases until the threshold velocity, local scour depth advances linearly under clear-water scour conditions. As the velocity passes the critical velocity, condition of transport is turned into live bed scour. Firstly, local scour depth decreases slightly and later increases again to second peak (live bed peak). The second

peak is smaller than the threshold peak because, the total strength of the flow is used to scour the base of the pier. However, in the case of live bed scour, the strength of the flow is used to scour the pier foundation and transport the sediment (Yanmaz, 2002).

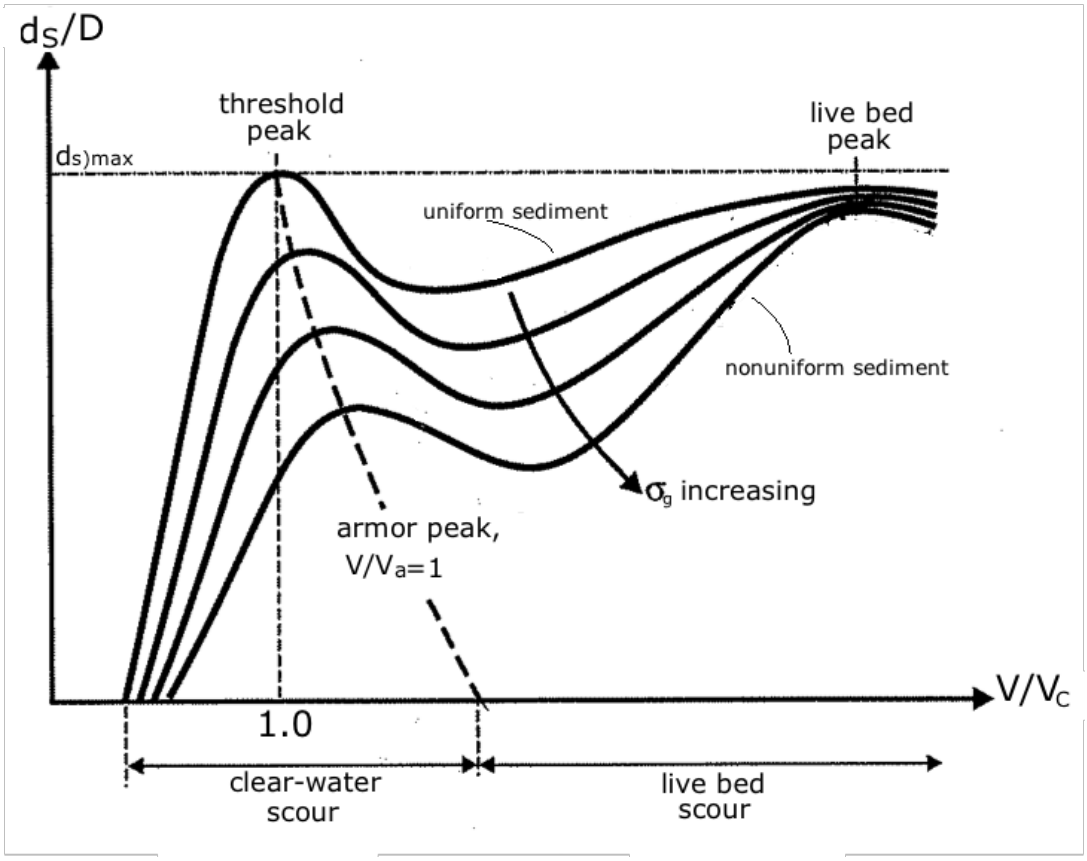

Figure 3.2: Local scour depth variation with flow intensity
(Reproduced from Melville and Coleman, 2000)

Melville and Coleman (2000) recommend various correction factors for scour depth estimation. K_1 represents the effects of flow intensity on local scour depth. Figure 3.3 and Figure 3.4 show the influence of flow intensity on local scour depth in uniform sediment and nonuniform sediment respectively. These are the plots of laboratory data from past studies for local scour at piers in terms of K_1. The following relationship is given (Melville and Coleman, 2000):

$$K_1 = \frac{V-(V_a-V_c)}{V_c} \quad \text{for} \quad \frac{V-(V_a-V_c)}{V_c} < 1 \qquad (3.9)$$

$$K_1 = 1 \quad \text{for} \quad \frac{V-(V_a-V_c)}{V_c} \geq 1 \qquad (3.10)$$

For uniform sediments, critical velocity and armor peak velocities can be taken as equal, while putting into the Eqs. (3.9) and (3.10). Thus, $[V-(V_a-V_c)]/V_c \equiv V/V_c$. It is obvious

that, when laboratory-based envelope curves are inspected, K_1 increases from 0 to 1 until the threshold condition and later it stays constant (Figure 3.3 and 3.4).

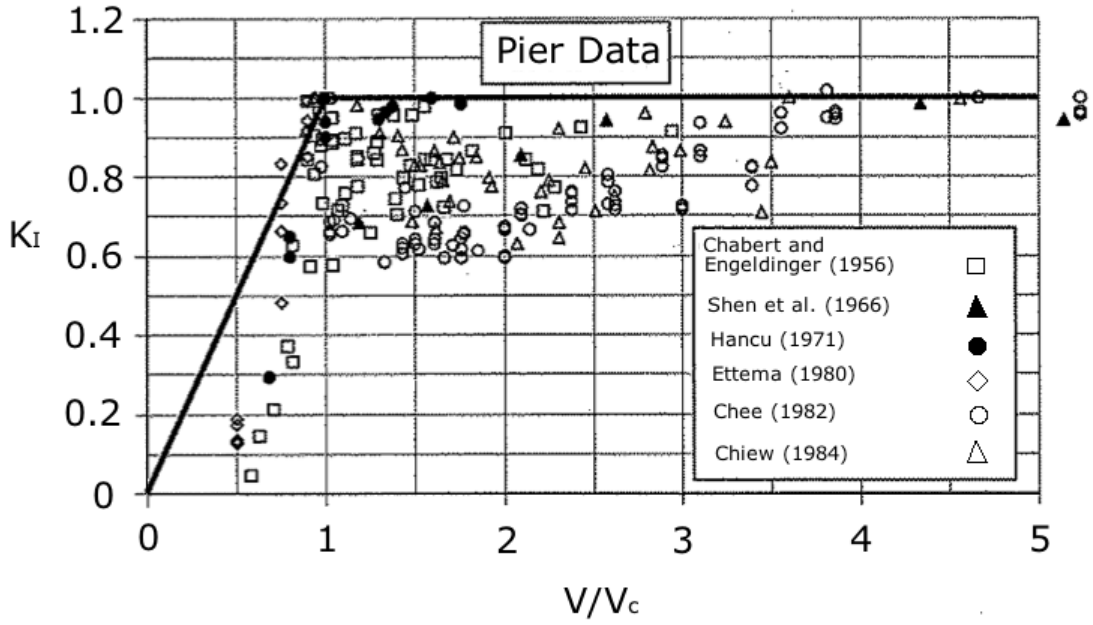

Figure 3.3: Influence of flow intensity on local scour depth in uniform sediment. (Reproduced from Melville and Coleman, 2000)

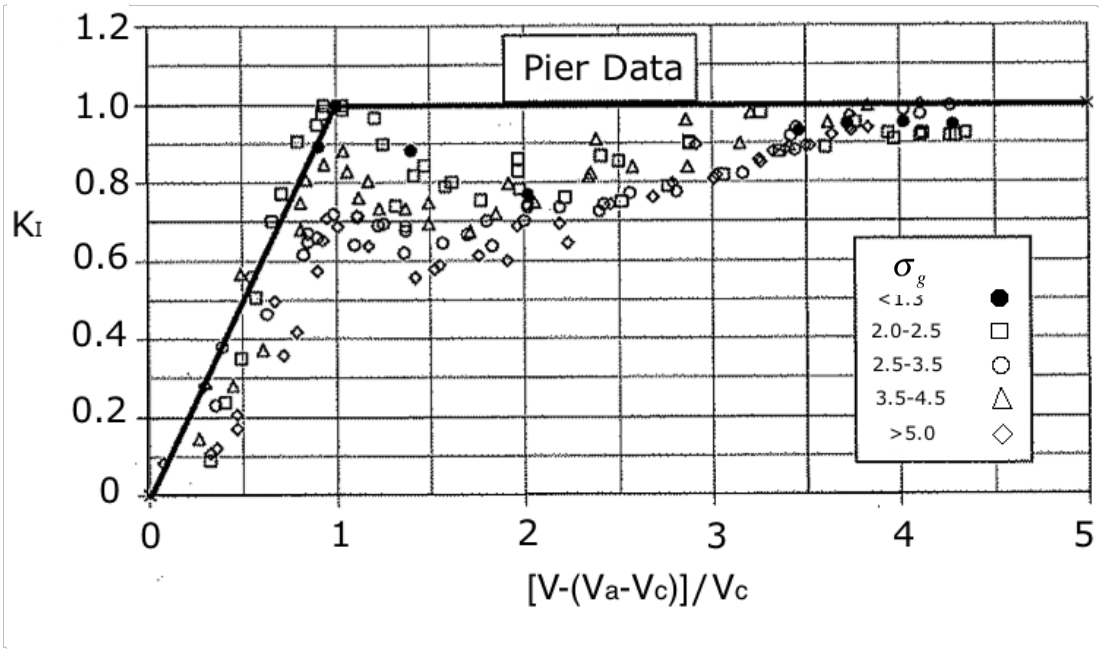

Figure 3.4: Influence of flow intensity on local scour depth in nonuniform sediment (Reproduced from Melville and Coleman, 2000)

3.2 Effect of Approach Flow Depth

In Chapter 2, the flow pattern around circular bridge piers is discussed and separated into four components as downflow, horseshoe vortex, wake vortices and bow wave. Existence of a pier in the direction of flow causes surface roller at the upstream and horseshoe vortex at the bed level. These eddy movements that are developed at the surface and the base, move in opposite direction (Figure 2.2). Dependence of the local scour on the approach flow depth is based on the interference of the eddy movements (Yanmaz, 2002). As a general rule, if two rollers do not interact with each other, the local scour depth is independent of flow depth. In other words, when depth of flow is large enough, the interference between the vortices loses its intensity (Raudkivi, 1991). The surface roller becomes more effective and leads the base vortices to undermine the base of the footing lesser with decreasing flow depth. Yanmaz (2002) indicates that, Melville and Sutherland (1988) ignore the effect of depth of flow for certain d_0 / D values for fine and coarse aggregates:

Fine aggregate, $d_0 / D \geq 3.0$ (3.11)

Coarse aggregate, $d_0 / D \geq 6.0$ (3.12)

Above these limits, the effect of approach flow depth on formation of local scour is negligible.

The scour depth equations, derived by past researchers, are typically in the form of $(D / d_0)^{\xi}$. Raudkivi (1991) states that, Neill (1964) derived an equation showing that depth of local scour is the function of flow depth by using the data by Laursen and Toch (1956), for constant discharge:

$$\frac{d_s}{d_0} = 1.5\left(\frac{D}{d_0}\right)^{0.7} \tag{3.13}$$

Figure 3.5 shows the variation of local scour depth with depth of flow that is presented in the literature by various studies.

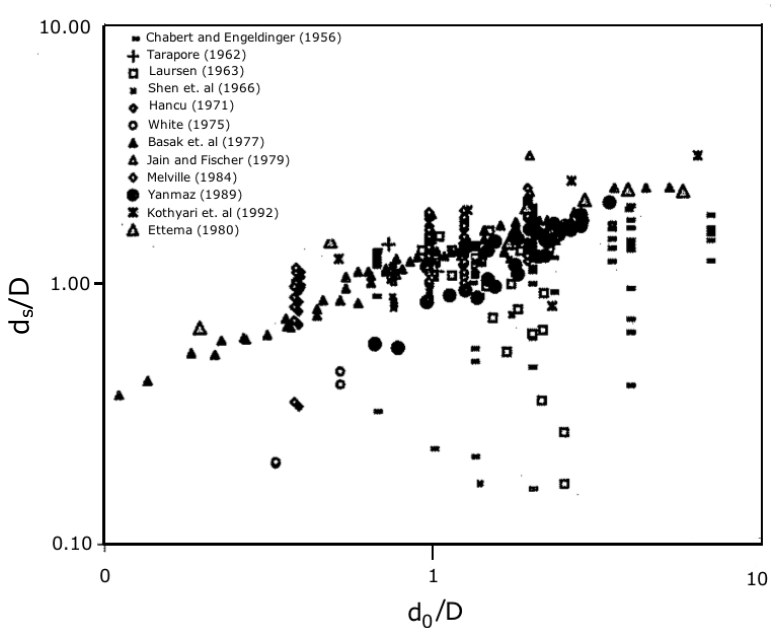

Figure 3.5: Variation of relative scour depth with relative depth of flow (Reproduced from Yanmaz, 2002)

Melville and Coleman (2000) classify the local scour process at bridge piers (Table 3.1). Figure 3.6 represents the effect of relative flow depth on relative scour depth (Melville and Chiew, 1999). The inequalities defining each class are obtained from the laboratory data. Furthermore, they propose a flow depth – foundation size factor, K_{yb}, as follows:

$$K_{yb} = 2.4D \quad \text{for} \quad \frac{D}{d_0} < 0.7 \tag{3.14}$$

$$K_{yb} = 2\sqrt{d_o D} \quad \text{for} \quad 0.7 < \frac{D}{d_0} < 5 \tag{3.15}$$

$$K_{yb} = 4.5d_0 \quad \text{for} \quad \frac{D}{d_0} > 5 \tag{3.16}$$

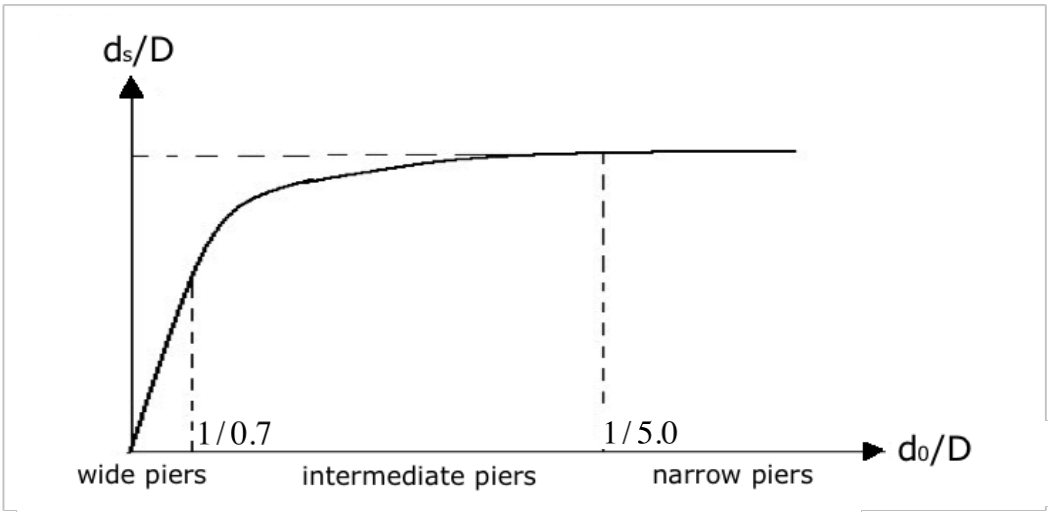

Figure 3.6: Effect of relative flow depth on relative scour depth

Table 3.1: Classification of local scour processes at bridge piers (Melville and Coleman, 2000)

Class	D/d_0	Local Scour Dependence
Narrow	$D/d_0 < 0.7$	$d_s \propto D$
Intermediate width	$0.7 < D/d_0 < 5$	$d_s \propto (Dd_0)^{0.5}$
Wide	$D/d_0 > 5$	$d_s \propto d_0$

Flow depth factor, K_y, that represents the correlation between relative scour depth and relative flow depth based on the data of many investigators is shown in Figure 3.7.

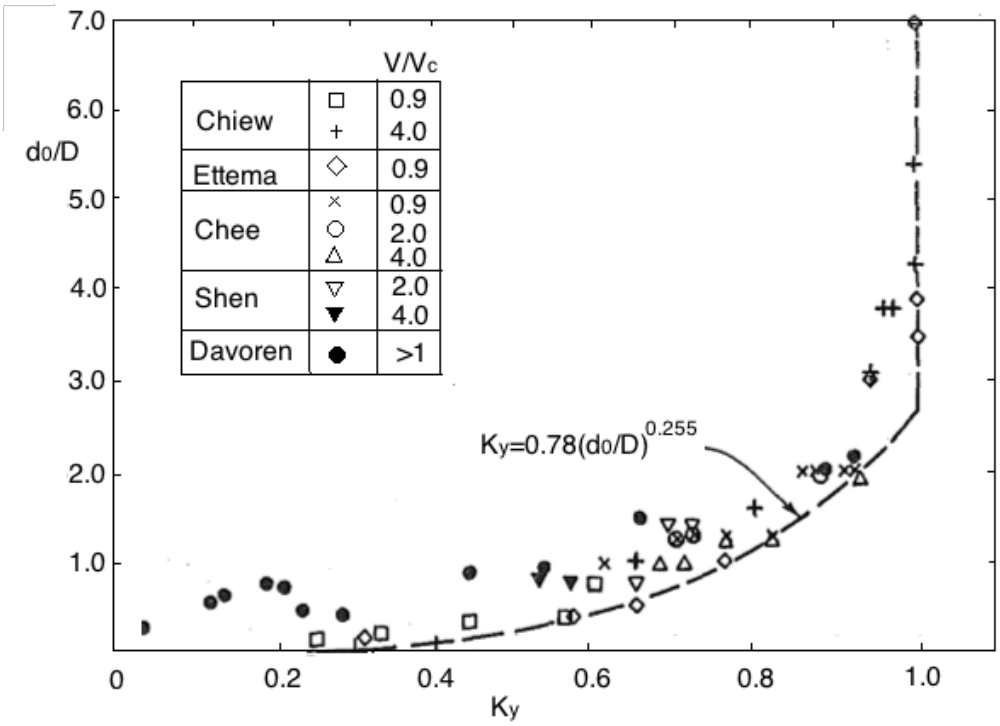

Figure 3.7: Influence of flow depth on scour depth (Reproduced from Melville and Sutherland, 1988)

3.3 Effect of Sediment Grading

Raudkivi and Ettema (1983) have studied the effect of sediment grading on local scour depth at clear-water conditions (Yanmaz, 2002). According to them, sediment grading substantially affects the scour depth. As long as standard deviation of sediment grading (σ_g) increases, armoring effect burst into prominence. Coarse particles spread over the fine particles, thus local scour depth reduces considerably. Yanmaz (2002) has obtained a regression equation, in an interval of $1.0 \le \sigma_g \le 5.0$, based on the correction factor (K_σ) given by Raudkivi (1986):

$$K_\sigma = 0.013462\sigma_g^5 - 0.2232\sigma_g^4 + 1.4066\sigma_g^3 - 4.0864\sigma_g^2 + 5.007\sigma_g - 1.1179 \qquad (3.17)$$

Considering the Eq. (3.17), the local scour depth in a nonuniform riverbed, where standard deviation of sediment grading is about 3.5 for a gravel river, decreases 80% when compared to the local scour depth in a river with uniform sediment (Yanmaz, 2002).

Melville and Sutherland (1988) summarize the results of the study made by Raudkivi and Ettema (1977) (Fig. 3.7). Equilibrium clear-water scour depth divided by pier diameter as a function of the sediment grading is shown (Raudkivi, 1991). They state that, grading does not change the time required to reach the equilibrium but affect the maximum value of d_s / D

.

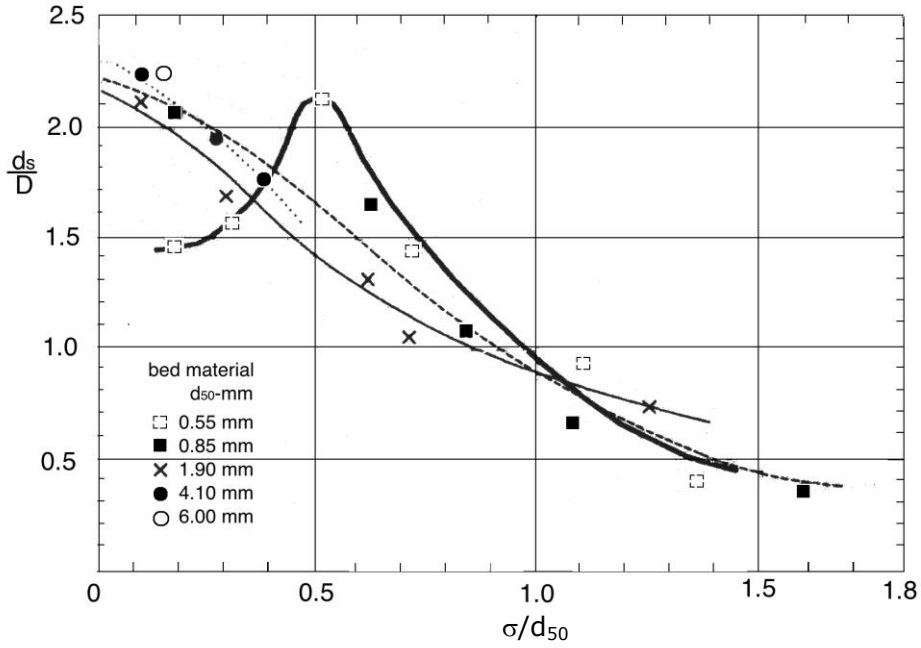

Figure 3.8: Equilibrium clear-water scour depth divided by pier diameter (ds/D) as a function of the sediment grading (Reproduced from Breusers and Raudkivi, 1991)

Raudkivi (1991) has derived an equation to estimate the possible maximum value of the equilibrium depth of clear-water scour:

$$\frac{d_{se}(\sigma)}{D} = K_\sigma \frac{d_{se}}{D} \tag{3.18}$$

where d_{se} is the equilibrium scour depth in uniform sediment, $\sigma_g = 1.0$. In parallel with Eq. (3.18), Figure 3.8 represents the coefficient K_σ as a function of the geometric standard deviation of the particle size distribution, σ_g.

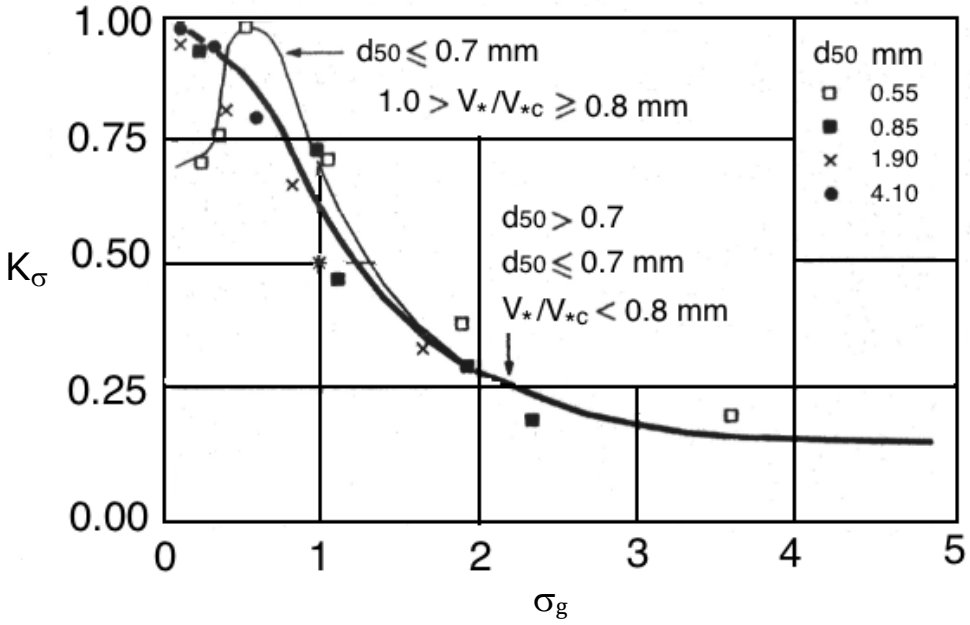

Figure 3.9: Coefficient K_σ as a function of the standard deviation of the particle size distribution (Reproduced from Breusers and Raudkivi, 1991)

3.4 Effect of Pier and Sediment Sizes

Ettema (1980) has investigated the effect of relative pier size, D / d_{50}, on scour depth and has made an inference. According to him, bed erosion is reduced when $D / d_{50} < 50$, just because bed material is considerably coarse and causes roughness at the bed level. The channel base absorbs the energy of the vertical flow, which is generated at the upstream of the pier (Breusers and Raudkivi, 1991). It is observed that relative scour depth is not affected by the particle size when $D / d_{50} > 50$ (Yanmaz, 2002). However, Raudkivi (1991) states that considering the work of Ettema (1980), relative scour depth is unaffected by particle size when $D / d_{50} \geq 25$ (Figure 3.10).

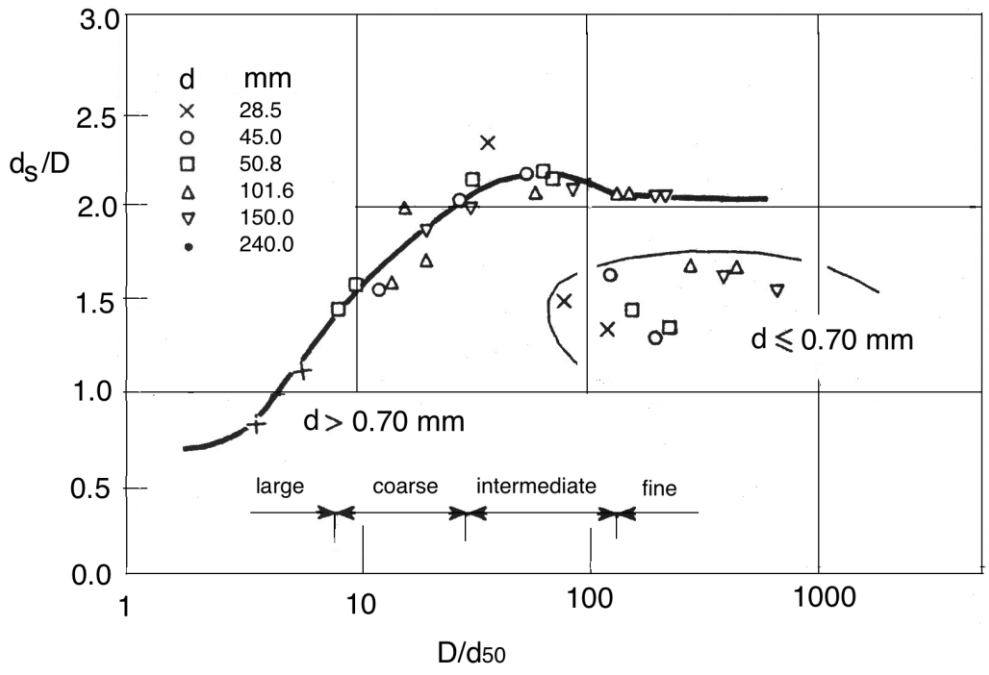

Figure 3.10: Equilibrium clear-water scour depth versus D/d_{50} (Reproduced from Breusers and Raudkivi, 1991)

Yanmaz (2002) has found the regression equations for the correction factor, K_D, which is introduced by Raudkivi (1986):

For $2.9 \le \frac{D}{d_{50}} < 21$,

$$K_D = 1.515 \times 10^{-4}\left(\frac{D}{d_{50}}\right)^3 - 7.53 \times 10^{-3}\left(\frac{D}{d_{50}}\right)^2 + 0.1349\left(\frac{D}{d_{50}}\right) - 0.0162 \quad (3.19)$$

For $21 \le \frac{D}{d_{50}} < 50$,

$$K_D = -8.167 \times 10^{-5}\left(\frac{D}{d_{50}}\right)^2 + 9.247 \times 10^{-3}\left(\frac{D}{d_{50}}\right) + 0.7418 \quad (3.20)$$

For $50 \le \frac{D}{d_{50}}$,

$$K_D = 1.0 \quad (3.21)$$

In Figure 3.11, the plotted pier data of Ettema (1980), Chiew (1984) and Baker (1986) are shown for both uniform and nonuniform sediments separately, in terms of the sediment size multiplying factor. Together with these envelope curves, Melville and Sutherland (1988) offered below equations:

$$\text{For } \frac{D}{d_{50}} \leq 25, \qquad K_D = 0.57 \log\left(2.24 \frac{D}{d_{50}}\right) \tag{3.22}$$

$$\text{For } \frac{D}{d_{50}} \geq 25, \qquad K_D = 1.0 \tag{3.23}$$

For nonuniform sediments, Eq. (3.22) is expressed in terms of D / d_{50a} rather than D / d_{50}. In Figure 3.21, L stands for abutment length.

When excluding the effects of relative depth and relative grain size, increasing the pier size affects the time to reach the maximum scour depth, not its relative magnitude. While estimating the local scour depth in the field, the effect of pier size is of primary interest (Raudkivi 1991).

Yanmaz and Altinbilek (1991) state that, as the size of the local scour hole around a circular bridge pier depends on the pier size, equilibrium scour depth and time to reach the equilibrium scour depth increases in case of larger piers. The usage of minimum pier size, which does not cause any structural problem, gives the optimal solution for hydraulic safety.

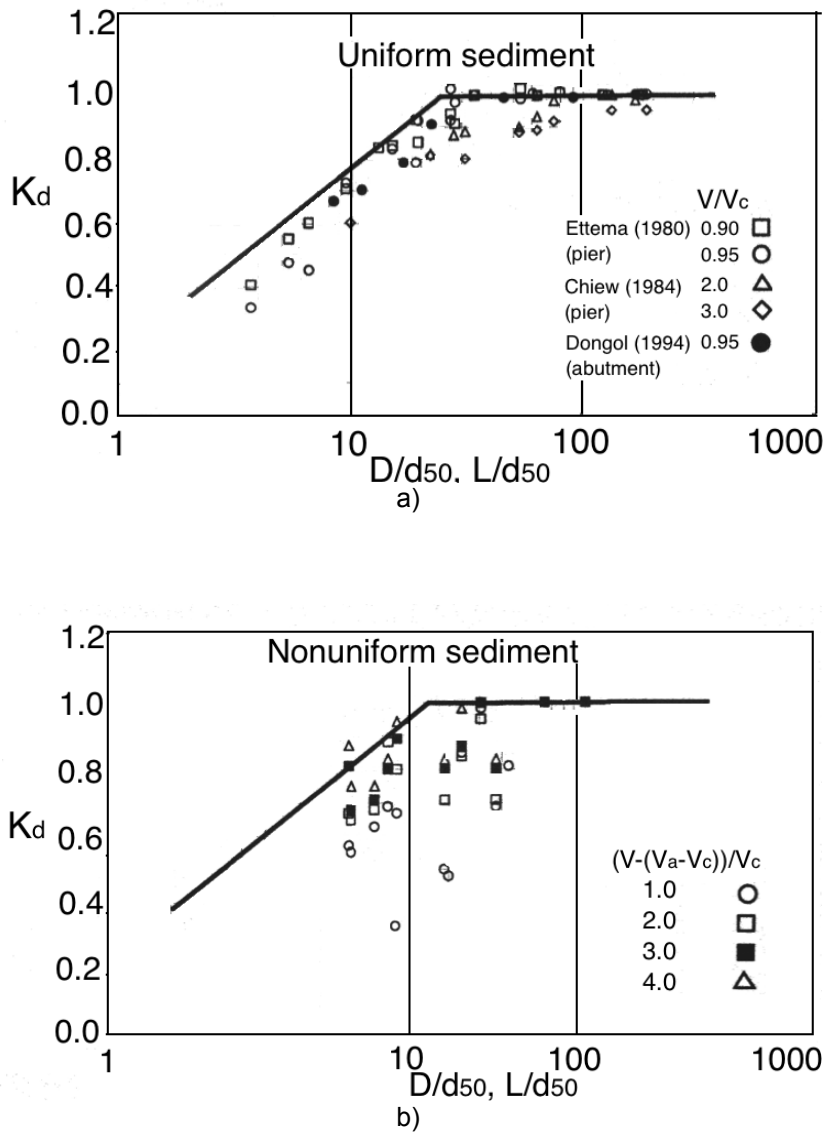

Figure 3.11: Influence of sediment coarseness on local scour depth a) uniform sediment b) nonuniform sediment
(Reproduced from Melville and Coleman, 2000)

3.5 Time Effect

In case of clear-water scour conditions; average shear stress, weight of water and turbulence stresses create balance simultaneously. Thus, it takes a long time to reach the equilibrium scour depth (Yanmaz, 2002). Yanmaz (2002) offers a regression equation for the variation of depth of scour with time according to his experimental study in specific conditions (Figure 3.12):

$$\frac{d_s}{d_{se}} = 0.12 \ln\left(\frac{t}{t_e}\right) + 1.0 \tag{3.24}$$

where d_{se} and t_e are equilibrium scour depth and time taken to reach the equilibrium scour depth respectively.

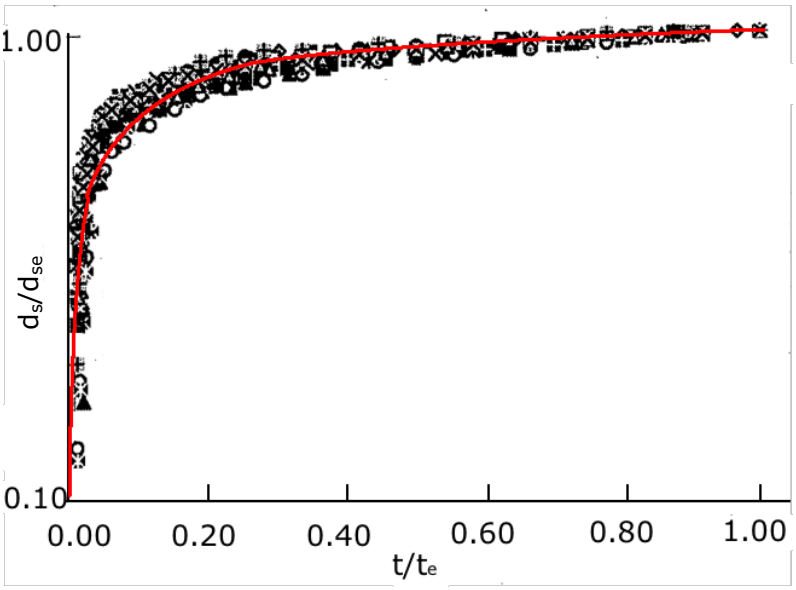

Figure 3.12: Temporal development of clear-water scour around a cylindrical pier (Reproduced from Yanmaz, 2002)

As can be seen from Figure 3.12, the rate of scour development is higher in initial phase of the development; however, scour deepens slowly and reaches equilibrium asymptotically after a while.

Melville and Coleman (2000) represent a time factor for cylindrical bridge piers:

$$K_t = \exp\left(-0.03 \left|\frac{u_c}{u} \ln\left(\frac{t}{t_e}\right)\right|^{1.6}\right) \tag{3.25}$$

The value K_t is equal to 1.0 if there are live-bed conditions, because equilibrium depth of local scour is attained rapidly.
Figure 3.13 shows the temporal development of local scour at circular bridge piers for various flow intensity values according to the laboratory studies done by Chiew and Melville (1996) and Melville and Chiew (1997). It is obvious that the rate of the development is reduced at lower flow intensities.

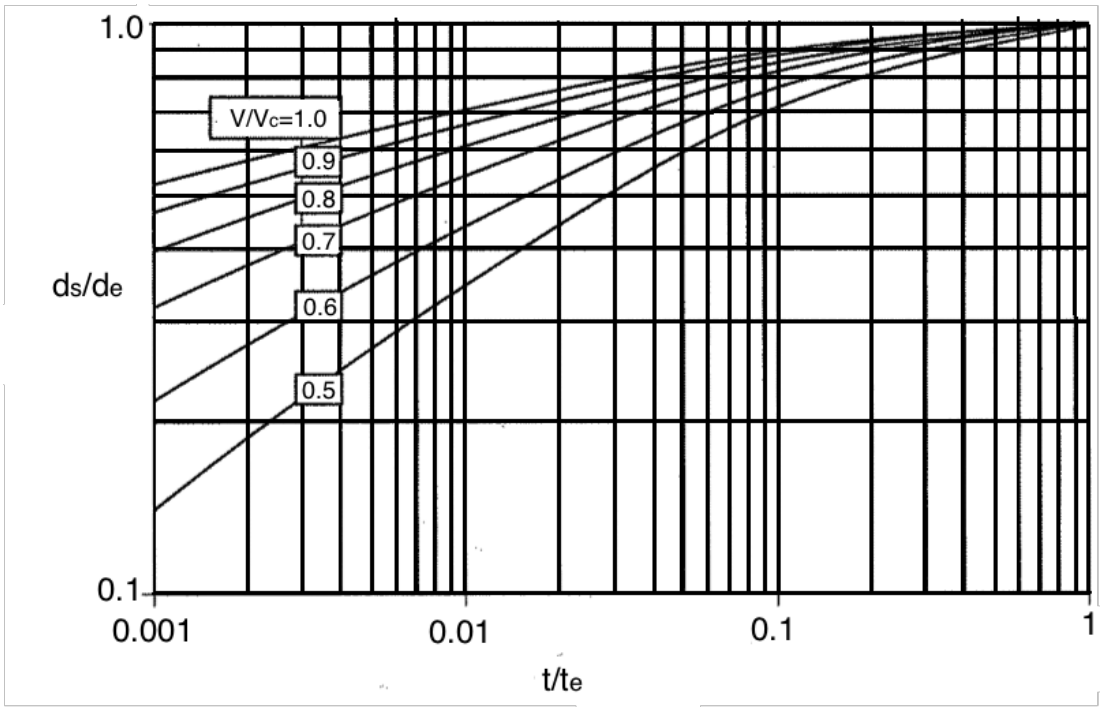

Figure 3.13: Temporal development of local scour depth at piers under clear-water conditions (Reproduced from Melville and Coleman, 2000)

Raudkivi (1986) states that, 50 hours is needed to reach equilibrium scour depth in laboratory conditions for clear-water scour (Yanmaz 2002). It is a very long time and makes studies harder for the researchers. As the trend of the development of scour hole is asymptotic, some researchers have decided on where to stop the experiments. Melville and Chiew (1999) have formalized the proposal as follows:

$$\frac{d(d_{se})}{d_t} \leq \frac{0.05D}{24h} \qquad (3.26)$$

From Equation 3.26, it can easily be said that when the development of scour hole does not exceed 5% of the pier diameter in 24 hours, the experiment is assumed to reach the equilibrium. Mia and Nago (2003) have expressed the issue in such a way that when the development of scour in 1 hour is less than 1mm, then the experiments can be stopped.

3.6 Effect of Pier Alignment

Another factor affecting the local scour depth is the pier alignment. As the alignment increases, the scour depth increases because depth of scour is the function of the projected width of the pier. Eq. (3.27) gives the relation between projected pier width with the length and the width of the pier:

$$b_t = b\cos\alpha + L_p \sin\alpha \tag{3.27}$$

Figure 3.14 shows the diagrammatic scour shapes at a pier aligned with flow and angled to the flow direction (Raudkivi 1991). Only cylindrical piers are not affected by the pier alignment as long as they show same behavior for every alignment angle. The ratio of the length of the pier to its width directly affects the development of scour hole at the downstream side of the pier (Figure 3.15).

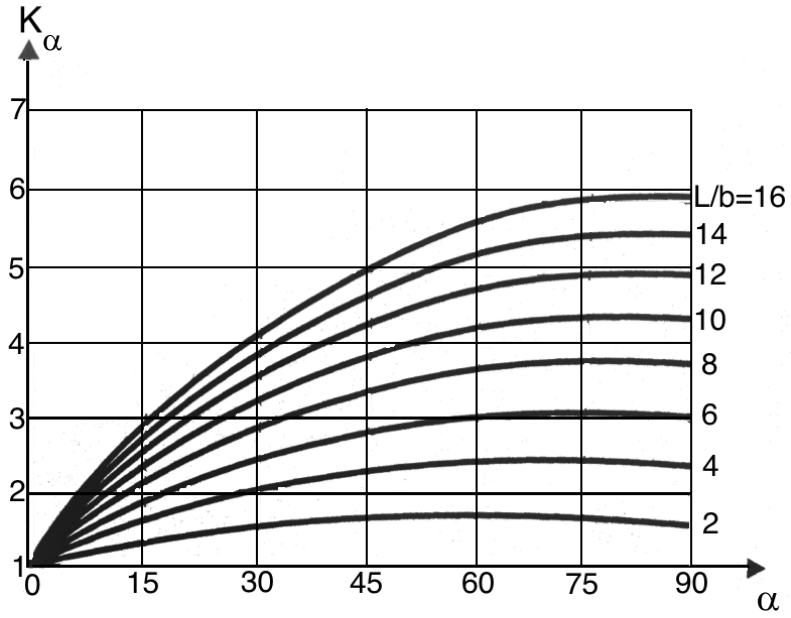

Figure 3.14: Alignment factor Kα for piers not aligned with flow (Reproduced from Breusers and Raudkivi, 1991)

Richardson and Davis (2001) propose an alignment factor for non-cylindrical piers:

$$K_\alpha = \left(\cos\alpha + \frac{L_p}{b}\sin\alpha\right)^{0.65} = \left(\frac{b_t}{b}\right)^{0.65} \tag{3.28}$$

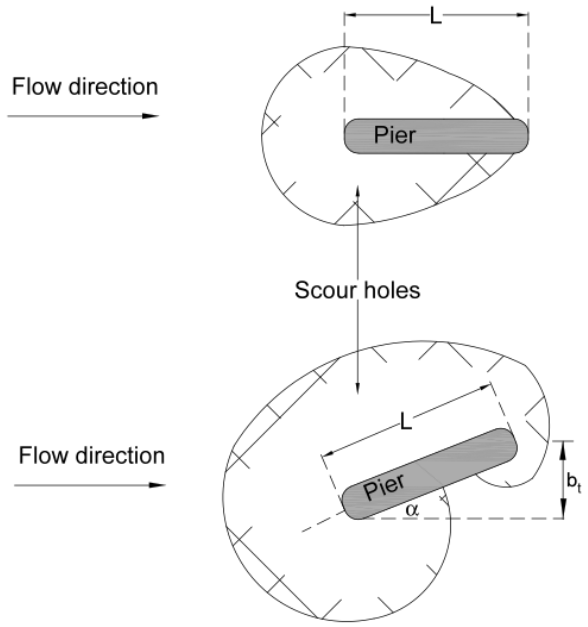

Figure 3.15: Diagrammatic scour shapes at a pier aligned with flow and another angled to the flow direction (Breusers and Raudkivi, 1991)

Raudkivi (1991) recommends that, angle of attack greater than 5-10° should be avoided or row of cylindrical pier should be used to reduce or remove the negative effects of the alignment.

3.7 Effect of Pier Shape

It is an advantage to place the piers streamlined to reduce the strength of general flow turbulence and vortices. Like that of alignment, the effect of pier shape can be represented by the factor K_s (Raudkivi, 1991). When the shape factor, K_s, decreases, the estimated scour depth also decreases. The shape factors for variety of shapes are given in Table 3.2 and the dimensions are defined in Figure 3.16.

Table 3.2: Pier shape factors (Breusers and Raudkivi, 1991)

Pier shape	b / L	b'/ L'	K_s
Cylindrical			1.0
Rectangular	1:1		1.22
	1:3		1.08
	1:5		0.99
Rectangular with semi-circular nose	1:3		0.90
Semicircular nose with wedge-shaped tail	1:5		0.86
Rectangular with chamfered corners	1:4		1.01
Rectangular with wedge-shaped nose	1:3	1:2	0.76
		1:4	0.65
Elliptic	1:2		0.83
	1:3		0.80
	1:5		0.61
Lenticular	1:2		0.80
	1:3		0.70
Aerofoil	1:3.5		0.80

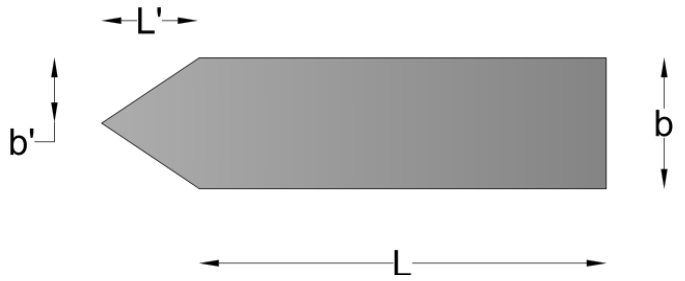

Figure 3.16: Rectangular pier with wedge shaped nose (Breusers and Raudkivi, 1991)

According to Raudkivi (1991), the shape factor of the cylinder is 1.0 and it has a comparable function among all shapes. Furthermore, when there is even a small angle of attack of the approach flow, there is no advantage of using a smooth pier shape (except cylindrical piers).

3.8 Effect of Vertical Angle of Attack

Placing the piers vertically inclined affects the local scour depth. Breusers and Raudkivi (1991) have given the shape factors, based on laboratory studies, for the piers whose widths change with depth (Table 3.3). Horseshoe vortex that are developed at the base can not be dragged along downstream, thus the depth of local scour increases with the result that the pier width increases upwards. On the contrary, depth of scour decreases for an upward narrowing pier. In addition, it is easily perceived that upward narrowing piers cause smaller stresses at the bottom (Yanmaz 2002). In Figure 3.17, local scour at piers tapered in elevation is shown.

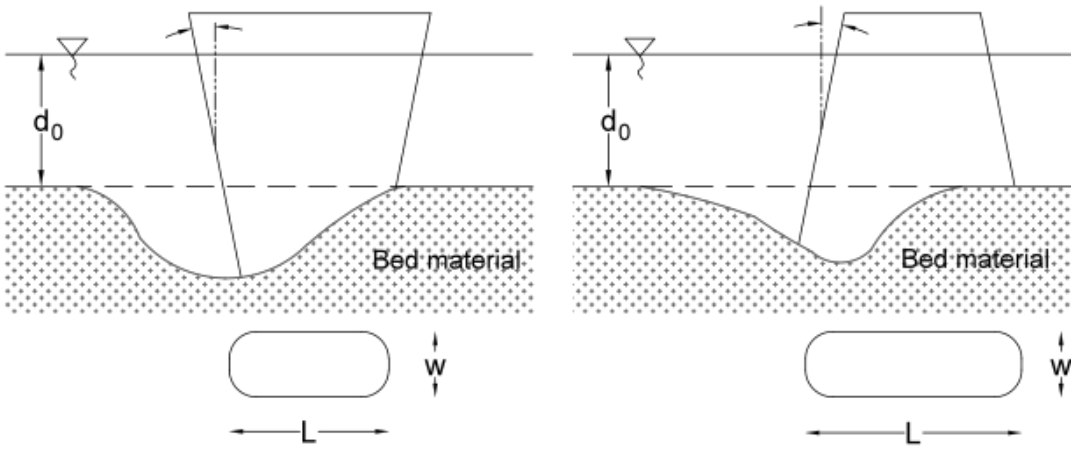

Figure 3.17: Local scour at piers tapered in elevation

Table 3.3: Shape factors for tapered piers (Breusers and Raudkivi, 1991)

Shape	$V(m/s)$	d_{se}/w	K_s
Cylinder	0.67	1.69	1.0
	0.81	1.71	1.0
Narrowing downward	0.67	2.03	1.20
	0.81	2.06	1.20
Narrowing upward	0.67	1.31	0.78
	0.81	1.26	0.74

Bozkus and Yildiz (2004) and Bozkus and Cesme (2010) have performed sets of experiments on inclination of cylindrical piers and derived various regression equations. The detailed explanation of these studies and comparison with this study is discussed in further chapters.

3.9 Group Effect of the Piers

According to the structural reasons, a group of piers that are arranged one after another rather than a massive pier can be constructed. In this case, negative flow conditions can occur because of the interference of the flow around piers. Group effect is generated by a group of piers, which are aligned in direction of flow and/or perpendicular to the flow. The group effect mainly depends on the distance between piers, direction and position of piers.

In literature, there are a few studies on bridge pier groups. Basak et al. (1975) have studied rectangular bridge pier groups and improved his research by studying cylindrical pier groups in 1977. He has investigated local scour depth around cylindrical bridge pier groups by running various experiments as well as changing some parameters such as angle of attack and distance between the piers with a constant Froude number ($Fr = 0.55$). In the pier group composed of cylindrical piers of equal sizes arranged in a linear axis at equal distances, the variation of scour depth observed on all surfaces of each pier forming the group, depending on the distance between piers, pier size and number and the angle of attack of flow have been studied (Basak et al., 1977).

When flow direction is parallel to the pier group axis ($\alpha = 0°$), the maximum scour depth takes place on upstream surface of the first pier, independent from number of piers forming the group; it is always equal to the individual scour of one single pier. The strength of flow reduces at rear piers because front piers are exposed to flow at first and they protect following piers against flow. In case of the flow direction forms an angle against the axis of the pier group ($\alpha > 0°$), the group effect tends to increase the scour depth and the scour becomes greater than that of an individual pier. Additionally, the flow approaching perpendicular to the pier group axis ($\alpha = 90°$), leads to an increase in maximum scour depth than that of a single pier (Basak, 1977).

Based on the experimental results, Basak concluded that if $a/D > 40$, all the piers constituting the pier group act as a single pier when $\alpha = 0°$ (Figure 3.18) and when $\alpha = 90°$, the pier group act as a single pier if $a/D > 7$ (Figure 3.19). Separate scour holes are formed around them and group effect is not observed. As the distance between piers is very small in case of $\alpha = 0°$, i.e. $a/D = 1$, a large and a single scour hole is formed as schematically drawn and shown in Figure 3.20. Moreover, when the flow is perpendicular to the pier group axis ($\alpha = 90°$), again a single hole is generated covering all piers if $a/D = 0.5$ (Figure 3.21). When the distance is between these limits, $a/D < 40$ for $\alpha = 0°$ and $a/D < 3$ for $\alpha = 90°$, separate but interfered scour holes are developed (Figure 3.22 and 3.23). Parallel to what was mentioned above, Basak (1977) also stated using a group of piers rather than a single massive pier, reduces the development of local scour depth.

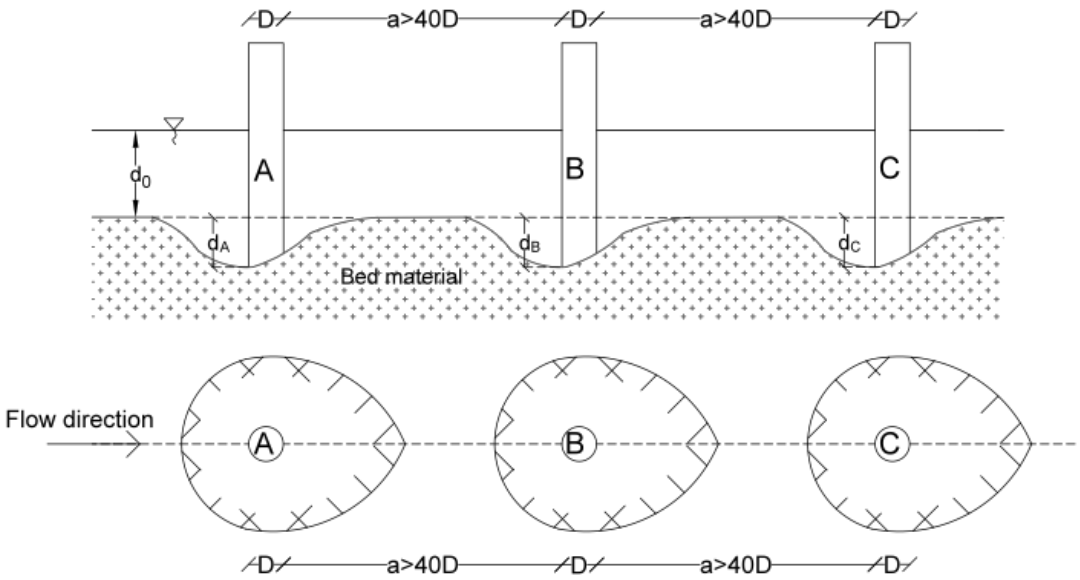

Figure 3.18: Formation of separate scour holes in case of $\alpha = 0°$ and $a/D > 40$

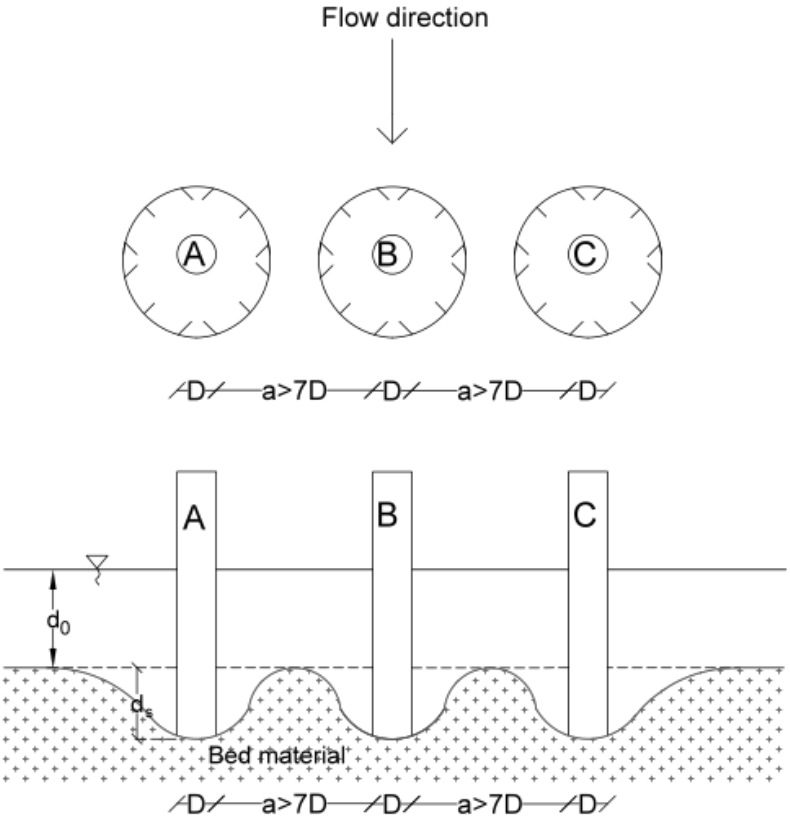

Figure 3.19: Formation of separate scour holes in case of $\alpha = 90°$ and $a > 7D$

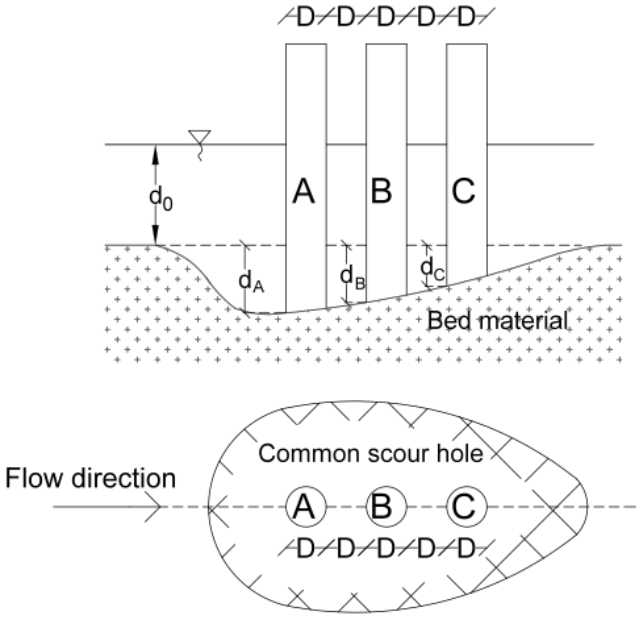

Figure 3.20: Formation of a common scour hole in case of $\alpha = 0°$ and $a = D$

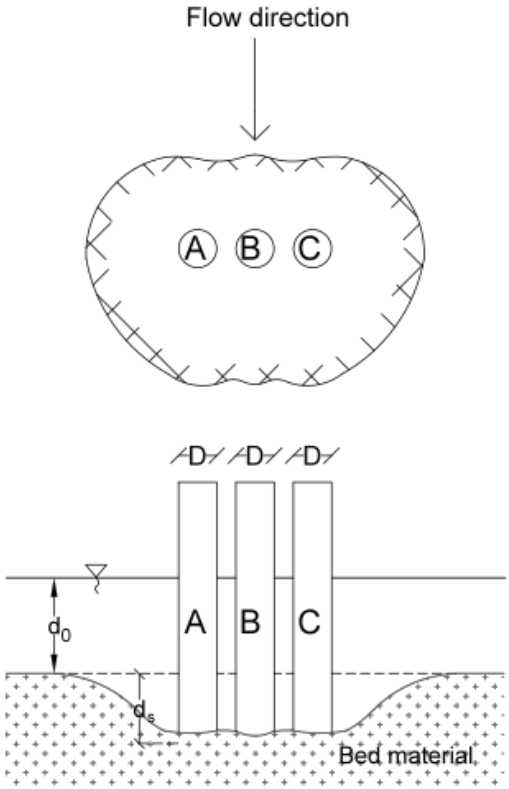

Figure 3.21: Formation of a common scour hole in case of $\alpha = 90°$ and $a < 0.5D$

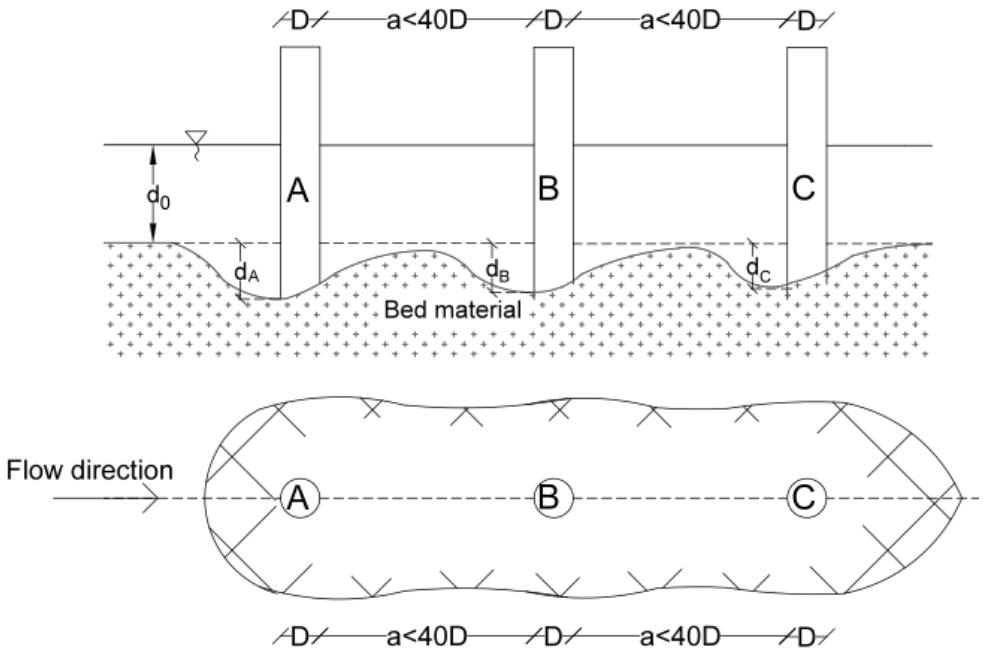

Figure 3.22: Formation of a scour hole in case of $\alpha = 0°$ and $a < 40D$

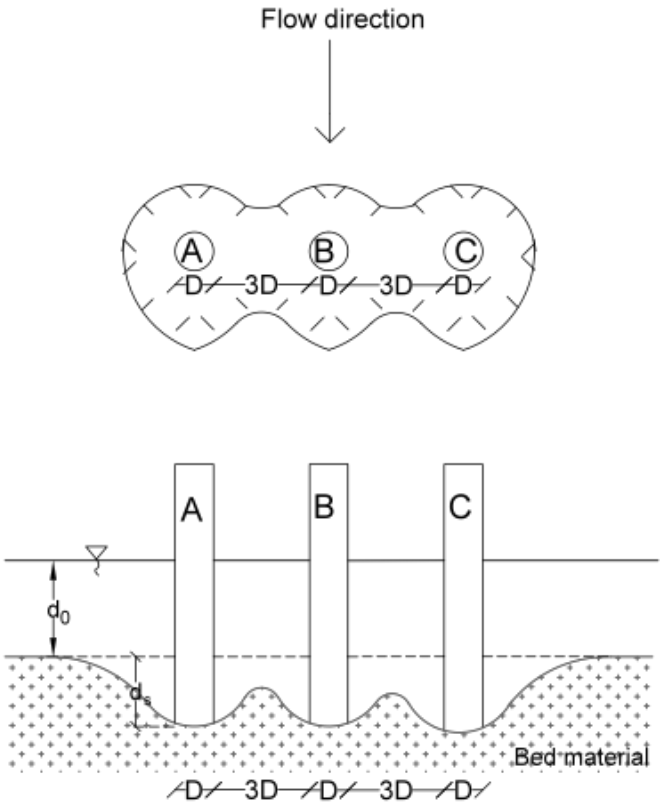

Figure 3.23: Formation of a scour hole in case of $\alpha = 90°$ and $a < 3D$

Hannah (1978) has studied the same subject with specific conditions and achieved some results showing the group effect. He founded that the local scour depth at the downstream side of the rear pier is smaller than the scour depth around a single pier. According to Yanmaz (2002), the main reason is the transportation of the bed material from the scour hole of upstream pier to the scour hole at the downstream pier partially.

A more recent study made by Salim and Jones (1999) focused on determining scour depths for pier groups by taking into consideration the spacing between the piers, the number of pier rows and a height factor for the pier length exposed to the flow (Richardson and Davis, 2000).

The study made by Vittal et al. (1994) considers a group of three smaller circular piers, which have an angular spacing of 120°, as a scour-reduction device. They have run the experiments in different orientations (Figure 3.24). They compared the local scour formation around a single pier whose diameter is equal to the circumscribing circle diameter of the pier group with the results from this group. Scour reduction of pier group is about 40% when compared to the local scour around solid pier. Moreover, maximum variation in scour depth due to the orientation is about 6%. The 30° orientation is considered as the best orientation and the 60° orientation resulted in maximum scour depth.

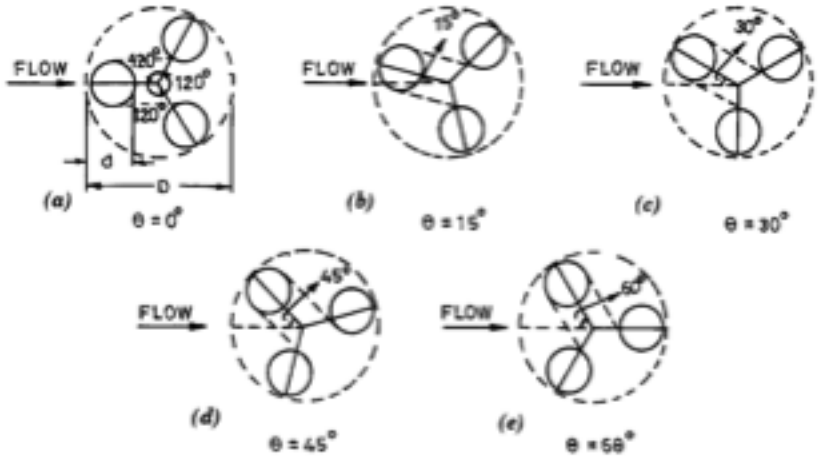

Figure 3.24: Approach flows: a) 0°; b) 15°; c) 30°; d) 45°; and e) 60° (Reproduced from Vittal et al. (1994))

CHAPTER 4

DIMENSIONAL ANALYSIS

Engineers should rely on interpretation and judgment based on experimental observations and experiences. Dimensional analysis is a powerful tool in formulating problems. Physical mechanism of the local scour can be understood better if appropriate dimensionless parameters describing the phenomenon are defined. A dimensional analysis is made below for the parameters that affect the local scour mechanism, which is suggested by Yanmaz (2002). The parameters are classified in terms of mass (M), length (L) and time (T).

1) Parameters characterizing the fluid

		Units	**Dimensions**
ρ	Density of the fluid	kg/m^3	ML^{-3}
ν	Kinematic viscosity of the fluid	m^2/s	L^2T^{-1}

2) Parameters characterizing the flow

g	Gravitational acceleration	m/s^2	LT^{-2}
d_0	Approach flow depth	m	L
u	Approach flow velocity	m/s	LT^{-1}
α	Angle of approach flow to the axis	-	-
u_*	Shear velocity	m/s	LT^{-1}

3) Parameters characterizing the flume

S_0	Channel bed slope	-	-
B	Channel width	m	L
K_a	Roughness effect of sidewalls	-	-
K_c	Channel alignment factor	m	L

4) Parameters characterizing the bed material

ρ_s	Density of the sediment	kg/m^3	ML^{-3}
d_{50}	Median sediment size	mm	L
σ_g	Standard deviation of particle size distribution	-	-
C	Cohesion	kg/ms^2	$ML^{-1}T^{-2}$

5) Parameters characterizing the pier

D	Pier diameter	m	L
K_s	Pier shape factor	-	-
K_g	Group effect of piers	-	-
K_r	Roughness of pier surface	-	-
β	Inclination angle of the pier with vertical axis	-	-

6) Time

t	Duration of flow	min	T

The variables, which affect the local scour mechanism, are summarized by this relationship:

$$f(d_s,\rho,g,\upsilon,d_0,V,\alpha,V_*,S_0,B,K_c,K_a,\rho_s,C,d_{50},\sigma_g,D,\beta,K_r,K_s,K_g,t)=0 \qquad (4.1)$$

Dimensionless parameters are found by Buckingham π-theorem and the repeated parameters are selected as ρ, V and D, indicating fluid, flow and geometric characteristics. Rearranging the dimensionless parameters gives the following relationship:

$$\frac{d_s}{D}=f_1\left(\frac{V}{\sqrt{gd_0}},\frac{Vd_{50}}{v},\frac{d_0}{D},\frac{V_*}{V},\frac{d_{50}}{B},\frac{\rho_s-\rho}{\rho},\frac{Vt}{D},\frac{K_c}{D},\sigma_g,\frac{C}{\rho V^2},\frac{d_{50}}{D},\alpha,\frac{K_r}{D},S_0,K_g,\beta,K_s,K_a\right) \qquad (4.2)$$

Where $V/\sqrt{gd_0}$ is Froude number (Fr), Vd_{50}/v is the particle Reynolds number (Re), $(\rho_s-\rho)/\rho$ is the relative density.

For the conditions in this study, the general statement can be simplified by the following assumptions:

a. The effect of Reynolds number is ignored for fully turbulent flow. Thus the term Vd_{50}/v is dropped.
b. In case of constant bed slope and sediment size, V_*/V is defined in terms of d_0/D, because it only depends on approach flow depth.
c. The sediment grain size (d_{50}) is very small compared to the channel width (B) ($d_{50}/B\approx 0$).
d. Densities of the fluid and sediment are constant throughout the study. In this way, relative density term $(\rho_s-\rho)/\rho$ is dismissed.
e. As the flow duration is long enough and equilibrium scour depth is studied, time development of local scour is ignored (Vt/D).
f. In a proper channel, the roughness of the sidewalls is ignored (K_c).
g. Bed material properties do not change, thus standard deviation of particle size distribution is constant (σ_c).
h. The bed material used in the experiments is non-cohesive ($C=0$), so the term $C/\rho u^2$ is dropped.
i. Angle of attack is zero in all experiments ($\alpha=0°$).
j. Smooth cylindrical piers are used, thereby the pier shape factor $K_s=1$ and roughness coefficient of the pier $K_r=1$.
k. The minimum pier diameter D=50mm and the median particle size $d_{50}=0.88mm$. As $D/d_{50}>50$, the effect of this term is neglected.
l. The flume is uniform and has a constant slope. S_0 and K_a terms are dropped.
m. K_g term (group effect) is ignored because local scour depth at the upstream face of the first pier is considered in regression calculations.

After simplifying the general relationship by determining the constant and ineffectual parameters, the below equation is derived for the experimental conditions in this study:

$$\frac{d_s}{D} = f_2\left(\frac{d_0}{D}, Fr, \beta\right) \tag{4.3}$$

Eq. (4.3) shows that relative scour depth is a function of the Froude number, inclination of pier with vertical axis and relative flow depth. However, flow intensity, V/V_c, is used rather than Froude number because the range of Froude number is very small ($0.292<F_r<0.370$). Then the Equation 4.4 becomes:

$$\frac{d_s}{D} = f_3\left(\frac{d_0}{D}, \frac{V}{V_c}, \beta\right) \tag{4.4}$$

CHAPTER 5

EXPERIMENTAL WORK

5.1 Introduction

The aim of this study is to experimentally investigate the effect of inclination of pier groups with vertical axis on local scour. The experimental approach for local scour around a bridge pier is the most common and significant method of analysis since the interaction between the flow and bed materials is hard to understand and quantify clearly due to the complexity of the flow field and properties of bed materials around a bridge pier. Experimental studies can be mainly divided into two categories: (1) those that focused on explanation of the three-dimensional flow field around a bridge pier and (2) those that developed empirical correlations to predict the maximum scour depth around a bridge pier.

5.2 Experimental Facilities

All the experiments of local scour around bridge pier groups were conducted in the Hydraulics Laboratory of Civil Engineering Department at Middle East Technical University, Ankara. The test channel is reconstructed to provide the necessary conditions. Old sediment is removed before maintenance work and clear, uniform and sieved bed material is placed afterwards. Detailed descriptions of the experimental equipment, the range of conditions tested and the method of testing are presented in the following sections.

5.2.1 The Test Channel

The test channel consists of 5 components:

1) Inflow pipe
2) Main channel
3) Settling pool
4) Outflow Pipe
5) Secondary channel

The plan view and side view of the test channel are given in Figure 5.1a and 5.1b respectively.

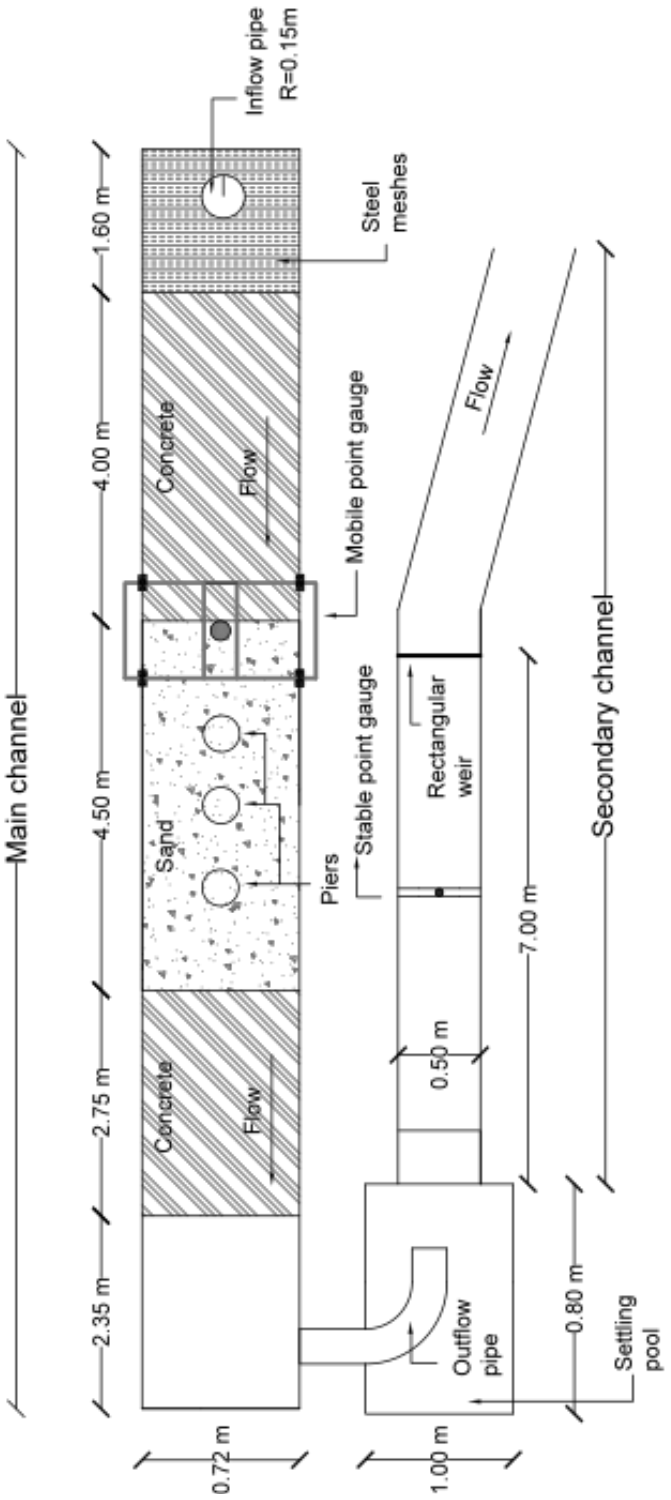

Figure 5.1a: Plan view of the test channel

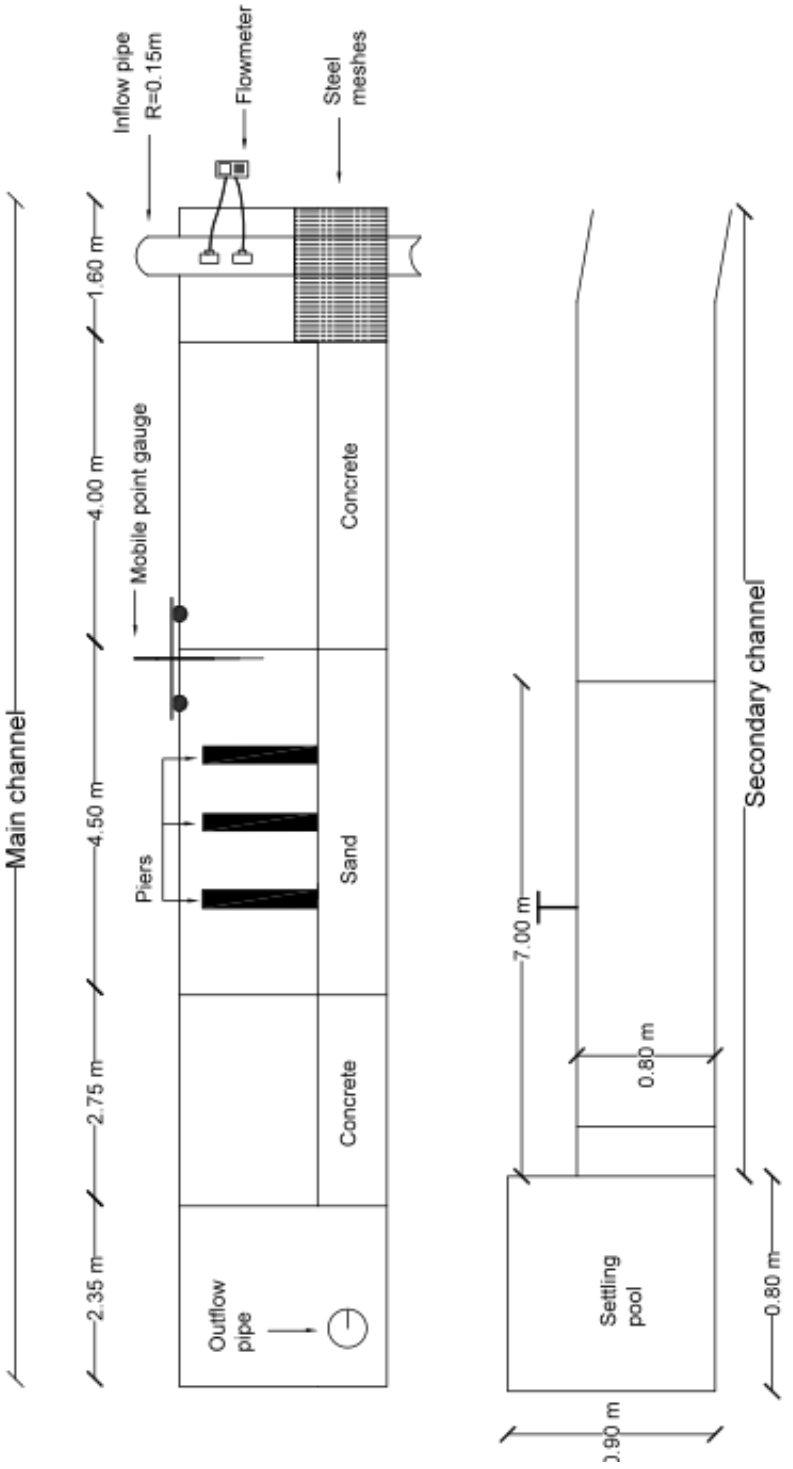

Figure 5.1b: Side view of the side channel (upper) and secondary channel (lower)

5.2.1.1 Inflow Pipe

Water is supplied to the channel through 0.15 m diameter pipe by a centrifugal pump from the sump located underneath of the lab floor. A valve with the same diameter as the pipe controls the flow rate. Flowmeter is installed on the inflow pipe and flow rate is measured by this device. The pipe is installed so that the pipe opening is very close to the bed level, in order not disturbing the bed material. Steel meshes of 1.6 m height is mounted at the beginning of the main channel to avoid the turbulence of water exiting from the inflow pipe. Inflow pipe, steel meshes and valve are shown in Appendix B.

5.2.1.2 Main Channel

All of the experiments were conducted at 14.00 m long, 0.72 m wide and 1.00 m deep channel. Steel meshes are located at the upstream of the test section to reduce turbulence created by the inflow. Considering the height of steel meshes, the total length of the main channel is 15.6 m. The backside of the channel is made of sheet iron, front side is of glass and the bottom is made of varnished concrete. As it is seen from Figure 5.1a and Figure 5.1b, the main channel is not filled only with sand. To ease the further works i.e. flattening the bed level, changing the pier model and adjusting the slope; only middle part of the test channel is filled with sand to the level of the channel bed. It is at this section that all scour experiments are performed. The initial and final parts are bricked up and covered with concrete mix. The pier model is placed in such a way that the midpoint of the pier group coincides with the middle of the sand section and where the approach flow is uniform. Small stones are placed at the upstream area of sand section to create a gradual transition surface between sand and concrete surfaces. Bed level and water surface height measurements are made with the help of mobile point gauge, which is placed on a wheeled tray. As the point gauge can be moved in 2 directions, measurements can be taken at different locations.

5.2.1.3 Outflow Pipe

The flow passing through the main channel is diverted to a settling pool through the outflow pipe, which has an inner diameter of 0.15 m. Outflow pipe is placed at the end of the main channel and a fully open valve is located on the pipe to maintain uniform flow.

5.2.1.4 Settling Pool

The aim of placing settling pool before secondary channel is to attain uniform flow. Without placing the settling pool, it is very hard to obtain uniform flow conditions in a very short distance. Water spilling from the outflow pipe, rests at settling pool and pass through hollow bricks and meshes to the secondary channel. It has the dimensions of 1.00 x 0.8 m and a depth of 0.90 m.

5.2.1.5 Secondary Channel

The secondary channel has been made of reinforced concrete, which has dimensions of 7.00 x 1.00 m and with a wall height of 0.90 m. The major function of the secondary channel is to calculate the discharge by means of a sharp crested weir located downstream of this channel. Discharge given to the main channel is actually the same discharge flowing over the sharp-crested weir in the secondary channel. The Rehbock Equation was used to obtain the discharge for each experiment also. The required water surface measurements for the equation were made by a stable point gauge located 3.0 m downstream of the settling pool in the secondary channel. Water is spilled to the laboratory sump after passing the secondary channel.

5.2.2 Materials Used

5.2.2.1 Bed Material

A uniform bed material that was available in the laboratory was sieved again and poured into the test section. The thickness of the bed material is 30 cm and the slope of the bed is adjusted in parallel with concrete surface as S_0=0.001. The properties of the sand and particle size distribution are given in Table 5.1 and Figure 5.2 respectively.

Table 5.1: Bed material properties

d_{10}	0.63mm	σ_g	1.284
$d_{15.9}$	0.68mm	C_u	1.460
d_{50}	0.88mm	$K\sigma$	0.947
d_{60}	0.92mm	γ_s	26.2 kN/m^3
$d_{84.1}$	1.13	d_m	0.950

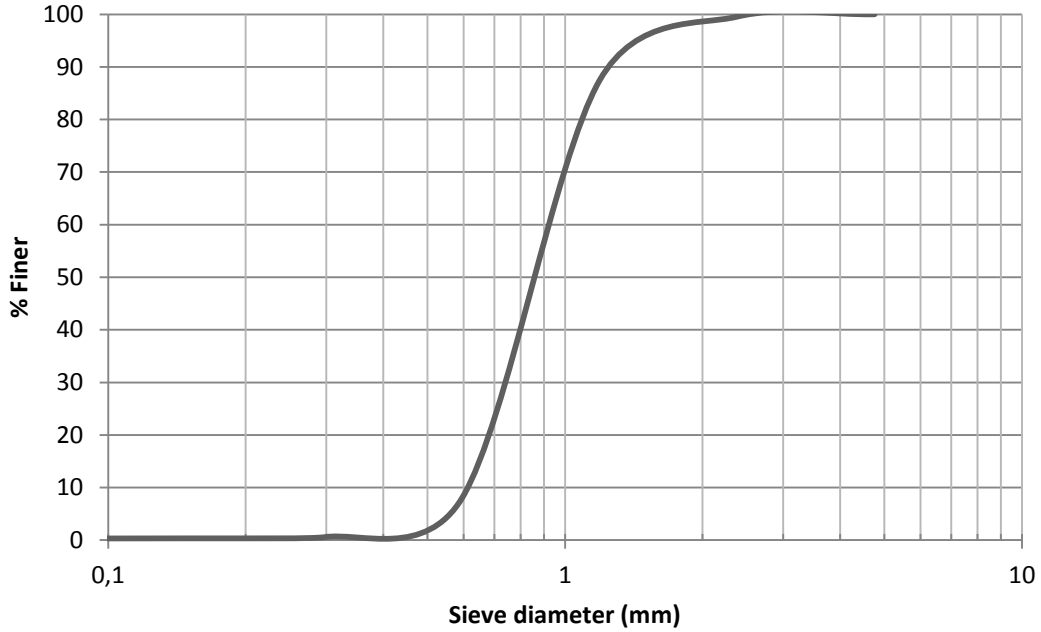

Figure 5.2: Particle size distribution of the bed material

As it is seen from Table 5.1, the geometric standard deviation is smaller than 1.3 and sediment distribution is defined as uniform for this value. Yanmaz (2002) states that when $\sigma_g < 1.3$ the bed material is considered to be uniform. Otherwise i.e. $\sigma_g > 1.3$, the sediment is said to be non-uniform. Geometric standard deviation shows the sediment gradation and it is calculated from the particle size distribution graph:

$$\sigma_g = \left(\frac{d_{84.1}}{d_{15.9}}\right)^{0.5} = \frac{d_{84.1}}{d_{50}} \qquad (5.1)$$

5.2.2.2 Piers

Cylindrical piers with diameter sizes of 50 and 70 mm are used in all of the experiments (Figure B.1 and B.2). The pier geometry and the pier sizes are chosen so that comparison can be made easily as other data is available. The cylinders are made of PVC and attached to the wooden plate with nails. The inclination angle is adjusted by electronic level and fixed by connectors.

In this study 2 configurations are tested: 1) 3 pier configurations and 2) 4 pier configurations (Figure 5.3 and 5.4). With various inclination angles and pier sizes, totally 12 bridge pier models are manufactured.

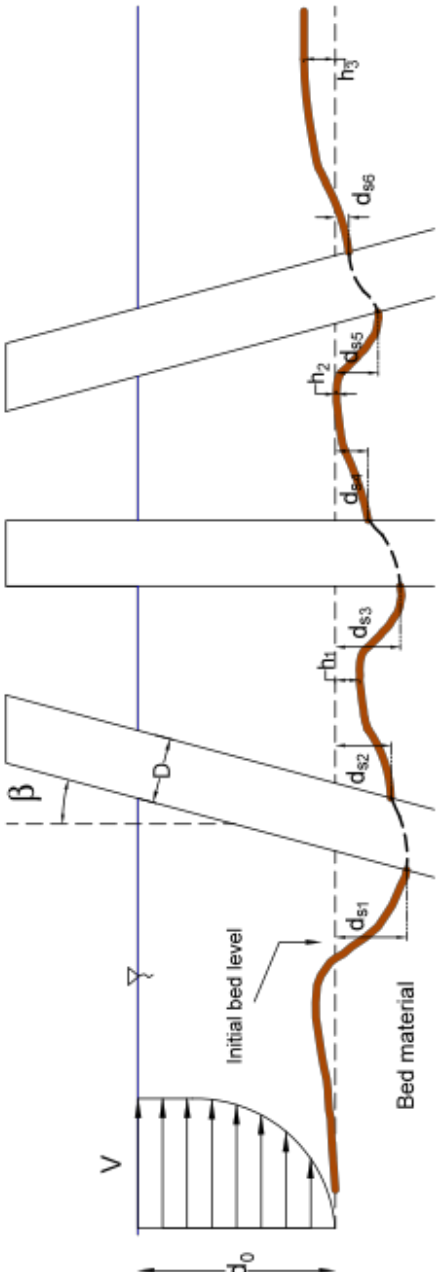

Figure 5.3: Illustration of the scour measurements around 3 piers (Present study)

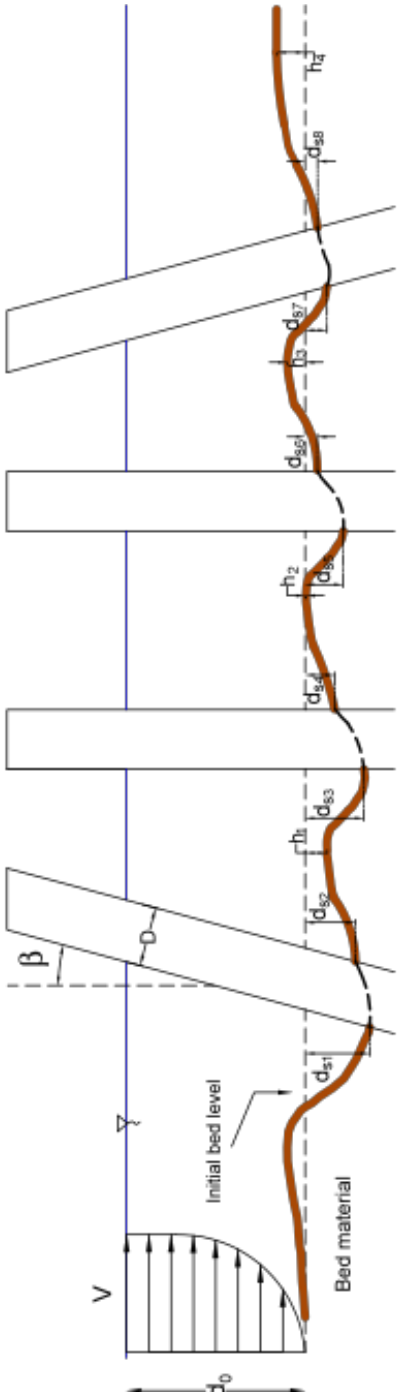

Figure 5.4: Illustration of the scour measurements around 4 piers (Present study)

5.3 Experimental Procedure

5.3.1 Preliminary Studies

The selected bridge pier model is placed in the channel by digging enough area in the channel bed and fixed with clamping system at the foundation. After filling the empty space by sand, the channel bed is carefully leveled using trowel and checked with mobile point gauge before starting each experiment to prevent the influence of surface irregularities on scour around bridge piers. The test channel is gently filled with water and the flow conditions are observed for a while. Next, the discharge is increased gradually and flow depth – discharge relationship is derived. A range of variables are determined according to the capacity of test channel, limits of flow conditions and scour behavior. Preliminary experiments have shown that, 6 hours is enough to reach the equilibrium scour depth because after 6 hours the increase in scour depth was found to be negligible. During each experiment, the volumetric flow rate was continuously monitored using the flowmeter that is installed on the inflow pipe and double-checked by measuring the head on the sharp crested weir located in the secondary channel. At the end of the tests, the valve was closed and the channel was allowed to drain. In experimental studies, errors can be made typically. So, all experiments were conducted using the same measurement equipment and selected experiments were repeated to confirm the reliability of the results.

5.3.2 Determination of Variables

In this study, the effect of inclination angle on local scour around bridge pier groups is examined mainly. Three different inclination angles are selected as 0°, 10°, and 15°. Over 15° were not preferred because of the structural difficulty in the field. In addition to that, Bozkus and Yildiz (2004) have studied the effect of an inclination angle on single bridge piers and did not observe remarkable change in the equilibrium scour depth between the range $0° < \beta < 10°$.

Time to reach the equilibrium depth is determined as 6 hours and initial measurements were taken at t_1=15 min and t_2=30 min. After that, every 30 minutes depth of scour hole around cylindrical piers and aggradations between them are measured until t_e=360 min. Table 5.2 defines the measurement points:

Table 5.2: Definition of the measured scour depths

d_0	Depth of flow
d_{s1}	Scour depth just at the upstream face of the 1st pier
d_{s2}	Scour depth just at the downstream face of the 1st pier
d_{s3}	Scour depth just at the upstream face of the 2nd pier
d_{s4}	Scour depth just at the downstream face of the 2nd pier
d_{s5}	Scour depth just at the upstream face of the 3rd pier
d_{s6}	Scour depth just at the downstream face of the 3rd pier
d_{s7}	Scour depth just at the upstream face of the 4th pier
d_{s8}	Scour depth just at the downstream face of the 4th pier
h_1	Aggradation height between 1st and 2nd piers.
h_2	Aggradation height between 2nd and 3rd piers.
h_3	Aggradation height between 3rd and 4th piers / at the downstream of 3rd pier
h_4	Aggradation height at the downstream of 4th pier

During the preliminary experiments discharge is adjusted by a valve placed on the inflow pipe and monitored from a flowmeter. In addition to that, discharge can be calculated from Rehbock equation (Eq. 5.2).

$$Q = \frac{2}{3} B \sqrt{2g} C_d H^{3/2} \tag{5.2}$$

$$C_d = 0.611 + 0.08 \frac{H}{W} \tag{5.3}$$

where Q= Discharge (m^3/s)

B= Width of the sharp crested weir (m)

C_d= Discharge coefficient

H= Head on the sharp-crested weir

W= Height of the sharp crested weir (m)

It is observed that the discharge values, which are read from the flowmeter are almost equal to the calculated ones from the Rehbock equation.

Depths of flow are measured at the main channel for various discharge values and mean approach velocity is calculated simply from the continuity equation below (Eq. 5.4).

$$V_{av} = Q / A \tag{5.4}$$

$$A = d_0 * w \tag{5.5}$$

where A= Net flow area (m^2)

d_0= Depth of flow (m)

w= Width of main channel (m)

The shear velocity and shear stress are found by the following equations:

$$V_* = \sqrt{gRS_0} \tag{5.6}$$

$$\tau = \gamma RS_0 \quad or \quad \tau = \rho V_*^2 \tag{5.7}$$

where R= Hydraulic radius of the channel cross-section

S_0= Slope of the channel cross-section

γ= Specific weight of water

ρ= Density of water

The critical shear stress, τ_c, can be found by the Shield's diagram and critical shear velocity is calculated either by Eq. (5.8) or statement given by Melville and Coleman (2000) (Eq. 5.9).

$$V_{*c} = \sqrt{\frac{\tau_c}{\rho}} \tag{5.8}$$

$$V_{*c} = 0.0115 + 0.0125 d_{50}^{1.4} \tag{5.9}$$

Finally, the mean critical velocity is found by below equation:

$$\frac{V_c}{V_{*c}} = 5.75 \log 5.53 \frac{d_0}{d_{50}} \tag{5.10}$$

Table 5.3 shows the critical velocity values against measured discharge and flow depth values, for the purpose verifying the flow conditions.

Table 5.3: Verification of clear-water conditions

Q (l/s)	d_0 (mm)	V (m/s)	V_c (m/s)	V/V_c	Clear-Water
4.698	37	0.176	*0.299*	0.589	<1.0 ✓
7.239	47	0.214	*0.312*	0.686	<1.0 ✓
10.125	54	0.260	*0.319*	0.814	<1.0 ✓
13.320	64	0.289	*0.329*	0.879	<1.0 ✓
15.025	69	0.302	*0.333*	0.907	<1.0 ✓
16.198	74	0.315	*0.337*	0.936	<1.0 ✓

5.4 Scope of the Experiments

The experiments are conducted under uniform, steady flow and clear-water scour conditions. Cylindrical piers made of PVC, which have diameter sizes of 50 mm and 70 mm are used. The distances between piers are fixed (a=4D). Bed material with the characteristics of σ_g=1.29, d_{50}=0.88mm and γ_s=26.2 kN/m^3 has been used during the experiments (Table 5.1). The bed slope S_0=0.001 remains constant and the bed level is smoothened before each run. Depth of scour measurements have been taken from just upstream and downstream sides of the pier and bed level between piers are measured (Table 5.2). Moreover, temporal development of scour is observed and measurements have been made every 30 minutes. Two configurations are tested: 1) *3 pier configuration (C1)* and 2) *4 pier configuration (C2)* for various flow depths, inclination angles and pier sizes. Totally 72 experiments were conducted with 12 pier group model. Table 5.4 shows the values of variables for each experiment:

Table 5.4: The values of parameters for each experiment

Exp.	Conf.	β°	D (mm)	Q (l/s)	d_0 (mm)	d_o/D	V (m/s)	V_c (m/s)	V/V_c
#1	C1	0	50	4.698	37	0.740	0.176	0.299	0.589
#2	C1	0	50	7.239	47	0.940	0.214	0.312	0.686
#3	C1	0	50	10.125	54	1.080	0.260	0.319	0.814
#4	C1	0	50	13.320	64	1.280	0.289	0.329	0.879
#5	C1	0	50	15.025	69	1.380	0.302	0.333	0.907
#6	C1	0	50	16.198	74	1.480	0.315	0.337	0.936
#7	C1	10	50	4.698	37	0.740	0.176	0.299	0.589
#8	C1	10	50	7.239	47	0.940	0.214	0.312	0.686
#9	C1	10	50	10.125	54	1.080	0.260	0.319	0.814
#10	C1	10	50	13.320	64	1.280	0.289	0.329	0.879
#11	C1	10	50	15.025	69	1.380	0.302	0.333	0.907
#12	C1	10	50	16.198	74	1.480	0.315	0.337	0.936
#13	C1	15	50	4.698	37	0.740	0.176	0.299	0.589
#14	C1	15	50	7.239	47	0.940	0.214	0.312	0.686
#15	C1	15	50	10.125	54	1.080	0.260	0.319	0.814
#16	C1	15	50	13.320	64	1.280	0.289	0.329	0.879
#17	C1	15	50	15.025	69	1.380	0.302	0.333	0.907
#18	C1	15	50	16.198	74	1.480	0.315	0.337	0.936
#19	C1	0	70	4.698	37	0.529	0.176	0.299	0.589
#20	C1	0	70	7.239	47	0.671	0.214	0.312	0.686
#21	C1	0	70	10.125	54	0.771	0.260	0.319	0.814
#22	C1	0	70	13.320	64	0.914	0.289	0.329	0.879
#23	C1	0	70	15.025	69	0.986	0.302	0.333	0.907
#24	C1	0	70	16.198	74	1.057	0.315	0.337	0.936
#25	C1	10	70	4.698	37	0.529	0.176	0.299	0.589
#26	C1	10	70	7.239	47	0.671	0.214	0.312	0.686
#27	C1	10	70	10.125	54	0.771	0.260	0.319	0.814
#28	C1	10	70	13.320	64	0.914	0.289	0.329	0.879
#29	C1	10	70	15.025	69	0.986	0.302	0.333	0.907
#30	C1	10	70	16.198	74	1.057	0.315	0.337	0.936
#31	C1	15	70	4.698	37	0.529	0.176	0.299	0.589
#32	C1	15	70	7.239	47	0.671	0.214	0.312	0.686
#33	C1	15	70	10.125	54	0.771	0.260	0.319	0.814
#34	C1	15	70	13.320	64	0.914	0.289	0.329	0.879
#35	C1	15	70	15.025	69	0.986	0.302	0.333	0.907
#36	C1	15	70	16.198	74	1.057	0.315	0.337	0.936

Table 5.4 (cont.): The values of parameters for each experiment

Exp.	Conf.	β°	D (mm)	Q (l/s)	d_0 (mm)	d_0/D	V (m/s)	V_c (m/s)	V/V_c
#37	C2	0	50	4.698	37	0.740	0.176	0.299	0.589
#38	C2	0	50	7.239	47	0.940	0.214	0.312	0.686
#39	C2	0	50	10.125	54	1.080	0.260	0.319	0.814
#40	C2	0	50	13.320	64	1.280	0.289	0.329	0.879
#41	C2	0	50	15.025	69	1.380	0.302	0.333	0.907
#42	C2	0	50	16.198	74	1.480	0.315	0.337	0.936
#43	C2	10	50	4.698	37	0.740	0.176	0.299	0.589
#44	C2	10	50	7.239	47	0.940	0.214	0.312	0.686
#45	C2	10	50	10.125	54	1.080	0.260	0.319	0.814
#46	C2	10	50	13.320	64	1.280	0.289	0.329	0.879
#47	C2	10	50	15.025	69	1.380	0.302	0.333	0.907
#48	C2	10	50	16.198	74	1.480	0.315	0.337	0.936
#49	C2	15	50	4.698	37	0.740	0.176	0.299	0.589
#50	C2	15	50	7.239	47	0.940	0.214	0.312	0.686
#51	C2	15	50	10.125	54	1.080	0.260	0.319	0.814
#52	C2	15	50	13.320	64	1.280	0.289	0.329	0.879
#53	C2	15	50	15.025	69	1.380	0.302	0.333	0.907
#54	C2	15	50	16.198	74	1.480	0.315	0.337	0.936
#55	C2	0	70	4.698	37	0.529	0.176	0.299	0.589
#56	C2	0	70	7.239	47	0.671	0.214	0.312	0.686
#57	C2	0	70	10.125	54	0.771	0.260	0.319	0.814
#58	C2	0	70	13.320	64	0.914	0.289	0.329	0.879
#59	C2	0	70	15.025	69	0.986	0.302	0.333	0.907
#60	C2	0	70	16.198	74	1.057	0.315	0.337	0.936
#61	C2	10	70	4.698	37	0.529	0.176	0.299	0.589
#62	C2	10	70	7.239	47	0.671	0.214	0.312	0.686
#63	C2	10	70	10.125	54	0.771	0.260	0.319	0.814
#64	C2	10	70	13.320	64	0.914	0.289	0.329	0.879
#65	C2	10	70	15.025	69	0.986	0.302	0.333	0.907
#66	C2	10	70	16.198	74	1.057	0.315	0.337	0.936
#67	C2	15	70	4.698	37	0.529	0.176	0.299	0.589
#68	C2	15	70	7.239	47	0.671	0.214	0.312	0.686
#69	C2	15	70	10.125	54	0.771	0.260	0.319	0.814
#70	C2	15	70	13.320	64	0.914	0.289	0.329	0.879
#71	C2	15	70	15.025	69	0.986	0.302	0.333	0.907
#72	C2	15	70	16.198	74	1.057	0.315	0.337	0.936

5.5 Analysis of Results

In this section, experimental results are presented with related figures and tables according to the variable factors affecting the development of local scour.

5.5.1 Local Scour Process

Figure C.3 and C.4 illustrate the typical scour hole and sediment deposit resulting from a bridge scour experiment for 4 pier and 3 pier configurations respectively. Sediment deposition height (h), sediment deposition width (w), scour hole depth (d_s), scour hole width (s) and pier diameter are shown in the figures.
Time evolution of scour is observed and the equilibrium scour depth is determined. The equilibrium condition is assumed to be reached when scour depth at all locations do not increase more than 1mm in an hour. This condition was met at 6th hour and flow is stopped. The movement of the bed material starts when the flow intensity reaches to a certain point. Particles at the upstream face of the piers are the first to be removed from the bed by a small vortex structure and at the just downstream of the piers small deposits are formed. It is observed that scour formation is very rapid in the first five minutes. Large deposits are formed in this period and sediment particles are lifted off the bed and travel downstream with velocities faster than the average velocity for all the other particles. After a few minutes, sediment particles, which are transported downstream around the piers, accumulate between the piers, thus aggradation is observed. When scour hole enlarges with respect to time, horseshoe vortices lose their strength and rate of scouring decreases. As it is predictable, scour holes around each pier are developed asymptotically in time and over 80% of the scour hole formation takes place in 2 hours (i.e. t/t_e=0.3) (Fig. 5.5).

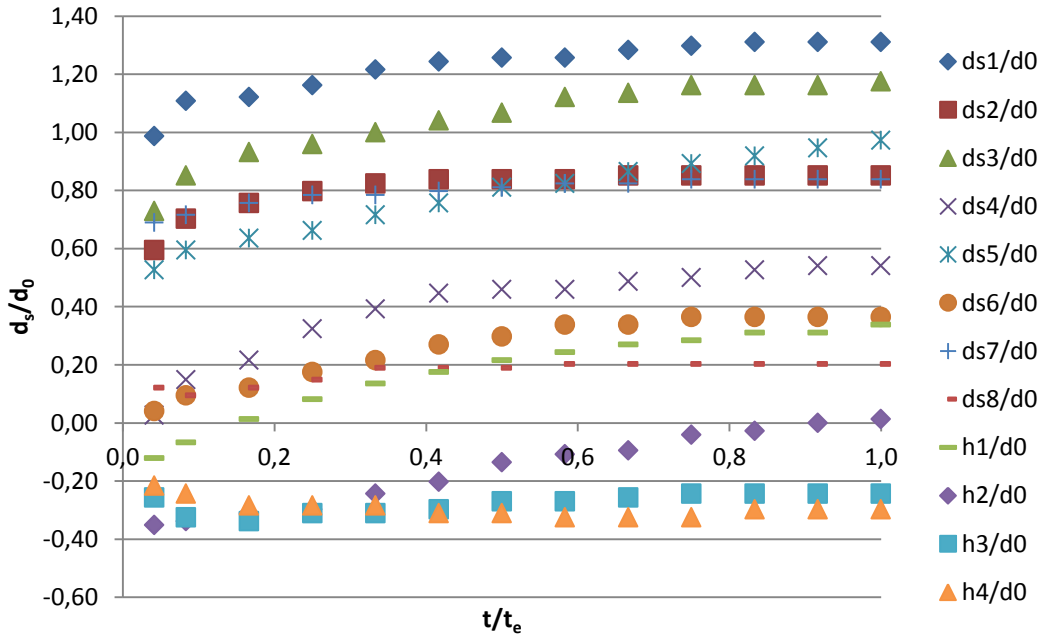

Figure 5.5: Evolution of scour holes in time

Moreover, sediment particles are deposited in a heart formation at the downstream side of the last pier (Figure C.3 and C.4). As time passes, the scour holes grow in x-y and z directions while deposit at the downstream side of the last pier elongates and the deposition between the piers slowly disappears. Magnitude of scour depths, which is generated at the upstream face of piers, reduces along the flow direction i.e. $d_{s1}>d_{s3}>d_{s5}$ for C1 and $d_{s1}>d_{s3}>d_{s5}>d_{s7}$ for C2 as it can be seen from the Figures C.3 and C.4. In the same manner, $d_{s2}>d_{s4}>d_{s6}$ for C1 and $d_{s2}>d_{s4}>d_{s6}>d_{s8}$ for C2, where even numbers represent the downstream sides of the piers. To add more, it can be said that the maximum local scour depth is observed at the midpoint of the upstream face of the piers.

As the pier spacing is fixed as a=4D for all experiments, separate but interfered scour holes are generated. The sediment depositions between piers are seen in very early stages but after a while sediment particles are transported downstream and scour holes that are not deeper than around the piers are formed between the piers (Figure C.3 and C.4). As Yanmaz and Altinbilek (1991) observed in a study that focused on time variation of local scour depth, it was again seen that the shape of the scour holes are in the shape of inverted cone having a circular base.

5.5.2 Effect of Flow Intensity

Six different flow intensities ranging between 0.589 and 0.936 are tested along all configurations. It is definite that, when flow intensity increases the local scour depth increases almost linearly. Figures 5.6 and 5.7 show the variation of equilibrium scour depth with flow intensity.

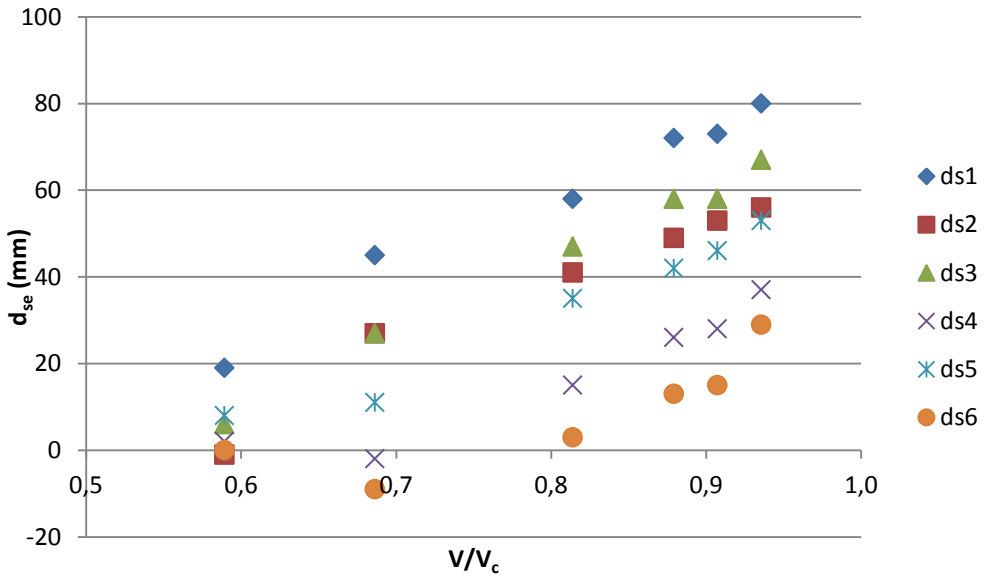

Figure 5.6: Variation of equilibrium scour depths with respect to flow intensity (β=10°, D=50mm, C1)

It is observed that at lower values of flow intensity, scour formation around the rear piers are not clearly noticed. Furthermore, aggradation takes place between the piers and sediment deposition between the upstream piers is greater than the deposition between downstream piers. Nevertheless, at higher intensities, local scour formation is faster, greater and scouring rather than sediment deposition appears between the piers. Changes in inclination angle or pier size do not affect the influence of the flow intensity on scour depth. In Appendix A, variations of relative scour depths with flow intensity for all inclination angles and pier sizes are shown.

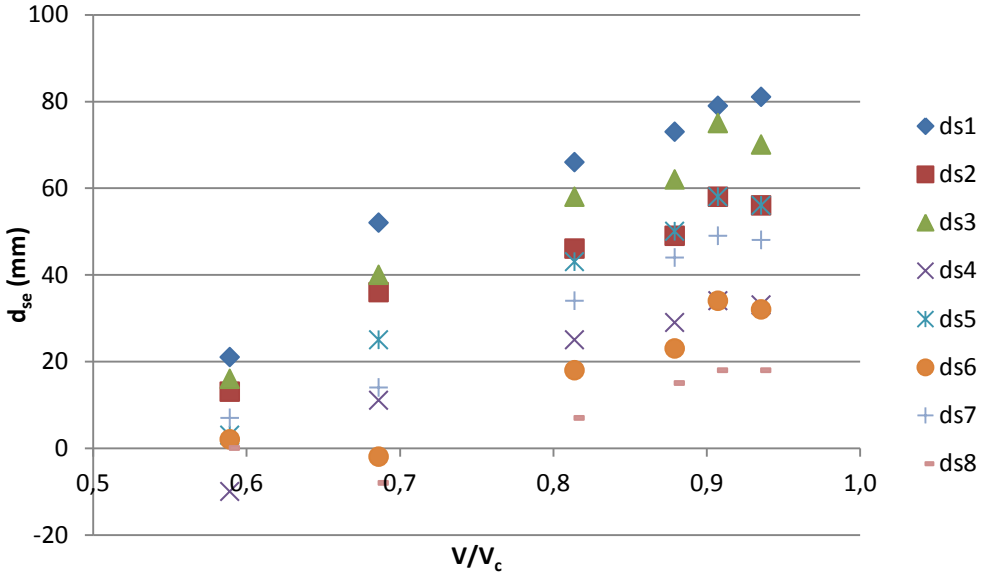

Figure 5.7: Variation of equilibrium scour depths with respect to flow intensity (β=10°, D=50mm, C2)

5.5.3 Effect of Pier Sizes

Equilibrium scour depth and time to reach the equilibrium scour depth increases in case of larger piers. In this study, 2 pier diameters of 50-mm and 70-mm are used along the experiments. Although rear piers are not affected too much, almost 25-30% increase in scour depth is observed around front piers when pier diameter is increased from 50-mm to 70-mm. Deposition, which is formed at the most downstream of the pier group, increases considerably and heart shaped formation is observed clearly when the pier sizes increase. Moreover, radius of the scour holes increases, thus scour hole expands in all directions. Variations of scour depths with respect to pier size are shown in Figures 5.8 and 5.9.

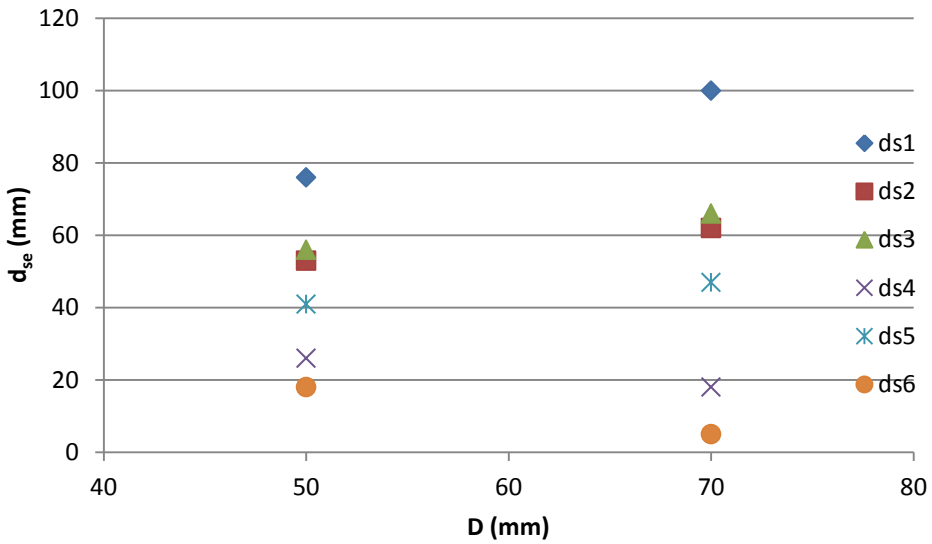

Figure 5.8: Variation of equilibrium scour depths with respect to pier size (β=0°, d_0=64mm, C1)

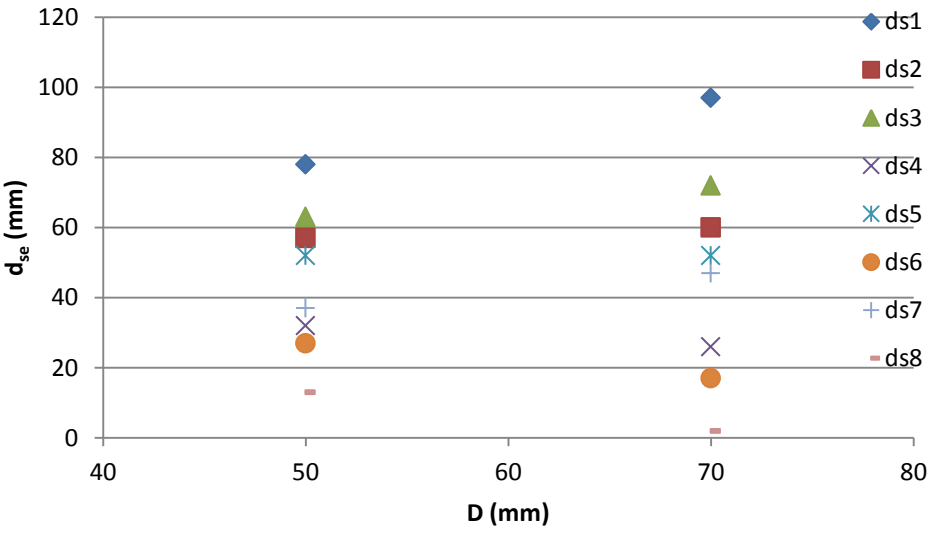

Figure 5.9: Variation of equilibrium scour depths with respect to pier size (β=0°, d_0=64mm, C2)

5.5.4 Effect of Relative Flow Depth

Flow depths that range from 37 mm to 74 mm are tested throughout the study. It can be said that, flow intensity and relative flow depth is directly proportional for a constant pier size and condition of bed material transport (i.e. clear-water scour). All experiments are conducted under clear-water scour conditions, but different pier sizes are used in experiments. Generally, when relative flow depth increases, scour hole size also increases. However, at a constant flow depth, it was observed that deeper scour holes are generated at lower relative flow depths. Effect of pier size outweighs the effect of relative flow depth (Figure 5.10.). When the strength of flow is kept constant while increasing the pier diameter, the scour geometry gradually increases. Variations of relative scour depth with respect to relative flow depth are shown in Figures 5.11 and 5.12.

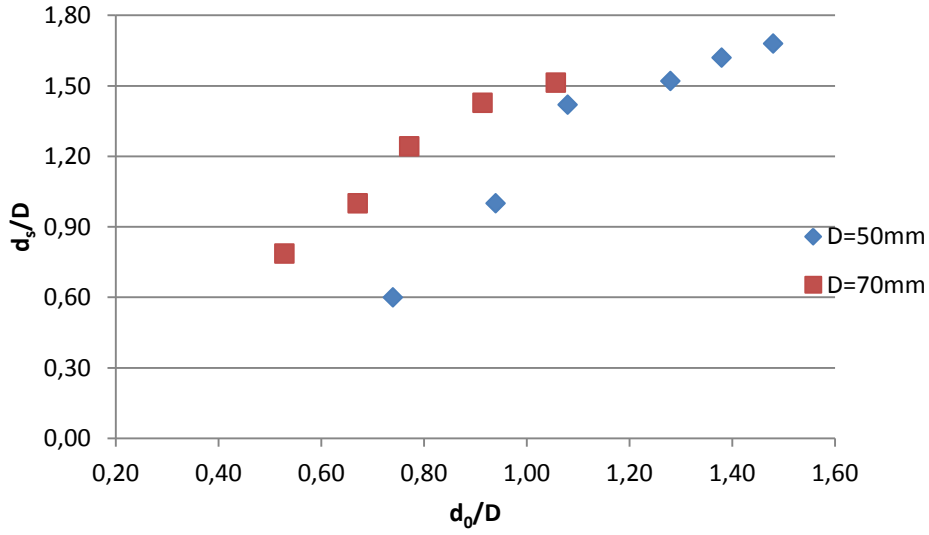

Figure 5.10: Variation of relative scour depth with respect to relative flow depth (β=0°, d_{s1}, C2)

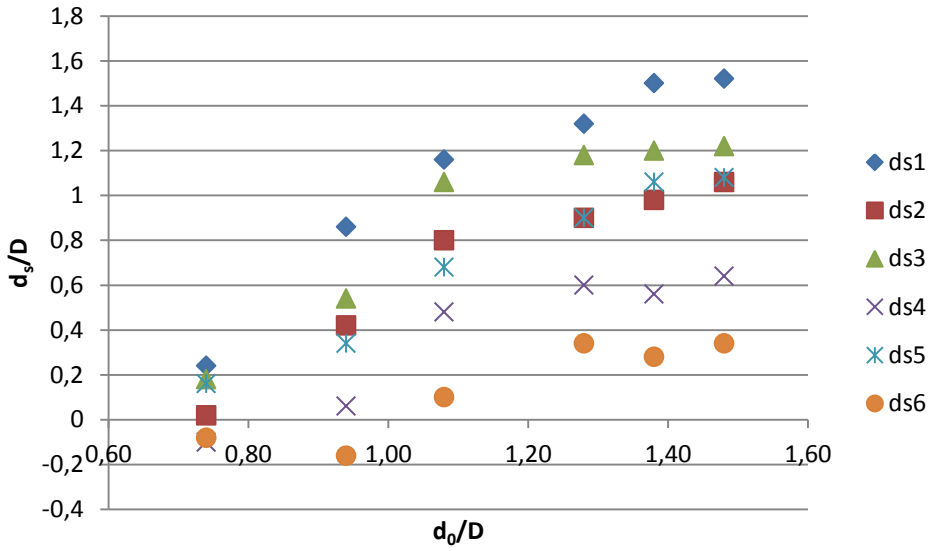

Figure 5.11: Variation of relative scour depth with respect to relative flow depth (β=15°, D=50mm, C1)

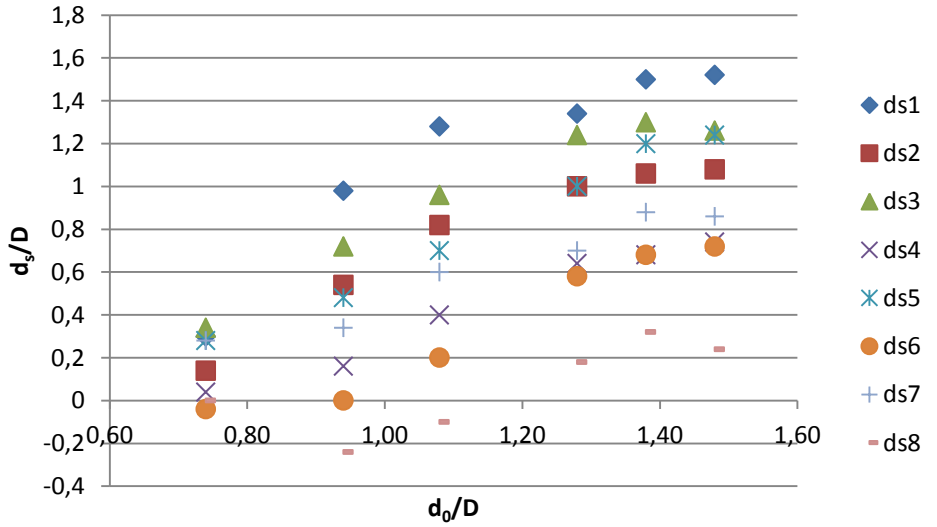

Figure 5.12: Variation of relative scour depth with respect to relative flow depth (β=15°, D=50mm, C2)

5.5.5 Effect of Inclination Angle

This is a follow up study of the previous studies conducted by Bozkus and Yildiz (2004) and Bozkus and Cesme (2010), as the inclination angle is the major parameter in all. However, different configurations are tested and rather than a single pier or dual piers, bridge pier groups that are comprised of 3 and 4 piers are investigated.

The experiments were performed for the angles β=0°, 10° and 15°. It can be said that on the whole, local scour depths decrease significantly as the inclination angle increases. However, this reduction is more apparent at the most upstream pier, which is inclined towards downstream. Reduction of almost 25-30% was measured around front piers when most upstream and most downstream piers are placed at an inclination angle of 15° through downstream and upstream directions respectively when compared to scours developed around vertical piers. The inclination angle of the middle piers was not changed throughout the experiments. Still, reduction in scour depths has been observed with the inclination of the very upstream pier. Approximately, the depth of scour reduction of 10-15% was noticed around the second pier. As the measurements proceed to the 3rd pier in configuration 2, which is placed vertically, the effect of inclination angle decreases and inconsiderable changes are observed when the inclination angle of most upstream pier is increased. The most downstream piers are inclined through upstream, thus an increase in scour depth is expected when inclination angle increases. However, based on the experimental data, no significant change in scour depth is observed.
The strength of the vortices that move sediment particles around piers decreases as the inclination angle increases. Downflow is resolved into its components when approach flow hits to the inclined pier, thus vertical component of the downflow decreases. Smaller scour holes are generated around cylindrical piers and aggradation at the most downstream of the pier group decreases. Following figures show the variation of equilibrium scour depths with respect to inclination angle, β.

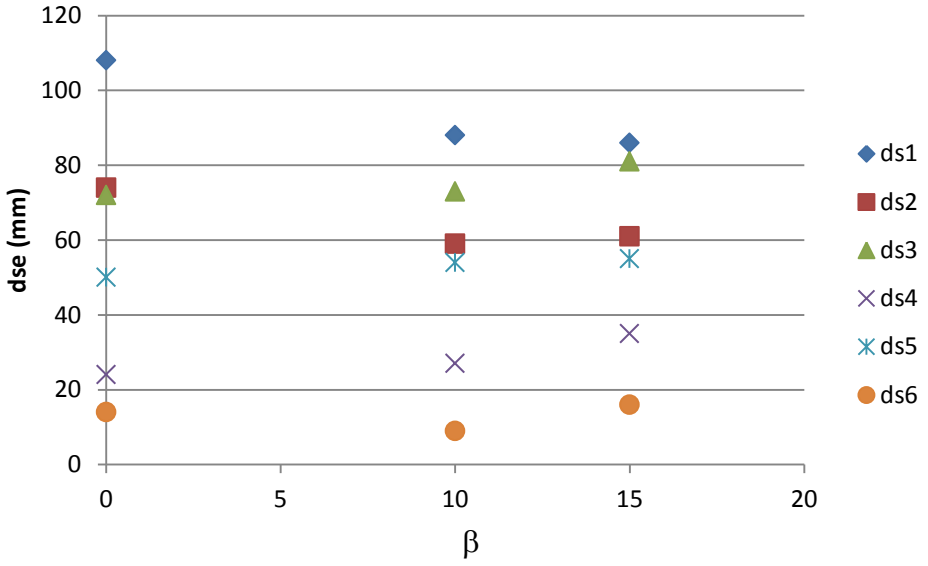

Figure 5.13: Variation of equilibrium scour depth with respect to inclination angle (d_0=69mm, D=70mm, C1)

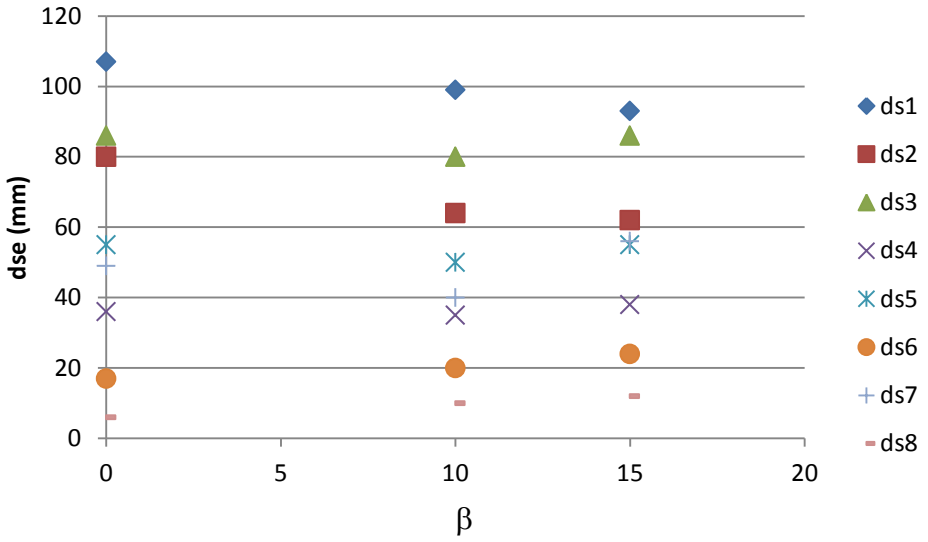

Figure 5.14: Variation of equilibrium scour depth with respect to inclination angle (d_0=69mm, D=70mm, C2)

The experimental data obtained for various inclination angles and configurations are shown in the following tables:

Table 5.5: Experiments conducted with β=0° and C1

Exp. #	Q (l/s)	D (mm)	d_0 (mm)	d_{s1} (mm)	d_{s2} (mm)	d_{s3} (mm)	d_{s4} (mm)	d_{s5} (mm)	d_{s6} (mm)
1	4.698	50	37	30	6	5	-6	6	0
2	7.239	50	47	50	25	30	1	19	-2
3	10.125	50	54	71	43	41	16	26	-3
4	13.320	50	64	76	53	56	26	41	18
5	15.025	50	69	81	60	60	34	52	27
6	16.798	50	74	84	61	67	32	56	28
19	4.698	70	37	55	13	8	4	18	-4
20	7.239	70	47	70	30	38	2	35	-2
21	10.125	70	54	87	60	62	20	43	4
22	13.320	70	64	100	62	66	18	47	5
23	15.025	70	69	108	74	72	24	50	14
24	16.798	70	74	106	76	68	31	60	14

Table 5.6: Experiments conducted with β=10° and C1

Exp. #	Q (l/s)	D (mm)	d_0 (mm)	d_{s1} (mm)	d_{s2} (mm)	d_{s3} (mm)	d_{s4} (mm)	d_{s5} (mm)	d_{s6} (mm)
7	4.698	50	37	19	-1	6	2	8	0
8	7.239	50	47	45	27	27	-2	11	-9
9	10.125	50	54	58	41	47	15	35	3
10	13.320	50	64	72	49	58	26	42	13
11	15.025	50	69	73	53	58	28	46	15
12	16.798	50	74	80	56	67	37	53	29
25	4.698	70	37	50	-4	14	4	30	5
26	7.239	70	47	66	32	41	-5	32	-6
27	10.125	70	54	77	42	52	8	40	-6
28	13.320	70	64	87	61	67	26	49	7
29	15.025	70	69	88	59	73	27	54	9
30	16.798	70	74	99	60	69	32	61	20

Table 5.7: Experiments conducted with β=15° and C1

Exp. #	Q (l/s)	D (mm)	d_0 (mm)	d_{s1} (mm)	d_{s2} (mm)	d_{s3} (mm)	d_{s4} (mm)	d_{s5} (mm)	d_{s6} (mm)
13	4.698	50	37	12	1	9	-5	8	-4
14	7.239	50	47	43	21	27	3	17	-8
15	10.125	50	54	58	40	53	24	34	5
16	13.320	50	64	66	45	59	30	45	17
17	15.025	50	69	75	49	60	28	53	14
18	16.798	50	74	76	53	61	32	54	17
31	4.698	70	37	43	4	42	7	22	-10
32	7.239	70	47	63	30	61	15	33	-15
33	10.125	70	54	73	39	60	17	34	2
34	13.320	70	64	85	55	64	30	47	15
35	15.025	70	69	86	61	81	35	55	16
36	16.798	70	74	92	64	80	34	62	18

Table 5.8: Experiments conducted with β=0° and C2

Exp. #	Q (l/s)	D (mm)	d_0 (mm)	d_{s1} (mm)	d_{s2} (mm)	d_{s3} (mm)	d_{s4} (mm)	d_{s5} (mm)	d_{s6} (mm)	d_{s7} (mm)	d_{s8} (mm)
37	4.698	50	37	26	12	12	0	7	0	9	-2
38	7.239	50	47	60	39	42	18	23	-4	16	-9
39	10.125	50	54	76	49	53	23	40	12	29	-7
40	13.320	50	64	78	57	63	32	52	27	37	13
41	15.025	50	69	85	69	67	37	62	35	45	17
42	16.798	50	74	90	66	70	38	57	36	42	15
55	4.698	70	37	60	30	21	-5	25	-5	26	5
56	7.239	70	47	81	45	45	2	29	-15	30	-4
57	10.125	70	54	93	59	69	23	38	-2	22	-13
58	13.320	70	64	97	60	72	26	52	17	47	2
59	15.025	70	69	107	80	86	36	55	17	49	6
60	16.798	70	74	109	75	80	37	57	17	53	13

Table 5.9: Experiments conducted with β=10° and C2

Exp. #	Q (l/s)	D (mm)	d_0 (mm)	d_{s1} (mm)	d_{s2} (mm)	d_{s3} (mm)	d_{s4} (mm)	d_{s5} (mm)	d_{s6} (mm)	d_{s7} (mm)	d_{s8} (mm)
43	4.698	50	37	21	13	16	-10	3	2	7	0
44	7.239	50	47	52	36	40	11	25	-2	14	-8
45	10.125	50	54	66	46	58	25	43	18	34	7
46	13.320	50	64	73	49	62	29	50	23	44	15
47	15.025	50	69	79	58	75	34	58	34	49	18
48	16.798	50	74	81	56	70	33	56	32	48	18
61	4.698	70	37	57	26	25	-14	27	-13	29	4
62	7.239	70	47	74	42	50	7	33	-15	26	-5
63	10.125	70	54	88	56	74	20	49	4	30	-4
64	13.320	70	64	93	61	73	26	52	16	42	1
65	15.025	70	69	99	64	80	35	50	20	40	10
66	16.798	70	74	104	68	82	36	67	27	59	19

Table 5.10: Experiments conducted with β=15° and C2

Exp. #	Q (l/s)	D (mm)	d_0 (mm)	d_{s1} (mm)	d_{s2} (mm)	d_{s3} (mm)	d_{s4} (mm)	d_{s5} (mm)	d_{s6} (mm)	d_{s7} (mm)	d_{s8} (mm)
49	4.698	50	37	15	7	17	2	14	-2	14	0
50	7.239	50	47	49	27	36	8	24	0	17	-12
51	10.125	50	54	64	41	48	20	35	10	30	-5
52	13.320	50	64	67	50	62	32	50	29	35	9
53	15.025	50	69	75	53	65	34	60	34	44	16
54	16.798	50	74	76	54	63	37	62	36	43	12
67	4.698	70	37	52	26	51	5	23	-14	8	-5
68	7.239	70	47	70	36	59	18	35	-16	24	-5
69	10.125	70	54	81	50	72	22	41	0	30	8
70	13.320	70	64	88	57	77	30	54	20	48	1
71	15.025	70	69	93	62	86	38	55	24	56	12
72	16.798	70	74	97	63	87	40	72	27	62	15

The following graphs display the interaction of parameters with each other on local scour depth at the upstream face of the most upstream pier (d_{s1}). Analyzing these graphs, one can easily conclude that when flow intensity or relative flow depth increases, depth of scour increases for all inclination angles. At the same time, when inclination increases, depth of scour decreases for all flow depths that are tested.

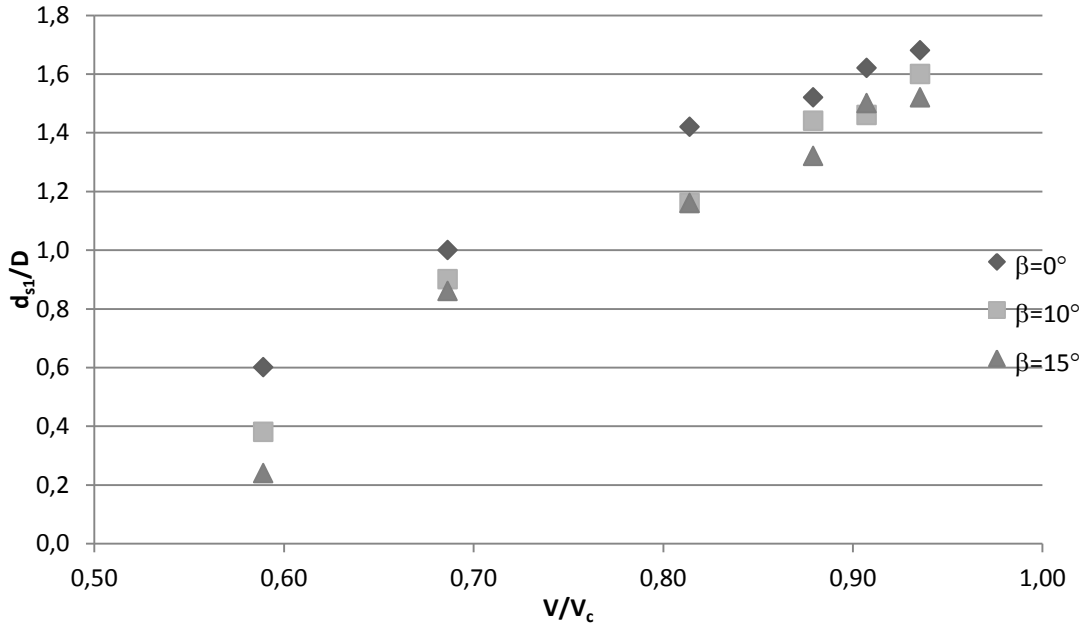

Figure 5.15: Variation of relative scour depth with flow intensity for all inclination angles (D=50 mm, C1)

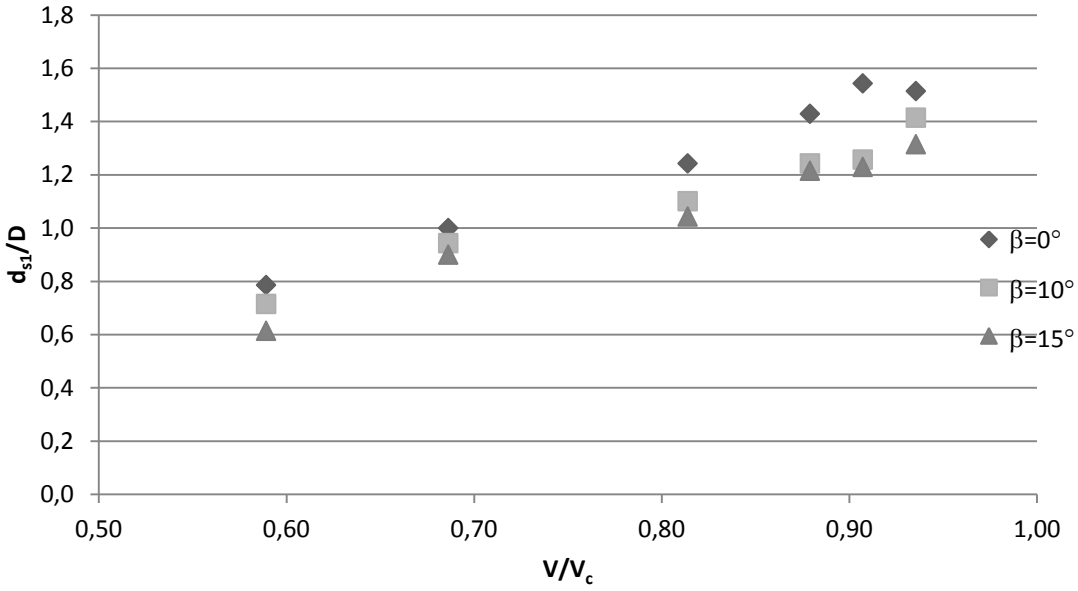

Figure 5.16: Variation of relative scour depth with flow intensity for all inclination angles (D=70mm, C1)

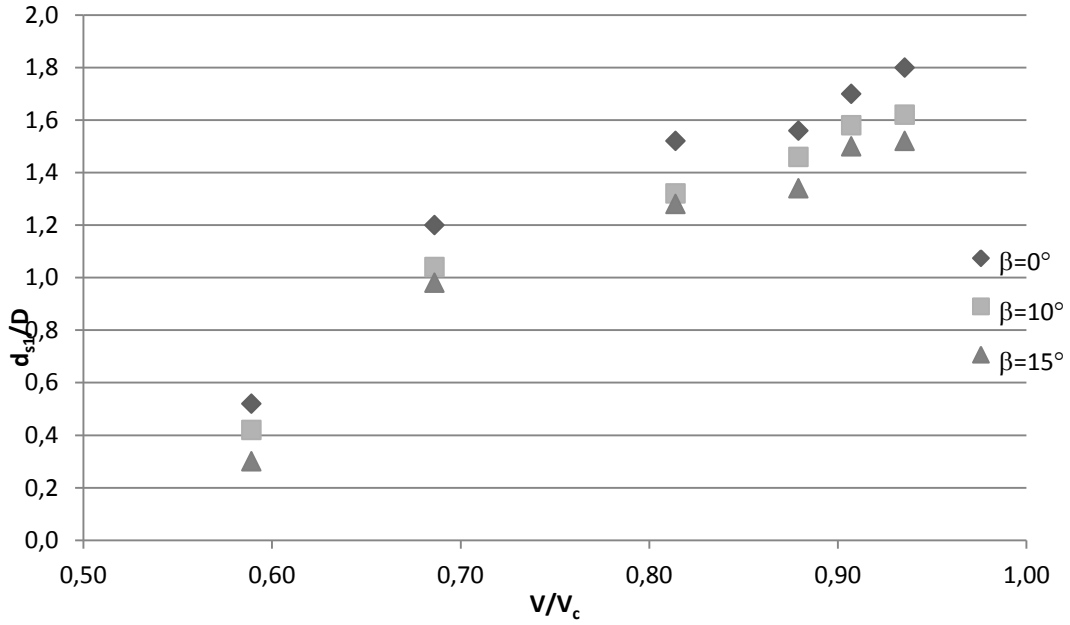

Figure 5.17: Variation of relative scour depth with flow intensity for all inclination angles (D=50mm, C2)

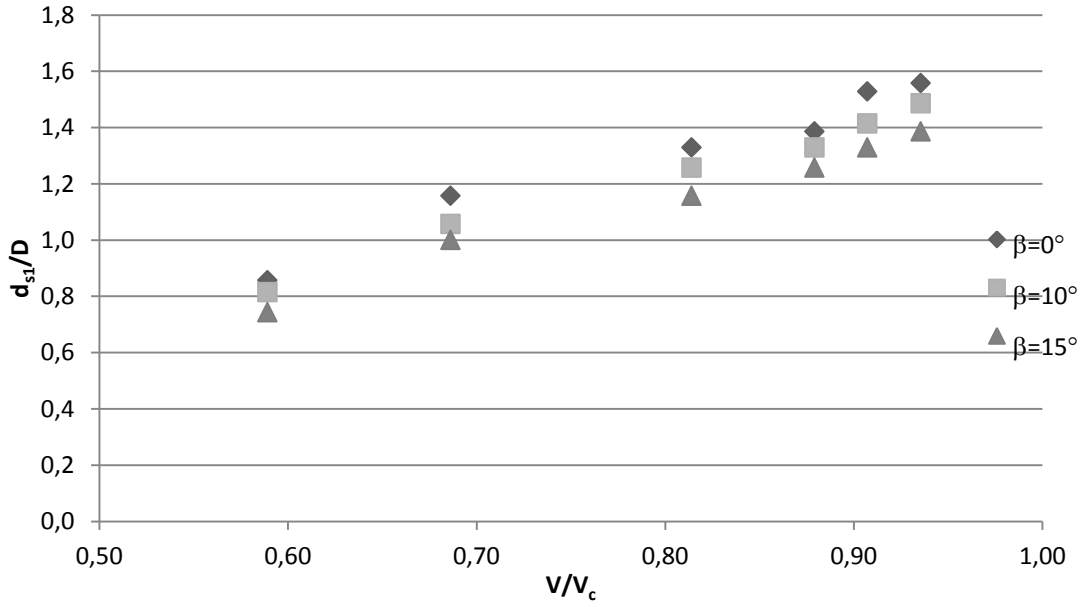

Figure 5.18: Variation of relative scour depth with flow intensity for all inclination angles (D=70mm, C2)

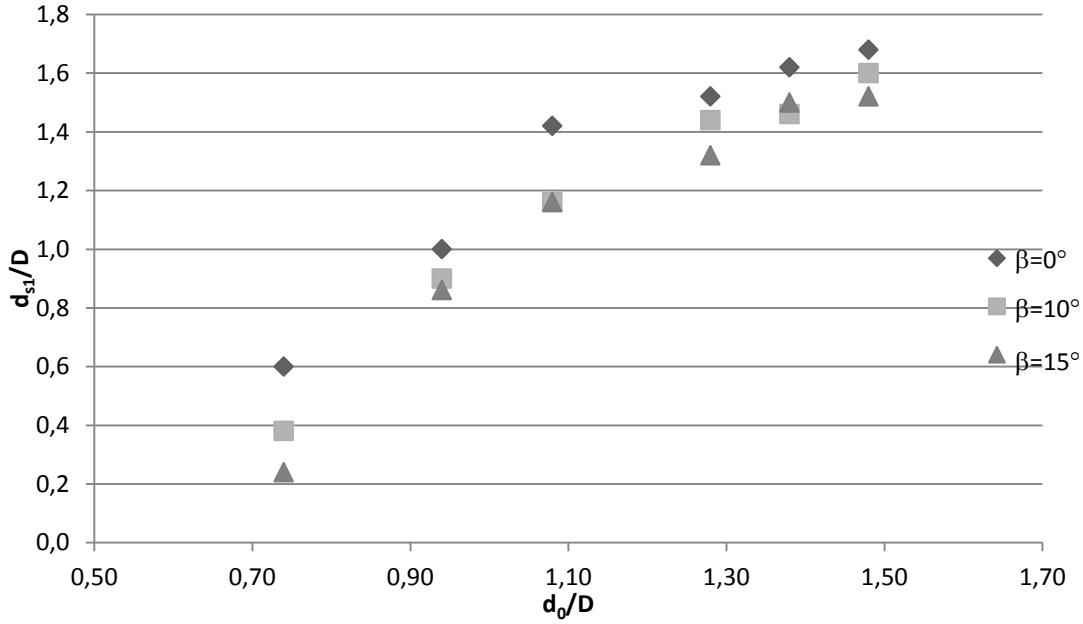

Figure 5.19: Variation of relative scour depth with relative flow depth for all inclination angles (D=50mm, C1)

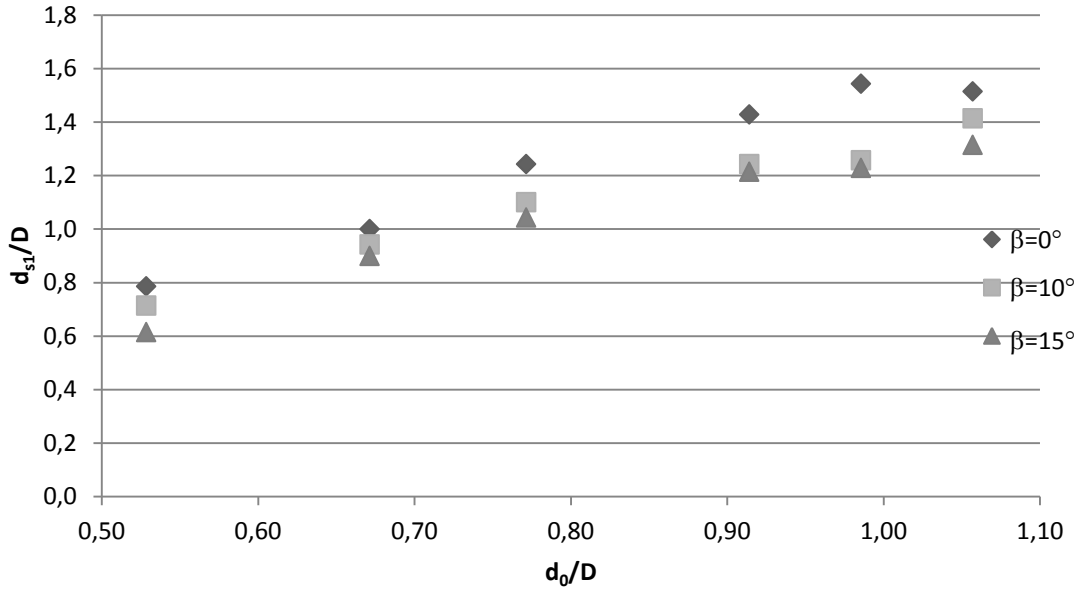

Figure 5.20: Variation of relative scour depth with relative flow depth for all inclination angles (D=70mm, C1)

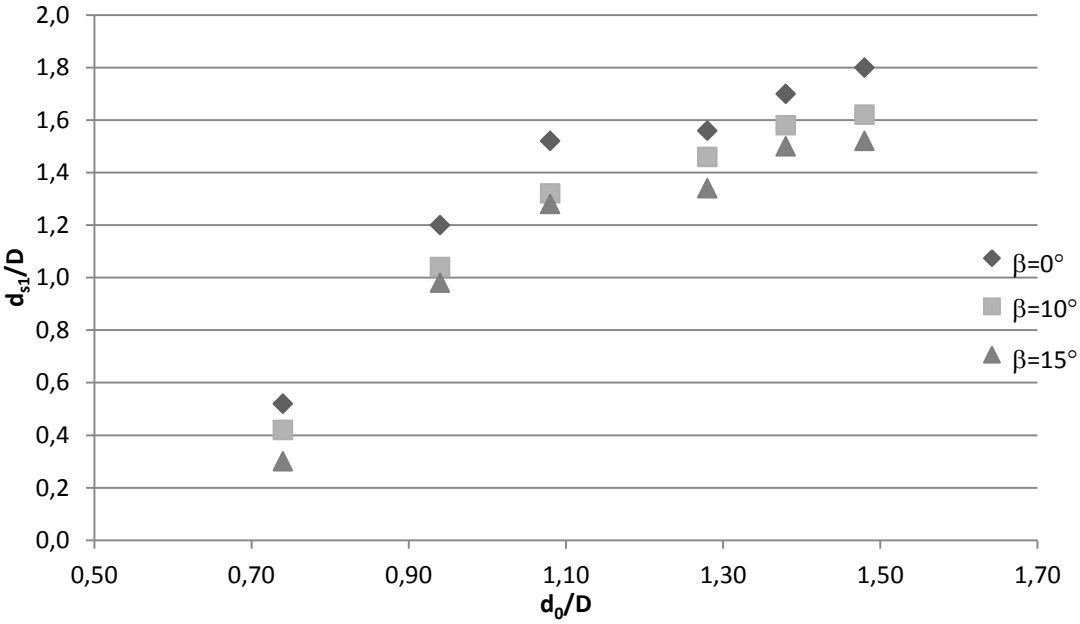

Figure 5.21: Variation of relative scour depth with relative flow depth for all inclination angles (D=50mm, C2)

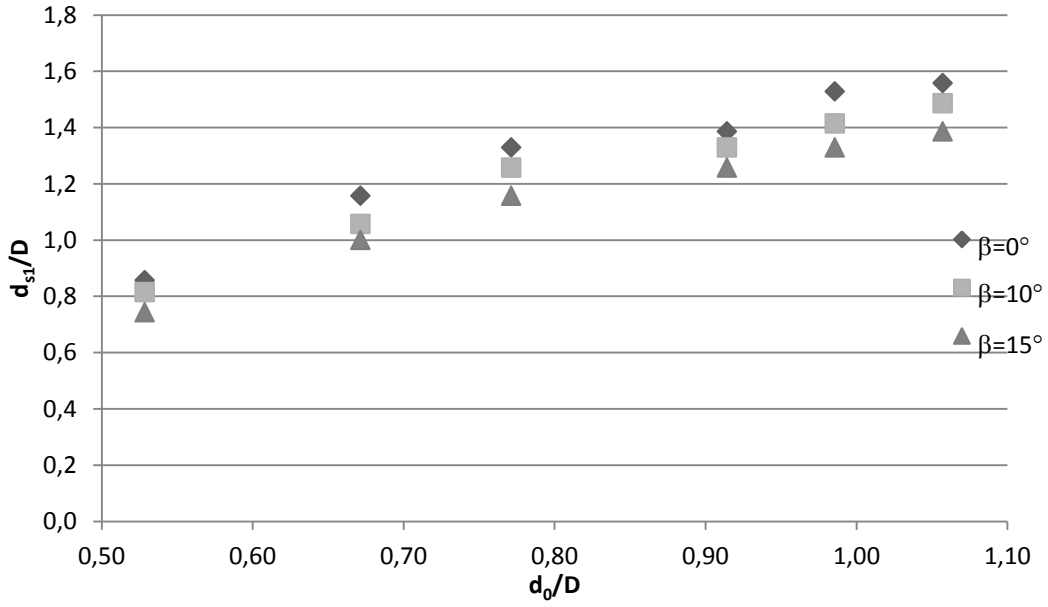

Figure 5.22: Variation of relative scour depth with relative flow depth for all inclination angles (D=70mm, C2)

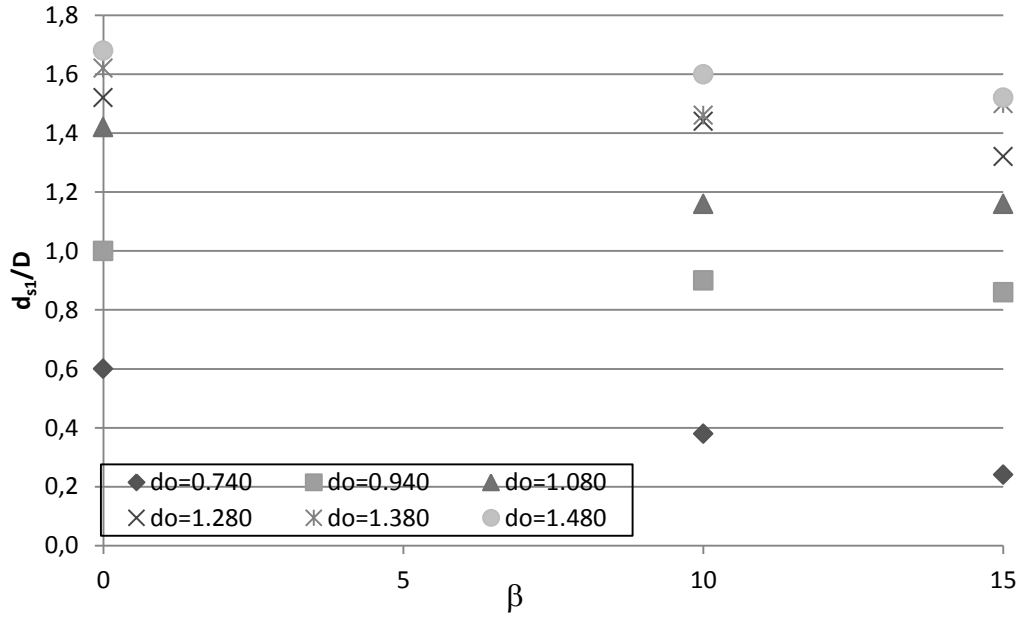

Figure 5.23: Variation of relative scour depth with an inclination angle, β, for all approach flow depths (D=50mm, C1)

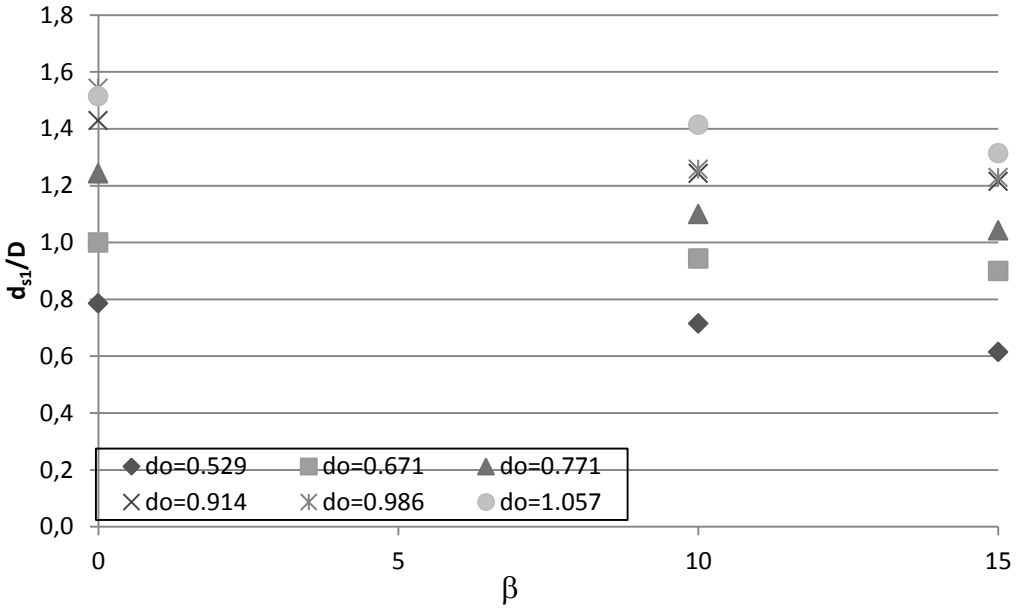

Figure 5.24: Variation of relative scour depth with an inclination angle, β, for all approach flow depths (D=70mm, C1)

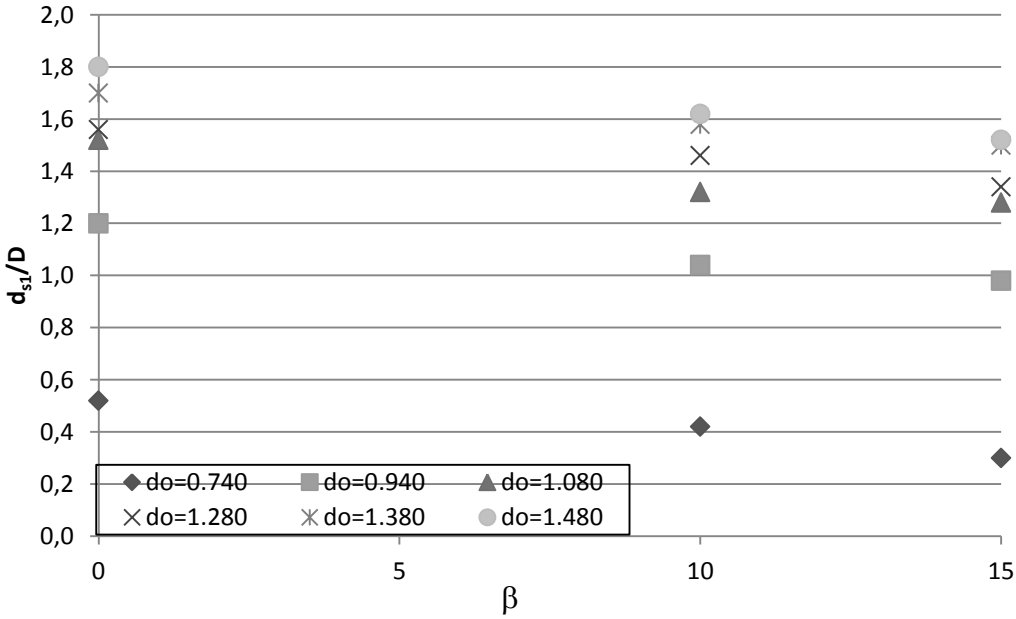

Figure 5.25: Variation of relative scour depth with an inclination angle, β, for all approach flow depths (D=50mm, C2)

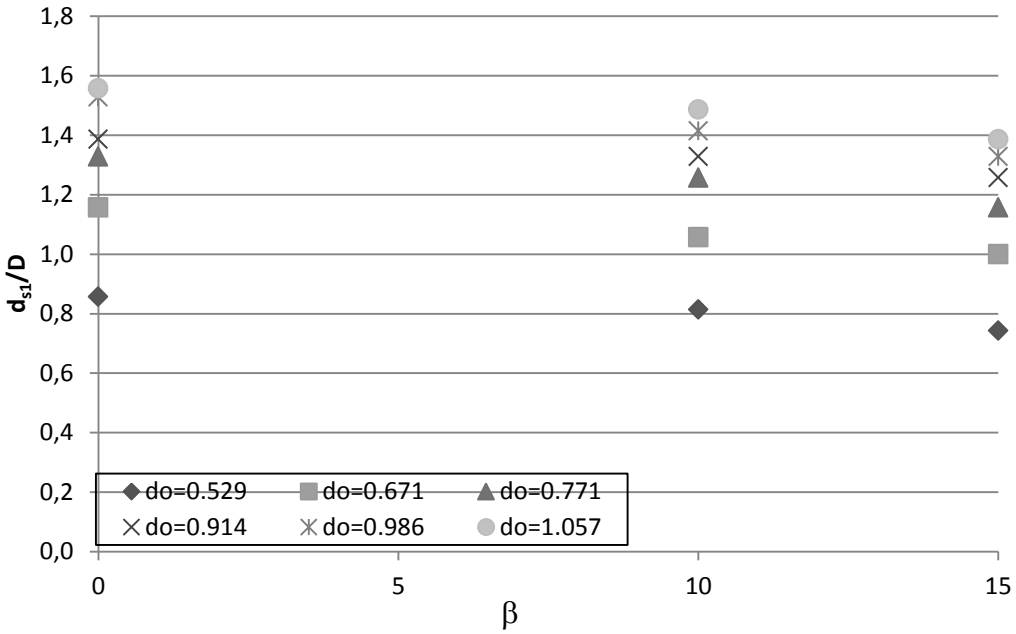

Figure 5.26: Variation of relative scour depth with an inclination angle, β, for all approach flow depths (D=70mm, C2)

5.6 Regression Analysis

In literature most of the pier scour equations are in the form of Eq. (5.11):

$$\frac{d_s}{D} = c_0 \left(\frac{d_0}{D}\right)^{c_1} (Fr)^{c_2} \tag{5.11}$$

where c_0, c_1 and c_2 are constants that are determined by the multiple regression analysis.

In chapter 4, dimensional analysis has been made for the local scour depth at the upstream face of the first pier (d_{s1}) and it is determined that the relative scour depth, d_s/D, is a function of relative flow depth, d_0/D, flow intensity, V/V_c and vertical inclination angle, β.

$$\frac{d_s}{D} = f\left(\frac{d_0}{D}, \frac{V}{V_c}, \beta\right) \tag{5.12}$$

The flow intensity variable, V/V_c, is used in the equations instead of Froude number because the Froude number range is very small. There is an extra variable in this case, which is the vertical inclination angle variable. In this study, mainly the effect of vertical inclination of bridge piers are discussed, so the pier scour equations include that parameter.

$$\frac{d_s}{D} = c_0 \left(\frac{d_0}{D}\right)^{c_1} \left(\frac{V}{V_c}\right)^{c_2} (\alpha)^{c_3} \tag{5.13}$$

where $\alpha = 90 - \beta$ in radians.

By taking the natural logarithm of both sides in Equation 5.13, the below equation is derived:

$$\ln\left(\frac{d_s}{D}\right) = \ln(c_0) + c_1 \ln\left(\frac{d_0}{D}\right) + c_2 \ln\left(\frac{V}{V_c}\right) + c_3 \ln(\alpha) \tag{5.14}$$

The below matrix is written to obtain a general multiple regression analysis formula by replacing $\ln(d_s / D)$ with Y, $\ln(d_0 / D)$ with X_1, $\ln(V / V_c)$ with X_2 and $\ln(\alpha)$ with X_3. N is the number of data points. As there are 4 unknowns, namely c_0, c_1, c_2 and c_3, 4x4 matrix is written and unknowns are found using the experimental data.

$$\begin{bmatrix} N & \sum X_1 & \sum X_2 & \sum X_3 \\ \sum X_1 & \sum X_1^2 & \sum X_1X_2 & \sum X_1X_3 \\ \sum X_2 & \sum X_2X_1 & \sum X_2^2 & \sum X_2X_3 \\ \sum X_3 & \sum X_3X_1 & \sum X_3X_2 & \sum X_3^2 \end{bmatrix} \begin{bmatrix} c_0 \\ c_1 \\ c_2 \\ c_3 \end{bmatrix} = \begin{bmatrix} \sum Y \\ \sum X_1Y \\ \sum X_2Y \\ \sum X_3Y \end{bmatrix} \tag{5.15}$$

Computational tables for regression analysis of configuration 1 and configuration 2 are shown in Tables 5.11 and 5.12 respectively. d_s/D, d_0/D, V/V_c and α data are placed into the columns 1 through 4 using the results of experiments. Then, natural logarithms of them are written into the columns 5 through 8. In the same manner X_1^2, X_2^2, X_3^2, X_1Y, X_2Y, X_3Y, X_1X_2, X_1X_3 and X_2X_3 values are computed and placed into the succeeding columns. Finally, equations are solved using the matrix algebra and the coefficients are computed. The pier scour equations are represented below:

Configuration 1:

$$\frac{d_s}{D} = 1.136 \left(\frac{d_0}{D}\right)^{0.250} \left(\frac{V}{V_c}\right)^{1.186} (\alpha)^{1.136} \tag{5.16}$$

$r = 0.99$ and $r^2 = 0.97$

Configuration 2:

$$\frac{d_s}{D} = 1.192 \left(\frac{d_0}{D}\right)^{0.251} \left(\frac{V}{V_c}\right)^{0.909} (\alpha)^{0.785} \tag{5.17}$$

$r = 0.99$ and $r^2 = 0.97$

As the rear piers do not affect the scour around most upstream pier, all the data is combined together and a general multiple regression analysis is made for all data (Eq. 5.18).

All Configurations:

$$\frac{d_s}{D} = 1.163\left(\frac{d_0}{D}\right)^{0.250}\left(\frac{V}{V_c}\right)^{1.047}(\alpha)^{0.828} \tag{5.18}$$

$r = 0.97$ and $r^2 = 0.95$

The correlation coefficient, r, is computed using Eq. (5.19):

$$r = \pm\sqrt{1 - \frac{\sum\left(\left(\frac{d_s}{D}\right)_{\exp} - \left(\frac{d_s}{D}\right)_{comp}\right)^2}{\sum\left(\left(\frac{d_s}{D}\right)_{\exp} - \left(\frac{d_s}{D}\right)_{ave}\right)^2}} \tag{5.19}$$

Table 5.11: Multiple regression analysis for 3 pier configurations (C1)

1	*2*	*3*	*4*	*5*	*6*	*7*	*8*	*9*	*10*	*11*	*12*	*13*	*14*	*15*	*16*	*17*	*18*	*19*	*20*
d_s/D^*	d_0/D	V/V_c	β (deg.)	α (deg.)	α (rad.)	Y	X_1	X_2	X_3	X_1^2	X_1X_2	X_1X_3	X_2^2	X_2X_3	X_3^2	X_1Y	X_2Y	X_3Y	d_s/D^{**}
1.000	0.940	0.686	0	90	1.571	0.000	-0.062	-0.376	0.452	0.004	0.023	-0.028	0.142	-0.170	0.204	0.000	0.000	0.000	1.060
1.420	1.080	0.814	0	90	1.571	0.351	0.077	-0.206	0.452	0.006	-0.016	0.035	0.042	-0.093	0.204	0.027	-0.072	0.158	1.344
1.520	1.280	0.879	0	90	1.571	0.419	0.247	-0.129	0.452	0.061	-0.032	0.111	0.017	-0.058	0.204	0.103	-0.054	0.189	1.537
1.620	1.380	0.907	0	90	1.571	0.482	0.322	-0.097	0.452	0.104	-0.031	0.145	0.009	-0.044	0.204	0.155	-0.047	0.218	1.625
1.680	1.480	0.936	0	90	1.571	0.519	0.392	-0.067	0.452	0.154	-0.026	0.177	0.004	-0.030	0.204	0.203	-0.035	0.234	1.715
0.786	0.529	0.589	0	90	1.571	-0.241	-0.638	-0.529	0.452	0.407	0.337	-0.288	0.280	-0.239	0.204	0.154	0.128	-0.109	0.766
1.000	0.671	0.686	0	90	1.571	0.000	-0.398	-0.376	0.452	0.159	0.150	-0.180	0.142	-0.170	0.204	0.000	0.000	0.000	0.975
1.243	0.771	0.814	0	90	1.571	0.217	-0.260	-0.206	0.452	0.067	0.053	-0.117	0.042	-0.093	0.204	-0.056	-0.045	0.098	1.236
1.429	0.914	0.879	0	90	1.571	0.357	-0.090	-0.129	0.452	0.008	0.012	-0.040	0.017	-0.058	0.204	-0.032	-0.046	0.161	1.413
1.543	0.986	0.907	0	90	1.571	0.434	-0.014	-0.097	0.452	0.000	0.001	-0.006	0.009	-0.044	0.204	-0.006	-0.042	0.196	1.494
1.514	1.057	0.936	0	90	1.571	0.415	0.056	-0.067	0.452	0.003	-0.004	0.025	0.004	-0.030	0.204	0.023	-0.028	0.187	1.577
0.900	0.940	0.686	10	80	1.396	-0.105	-0.062	-0.376	0.334	0.004	0.023	-0.021	0.142	-0.126	0.111	0.007	0.040	-0.035	0.957
1.160	1.080	0.814	10	80	1.396	0.148	0.077	-0.206	0.334	0.006	-0.016	0.026	0.042	-0.069	0.111	0.011	-0.031	0.050	1.213
1.440	1.280	0.879	10	80	1.396	0.365	0.247	-0.129	0.334	0.061	-0.032	0.082	0.017	-0.043	0.111	0.090	-0.047	0.122	1.387
1.460	1.380	0.907	10	80	1.396	0.378	0.322	-0.097	0.334	0.104	-0.031	0.108	0.009	-0.032	0.111	0.122	-0.037	0.126	1.467
1.600	1.480	0.936	10	80	1.396	0.470	0.392	-0.067	0.334	0.154	-0.026	0.131	0.004	-0.022	0.111	0.184	-0.031	0.157	1.548
0.714	0.529	0.589	10	80	1.396	-0.336	-0.638	-0.529	0.334	0.407	0.337	-0.213	0.280	-0.177	0.111	0.215	0.178	-0.112	0.692
0.943	0.671	0.686	10	80	1.396	-0.059	-0.398	-0.376	0.334	0.159	0.150	-0.133	0.142	-0.126	0.111	0.023	0.022	-0.020	0.880
1.100	0.771	0.814	10	80	1.396	0.095	-0.260	-0.206	0.334	0.067	0.053	-0.087	0.042	-0.069	0.111	-0.025	-0.020	0.032	1.115
1.243	0.914	0.879	10	80	1.396	0.217	-0.090	-0.129	0.334	0.008	0.012	-0.030	0.017	-0.043	0.111	-0.019	-0.028	0.073	1.275
1.257	0.986	0.907	10	80	1.396	0.229	-0.014	-0.097	0.334	0.000	0.001	-0.005	0.009	-0.032	0.111	-0.003	-0.022	0.076	1.349
1.414	1.057	0.936	10	80	1.396	0.347	0.056	-0.067	0.334	0.003	-0.004	0.019	0.004	-0.022	0.111	0.019	-0.023	0.116	1.423
0.860	0.940	0.686	15	75	1.309	-0.151	-0.062	-0.376	0.269	0.004	0.023	-0.017	0.142	-0.101	0.073	0.009	0.057	-0.041	0.905
1.160	1.080	0.814	15	75	1.309	0.148	0.077	-0.206	0.269	0.006	-0.016	0.021	0.042	-0.055	0.073	0.011	-0.031	0.040	1.147
1.320	1.280	0.879	15	75	1.309	0.278	0.247	-0.129	0.269	0.061	-0.032	0.066	0.017	-0.035	0.073	0.069	-0.036	0.075	1.311
1.500	1.380	0.907	15	75	1.309	0.405	0.322	-0.097	0.269	0.104	-0.031	0.087	0.009	-0.026	0.073	0.131	-0.039	0.109	1.387
1.520	1.480	0.936	15	75	1.309	0.419	0.392	-0.067	0.269	0.154	-0.026	0.106	0.004	-0.018	0.073	0.164	-0.028	0.113	1.464
0.614	0.529	0.589	15	75	1.309	-0.487	-0.638	-0.529	0.269	0.407	0.337	-0.172	0.280	-0.142	0.073	0.311	0.258	-0.131	0.654
0.900	0.671	0.686	15	75	1.309	-0.105	-0.398	-0.376	0.269	0.159	0.150	-0.107	0.142	-0.101	0.073	0.042	0.040	-0.028	0.832
1.043	0.771	0.814	15	75	1.309	0.042	-0.260	-0.206	0.269	0.067	0.053	-0.070	0.042	-0.055	0.073	-0.011	-0.009	0.011	1.054
1.214	0.914	0.879	15	75	1.309	0.194	-0.090	-0.129	0.269	0.008	0.012	-0.024	0.017	-0.035	0.073	-0.017	-0.025	0.052	1.205
1.229	0.986	0.907	15	75	1.309	0.206	-0.014	-0.097	0.269	0.000	0.001	-0.004	0.009	-0.026	0.073	-0.003	-0.020	0.055	1.275
1.314	1.057	0.936	15	75	1.309	0.273	0.056	-0.067	0.269	0.003	-0.004	0.015	0.004	-0.018	0.073	0.015	-0.018	0.074	1.346
						ΣY	ΣX_1	ΣX_2	ΣX_3	ΣX_1^2	ΣX_1X_2	ΣX_1X_3	ΣX_2^2	ΣX_2X_3	ΣX_3^2	ΣX_1Y	ΣX_2Y	ΣX_3Y	
						5.923	-1.103	-6.837	11.601	2.916	1.404	-0.388	2.127	-2.403	4.266	1.916	-0.091	2.246	

Table 5.12: Multiple regression analysis for 4 pier configurations (C2)

1	*2*	*3*	*4*	*5*	*6*	*7*	*8*	*9*	*10*	*11*	*12*	*13*	*14*	*15*	*16*	*17*	*18*	*19*	*20*
d_s/D^*	d_0/D	V/V_c	β (deg.)	α (deg.)	α (rad.)	Y	X_1	X_2	X_3	X_1^2	X_1X_2	X_1X_3	X_2^2	X_2X_3	X_3^2	X_1Y	X_2Y	X_3Y	d_s/D^{**}
1.200	0.940	0.686	0	90	1.571	0.182	-0.062	-0.376	0.452	0.004	0.023	-0.028	0.142	-0.170	0.204	-0.011	-0.069	0.082	1.188
1.520	1.080	0.814	0	90	1.571	0.419	0.077	-0.206	0.452	0.006	-0.016	0.035	0.042	-0.093	0.204	0.032	-0.086	0.189	1.437
1.560	1.280	0.879	0	90	1.571	0.445	0.247	-0.129	0.452	0.061	-0.032	0.111	0.017	-0.058	0.204	0.110	-0.057	0.201	1.608
1.700	1.380	0.907	0	90	1.571	0.531	0.322	-0.097	0.452	0.104	-0.031	0.145	0.009	-0.044	0.204	0.171	-0.052	0.240	1.686
1.800	1.480	0.936	0	90	1.571	0.588	0.392	-0.067	0.452	0.154	-0.026	0.177	0.004	-0.030	0.204	0.230	-0.039	0.265	1.764
0.857	0.529	0.589	0	90	1.571	-0.154	-0.638	-0.529	0.452	0.407	0.337	-0.288	0.280	-0.239	0.204	0.098	0.082	-0.070	0.895
1.157	0.671	0.686	0	90	1.571	0.146	-0.398	-0.376	0.452	0.159	0.150	-0.180	0.142	-0.170	0.204	-0.058	-0.055	0.066	1.092
1.329	0.771	0.814	0	90	1.571	0.284	-0.260	-0.206	0.452	0.067	0.053	-0.117	0.042	-0.093	0.204	-0.074	-0.058	0.128	1.320
1.386	0.914	0.879	0	90	1.571	0.326	-0.090	-0.129	0.452	0.008	0.012	-0.040	0.017	-0.058	0.204	-0.029	-0.042	0.147	1.478
1.529	0.986	0.907	0	90	1.571	0.424	-0.014	-0.097	0.452	0.000	0.001	-0.006	0.009	-0.044	0.204	-0.006	-0.041	0.192	1.549
1.557	1.057	0.936	0	90	1.571	0.443	0.056	-0.067	0.452	0.003	-0.004	0.025	0.004	-0.030	0.204	0.025	-0.029	0.200	1.621
1.040	0.940	0.686	10	80	1.396	0.039	-0.062	-0.376	0.334	0.004	0.023	-0.021	0.142	-0.126	0.111	-0.002	-0.015	0.013	1.083
1.320	1.080	0.814	10	80	1.396	0.278	0.077	-0.206	0.334	0.006	-0.016	0.026	0.042	-0.069	0.111	0.021	-0.057	0.093	1.310
1.460	1.280	0.879	10	80	1.396	0.378	0.247	-0.129	0.334	0.061	-0.032	0.082	0.017	-0.043	0.111	0.093	-0.049	0.126	1.466
1.580	1.380	0.907	10	80	1.396	0.457	0.322	-0.097	0.334	0.104	-0.031	0.108	0.009	-0.032	0.111	0.147	-0.045	0.153	1.537
1.620	1.480	0.936	10	80	1.396	0.482	0.392	-0.067	0.334	0.154	-0.026	0.131	0.004	-0.022	0.111	0.189	-0.032	0.161	1.609
0.814	0.529	0.589	10	80	1.396	-0.205	-0.638	-0.529	0.334	0.407	0.337	-0.213	0.280	-0.177	0.111	0.131	0.109	-0.069	0.816
1.057	0.671	0.686	10	80	1.396	0.056	-0.398	-0.376	0.334	0.159	0.150	-0.133	0.142	-0.126	0.111	-0.022	-0.021	0.019	0.995
1.257	0.771	0.814	10	80	1.396	0.229	-0.260	-0.206	0.334	0.067	0.053	-0.087	0.042	-0.069	0.111	-0.059	-0.047	0.076	1.203
1.329	0.914	0.879	10	80	1.396	0.284	-0.090	-0.129	0.334	0.008	0.012	-0.030	0.017	-0.043	0.111	-0.025	-0.037	0.095	1.347
1.414	0.986	0.907	10	80	1.396	0.347	-0.014	-0.097	0.334	0.000	0.001	-0.005	0.009	-0.032	0.111	-0.005	-0.034	0.116	1.413
1.486	1.057	0.936	10	80	1.396	0.396	0.056	-0.067	0.334	0.003	-0.004	0.019	0.004	-0.022	0.111	0.022	-0.026	0.132	1.478
0.980	0.940	0.686	15	75	1.309	-0.020	-0.062	-0.376	0.269	0.004	0.023	-0.017	0.142	-0.101	0.073	0.001	0.008	-0.005	1.030
1.280	1.080	0.814	15	75	1.309	0.247	0.077	-0.206	0.269	0.006	-0.016	0.021	0.042	-0.055	0.073	0.019	-0.051	0.066	1.245
1.340	1.280	0.879	15	75	1.309	0.293	0.247	-0.129	0.269	0.061	-0.032	0.066	0.017	-0.035	0.073	0.072	-0.038	0.079	1.393
1.500	1.380	0.907	15	75	1.309	0.405	0.322	-0.097	0.269	0.104	-0.031	0.087	0.009	-0.026	0.073	0.131	-0.039	0.109	1.461
1.520	1.480	0.936	15	75	1.309	0.419	0.392	-0.067	0.269	0.154	-0.026	0.106	0.004	-0.018	0.073	0.164	-0.028	0.113	1.529
0.743	0.529	0.589	15	75	1.309	-0.297	-0.638	-0.529	0.269	0.407	0.337	-0.172	0.280	-0.142	0.073	0.190	0.157	-0.080	0.776
1.000	0.671	0.686	15	75	1.309	0.000	-0.398	-0.376	0.269	0.159	0.150	-0.107	0.142	-0.101	0.073	0.000	0.000	0.000	0.946
1.157	0.771	0.814	15	75	1.309	0.146	-0.260	-0.206	0.269	0.067	0.053	-0.070	0.042	-0.055	0.073	-0.038	-0.030	0.039	1.144
1.257	0.914	0.879	15	75	1.309	0.229	-0.090	-0.129	0.269	0.008	0.012	-0.024	0.017	-0.035	0.073	-0.021	-0.029	0.062	1.280
1.329	0.986	0.907	15	75	1.309	0.284	-0.014	-0.097	0.269	0.000	0.001	-0.004	0.009	-0.026	0.073	-0.004	-0.028	0.076	1.343
1.386	1.057	0.936	15	75	1.309	0.326	0.056	-0.067	0.269	0.003	-0.004	0.015	0.004	-0.018	0.073	0.018	-0.022	0.088	1.405
						ΣY	ΣX_1	ΣX_2	ΣX_3	ΣX_1^2	ΣX_1X_2	ΣX_1X_3	ΣX_2^2	ΣX_2X_3	ΣX_3^2	ΣX_1Y	ΣX_2Y	ΣX_3Y	
						8.406	-1.103	-6.837	11.601	2.916	1.404	-0.388	2.127	-2.403	4.266	1.510	-0.801	3.103	

5.7 Comparison of the Results

In this section, the results of the present study are compared with the results of the studies done by Yildiz (2001) and Cesme (2005) graphically. Regression analyses are made for the equilibrium local scour depth around first pier in all studies.

Yildiz (2001) and Cesme (2005) derived the following equations by using regression analysis:

$$\frac{d_s}{D} = 0.455\left(\frac{d_0}{D}\right)^{0.202}\left(\frac{V}{V_c}\right)^{0.591}\alpha^{1.725} \qquad \text{Yildiz (2001)} \qquad (5.20)$$

$$\frac{d_s}{D} = 0.232\left(\frac{d_0}{D}\right)^{0.173}\left(\frac{V}{V_c}\right)^{0.351}\alpha^{2.888} \qquad \text{Cesme (2005)} \qquad (5.21)$$

By using the Eqs. (5.20) and (5.21) and the existing data, measured and computed flow depths are compared.

Depth of local scour was measured for different ranges of approach velocity and flow depths in all studies. In addition to the flow parameters, bed material size and gradation are completely different. Yildiz (2001) conducted the experiments with uniform sediments, however Cesme (2005) conducted with nonuniform sediments where armoring effect is observed. Nevertheless, Figures from 5.27 to 5.37 give an idea on variation of depth of local scour with respect to inclination angle, relative flow depth and flow intensity. Multiple comparisons are done between this study and Yildiz (2001) and Cesme (2005) because, they all focused on the effect of inclination of bridge piers on local scour depth.

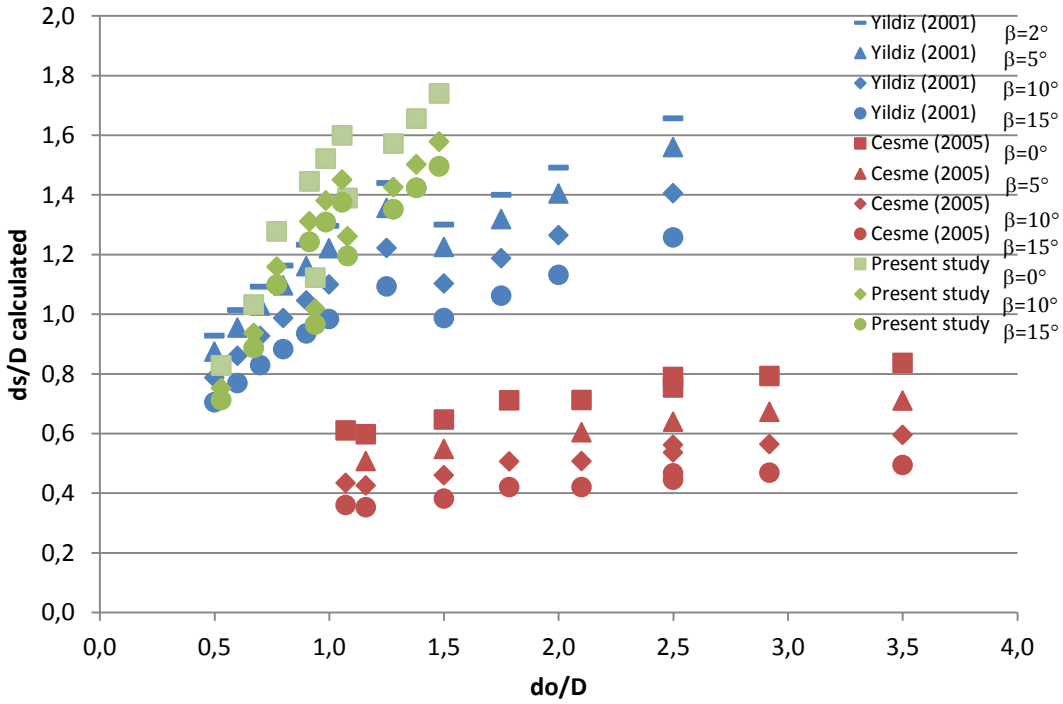

Figure 5.27: Calculated depth of local scour at the upstream side of the first pier (ds1) for all configurations

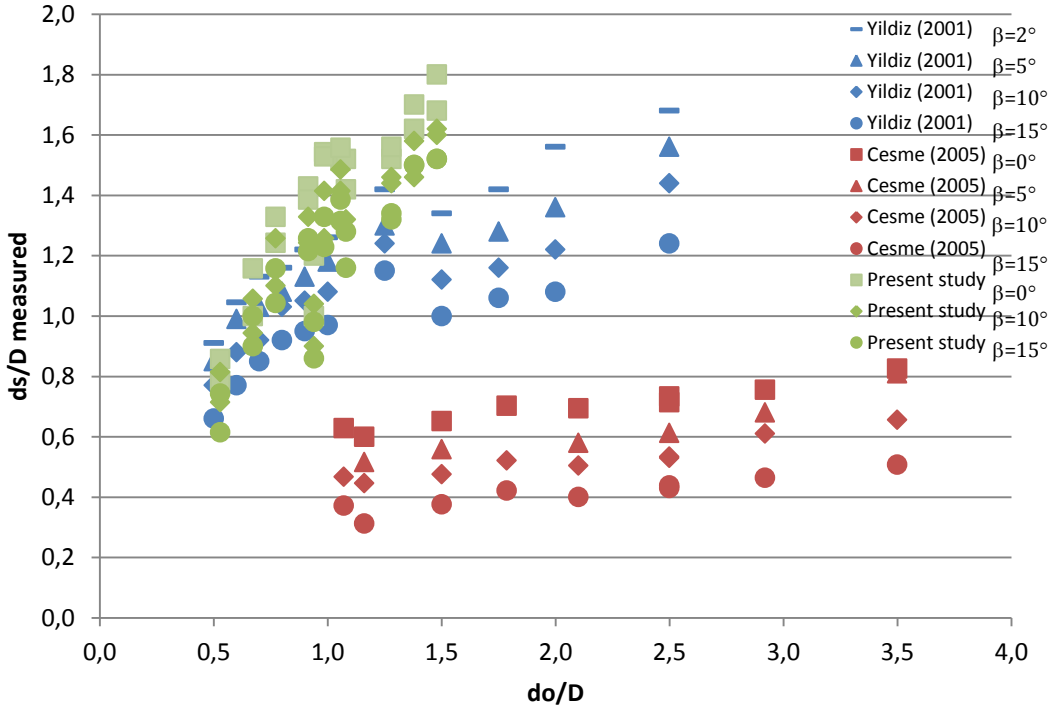

Figure 5.28: Measured depth of local scour at the upstream side of the first pier (ds1) for all configurations

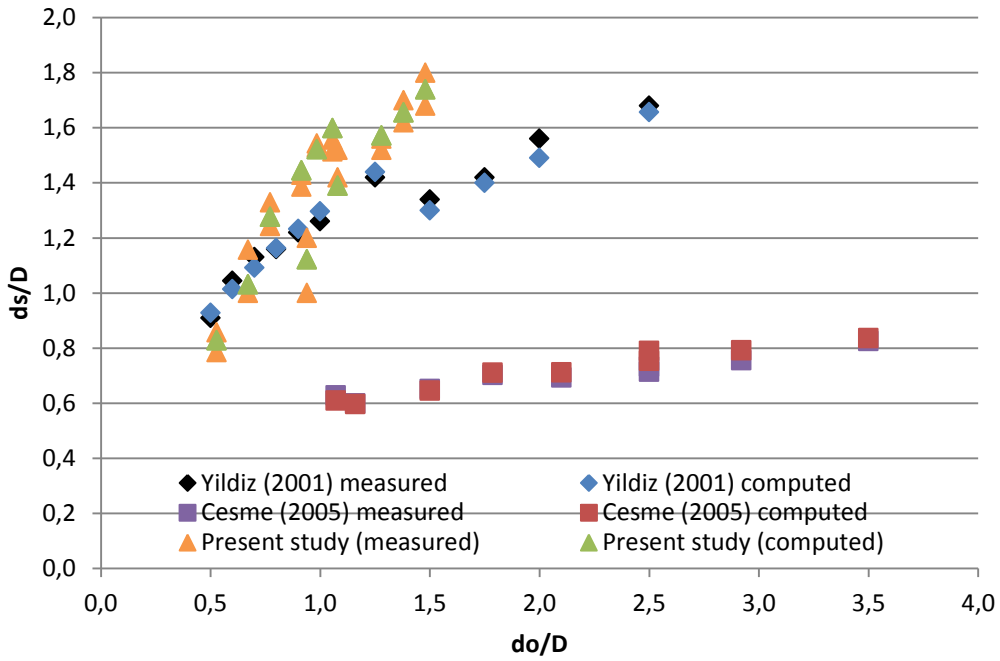

Figure 5.29: Variation of relative depth of local scour with relative flow depth for vertical piers (β=0°)

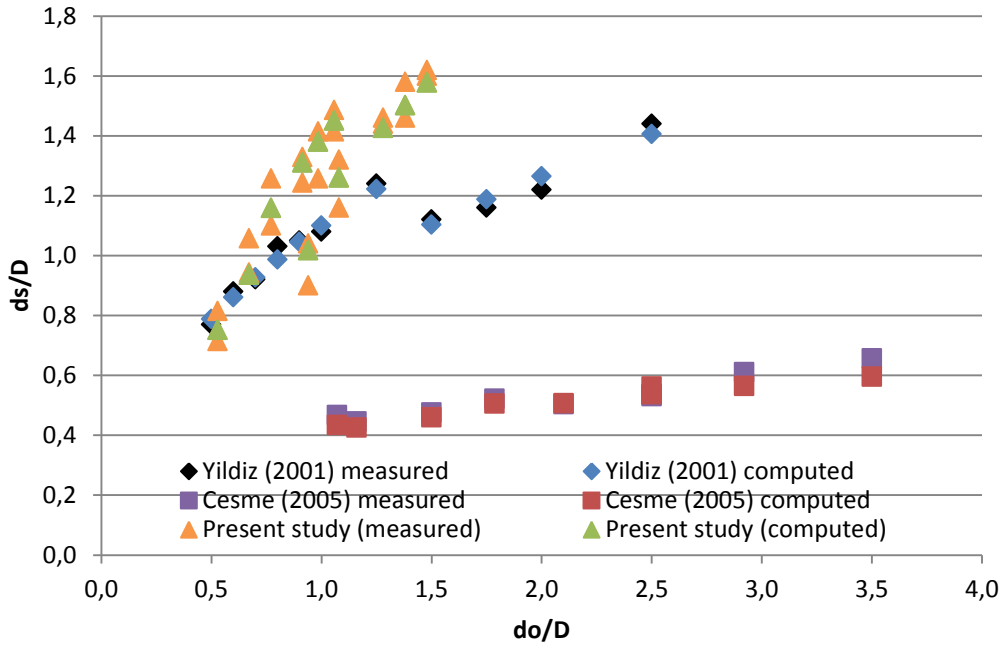

Figure 5.30: Variation of relative depth of local scour with relative flow depth for vertically inclined piers (β=10°)

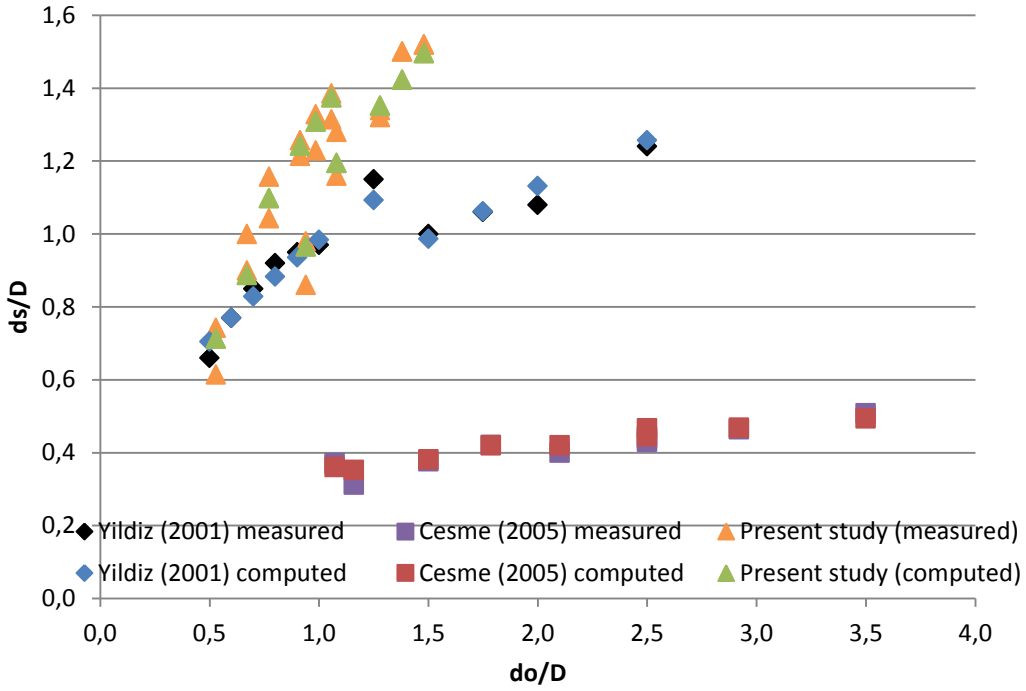

Figure 5.31: Variation of relative depth of local scour with relative flow depth for vertically inclined piers (β=15°)

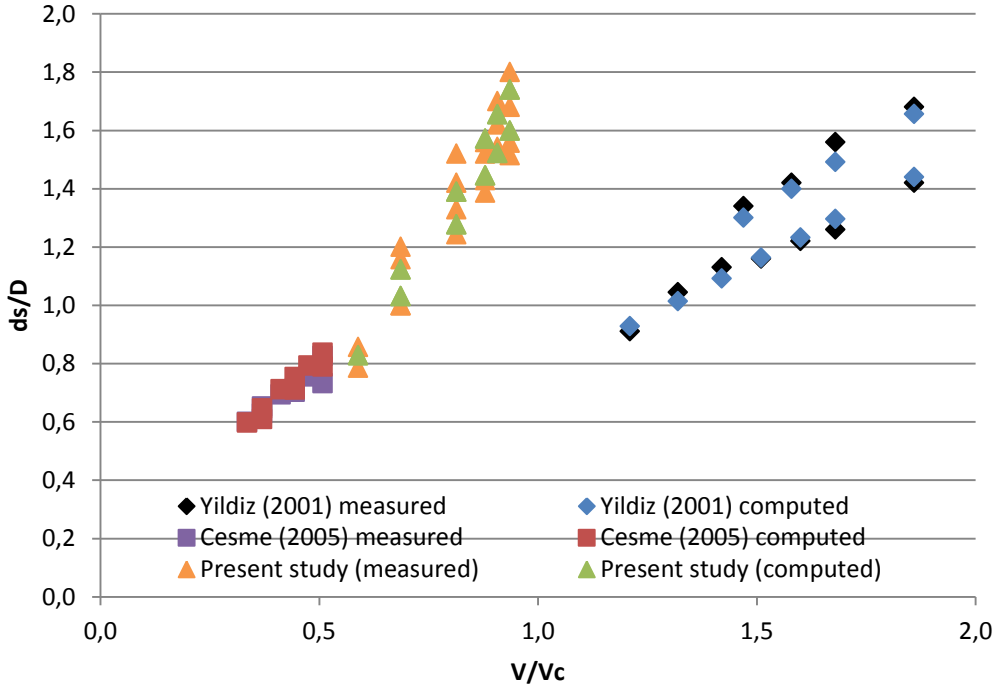

Figure 5.32: Variation of relative depth of local scour with flow intensity for vertical piers (β=0°)

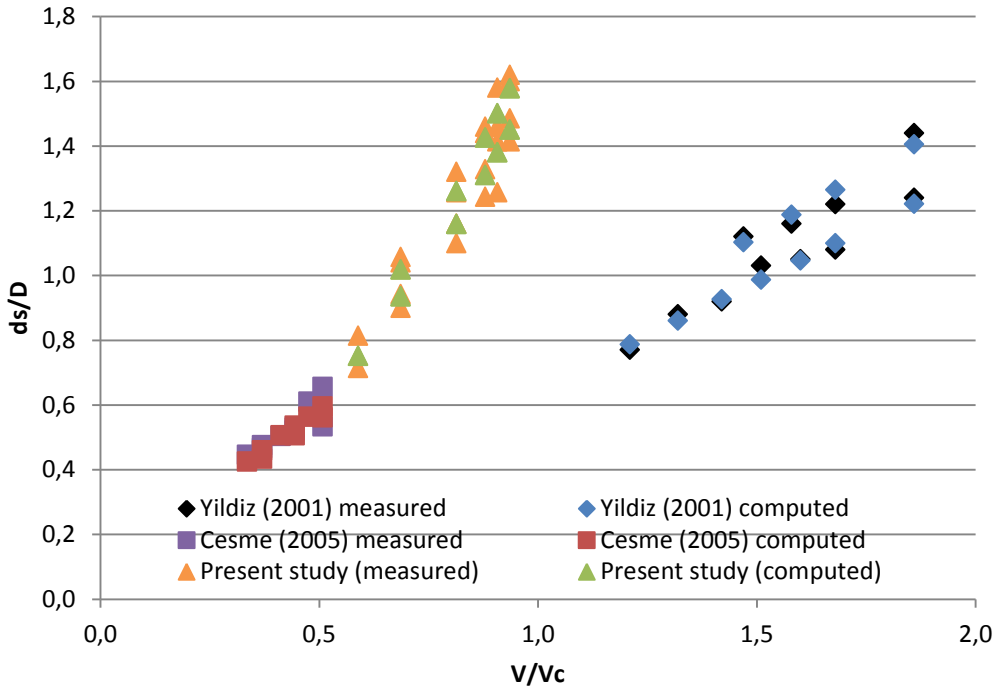

Figure 5.33: Variation of relative depth of local scour with flow intensity for vertically inclined piers (β=10°)

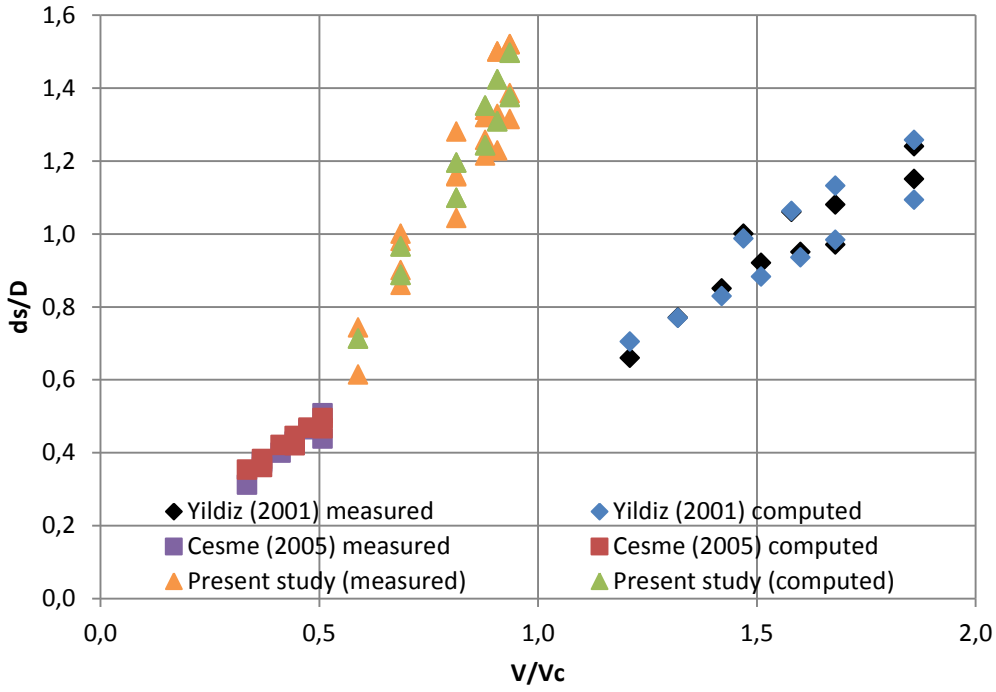

Figure 5.34: Variation of relative depth of local scour with flow intensity for vertically inclined piers (β=15°)

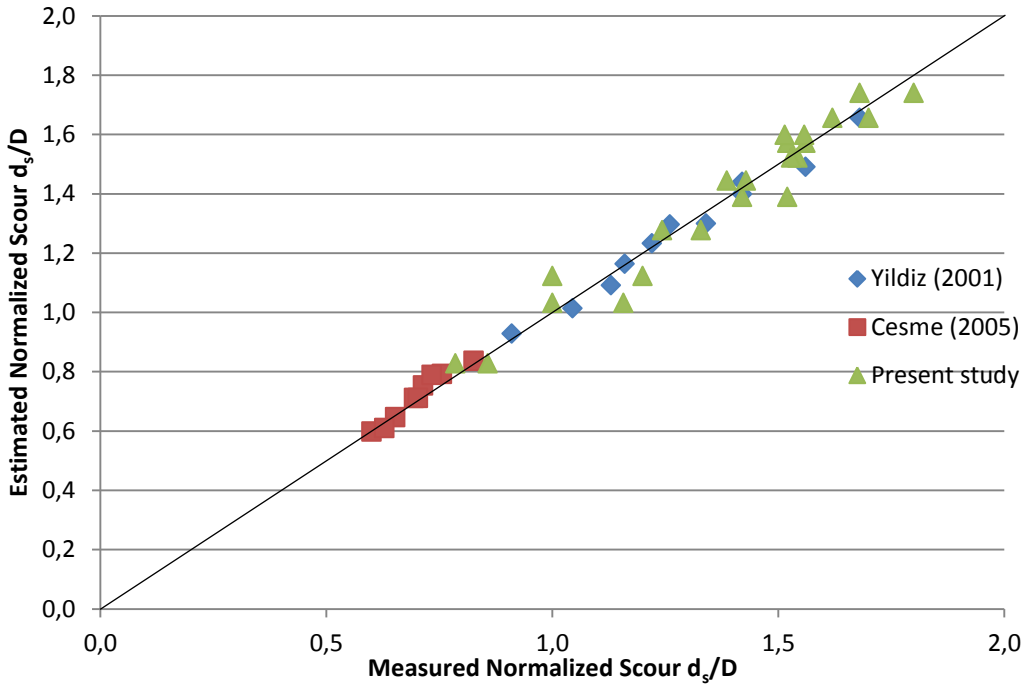

Figure 5.35: Comparison of all normalized measured scour depths with those computed with proposed equations at vertical piers

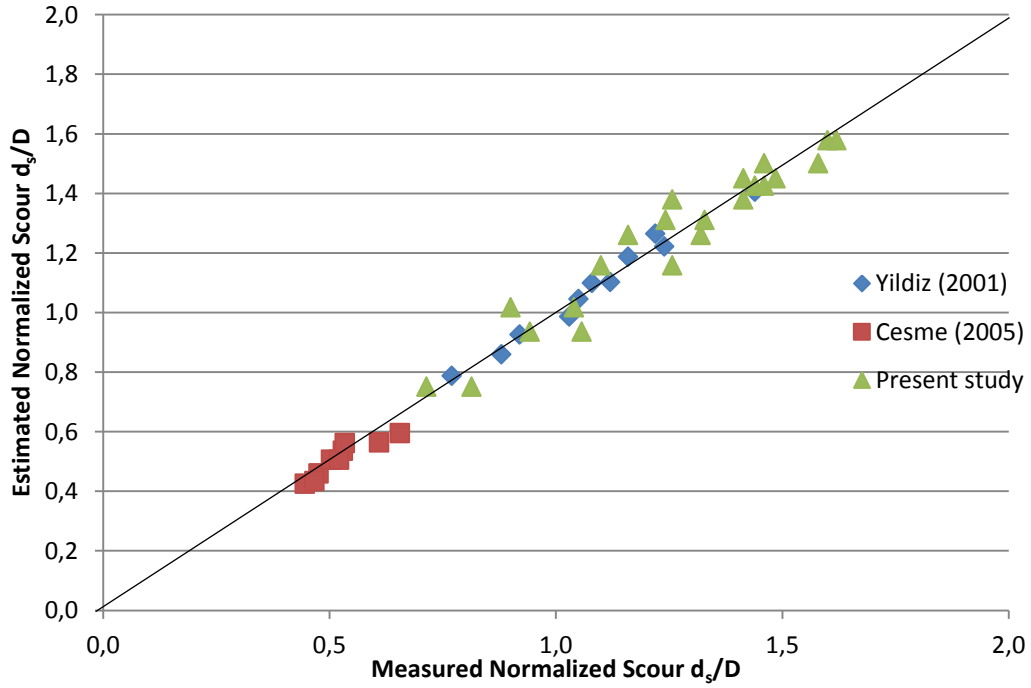

Figure 5.36: Comparison of all normalized measured scour depths with those computed with proposed equations with β=10°

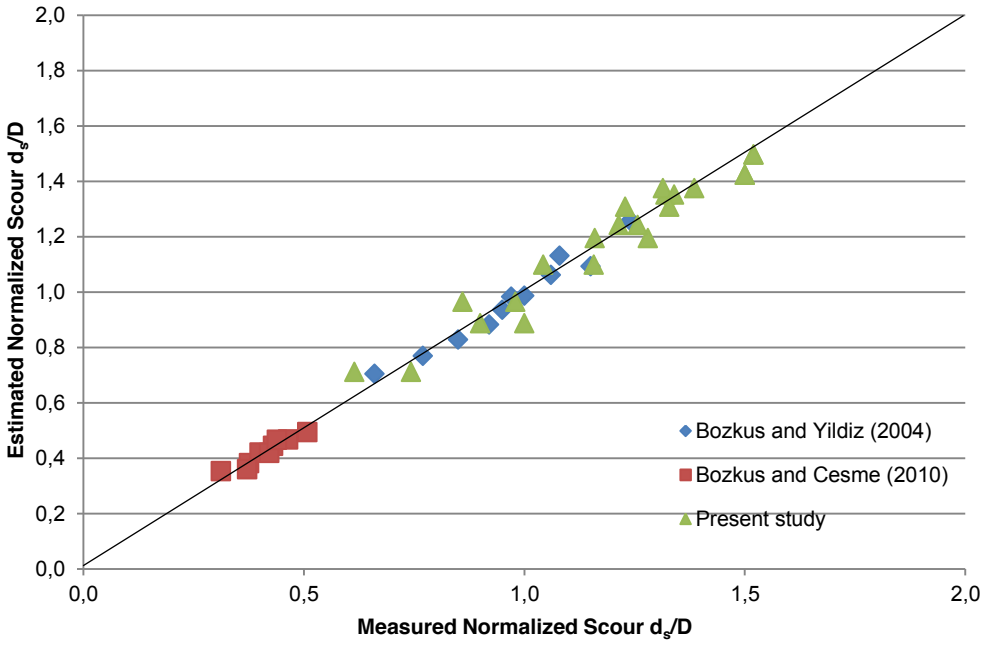

Figure 5.37: Comparison of all normalized measured scour depths with those computed with proposed equations with β=15°

The pier scour equation obtained from the present study represent the behavior of the scour, but valid only in the range of the experimental data. Richardson and Davis (2001) (HEC-18 pier scour equation) proposed pier scour equations, which are valid for all cases:

$$\frac{d_s}{d_0} = 2.0 K_1 K_2 K_3 \left(\frac{D}{d_0}\right)^{0.65} Fr^{0.43} \qquad \text{(HEC-18 pier scour equation)} \qquad 5.22$$

where K_1, K_2 and K_3 are correction factors for pier shape, angle of attack of flow and bed condition respectively.

Equation 5.22 predicts the maximum scour depth. The below figure shows the maximum scour depths that are founded by the related equation and the equation that is derived by this study:

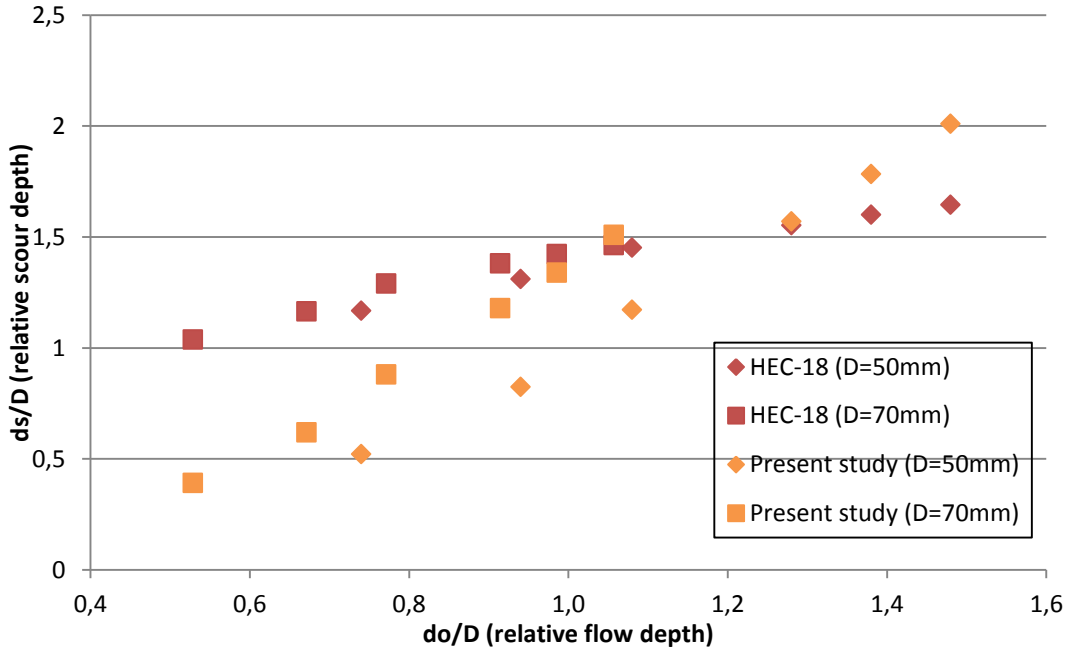

Figure 5.38: Variation of the maximum relative scour depth with respect to the relative depth of flow for various pier diameters

Table 5.13: The maximum relative depth of local scour values for D=50mm founded by various equations

						HEC-18	**Present study**
d_0 (mm)	V/V_c	Fr	D (mm)	d_0/D	D/d_0	d_s/D (mm)	d_s/D (mm)
37	0.589	0.293	50	0.740	1.351	1.168	0.521
47	0.686	0.315	50	0.940	1.064	1.310	0.824
54	0.814	0.357	50	1.080	0.926	1.451	1.172
64	0.879	0.364	50	1.280	0.781	1.553	1.571
69	0.907	0.367	50	1.380	0.725	1.600	1.783
74	0.936	0.370	50	1.480	0.676	1.646	2.010

Table 5.14: The maximum relative depth of local scour values for D=70 mm founded by various equations.

						HEC-18	Present study
d_0 (mm)	V/V_c	Fr	D (mm)	d_0/D	D/d_0	d_s/D (mm)	d_s/D (mm)
37	0.589	0.293	70	0.529	1.892	1.038	0.391
47	0.686	0.315	70	0.671	1.489	1.165	0.619
54	0.814	0.357	70	0.771	1.296	1.290	0.880
64	0.879	0.364	70	0.914	1.094	1.381	1.180
69	0.907	0.367	70	0.986	1.014	1.422	1.340
74	0.936	0.370	70	1.057	0.946	1.463	1.510

The HEC-18 pier scour equation is recommended for both live-bed and clear-water scour. The equation predicts maximum scour depths (Richardson and Davis, 2001). Thus, the equation that is founded from this study is compared with the HEC-18 pier scour equation.

CHAPTER 6

CONCLUSIONS AND RECOMMENDATIONS

Scour hole that is developed around bridge piers can be the main cause of a failure. As discussed in the previous chapters, the scour around bridge piers is developed by the high shear stress due to 3-dimensional separation of the boundary layer around the cylindrical pier. Predicting local scour around bridge piers is very important because underestimation of scour depth results in designing shallow foundations, which is dangerous for the bridge safety. Besides, bridge foundations are designed uneconomically if scour depth is overestimated.

Past studies show that there are many factors affecting the formation of local scour and some researchers developed various countermeasures to reduce the scour depth. As it was investigated before, the inclination angle of bridge piers affect the scour hole generation around a single cylindrical pier. In this study 72 experiments were carried out to find out the effect of inclination angle on scour depth around the cylindrical bridge pier groups. At the same time, effect of flow intensity and blockage ratio is examined and temporal variation of scour is observed. By using the experimental data, regression analysis is made and scour depth equations are derived. These equations are compared graphically with existing equations, which are derived by Bozkus and Yildiz (2004), Bozkus and Cesme (2010), Richardson and Davis (2001) and Melville (1988).

The following conclusions can be drawn from the study:

1. Local scour around bridge piers are developed asymptotically in time for constant flow conditions.
2. Increasing the flow intensity and pier size lead to increase in scour depth, surface area of scour hole and volume.
3. When inclination angle towards downstream increases, the local scour around a single pier decreases significantly. The largest reduction in the scour depth occurs around the most upstream pier. The inclination of most upstream and most downstream piers do not cause any problem to the middle piers; in fact scour depth reduction also is observed around the middle piers.
4. Inclination angle of β=10° seems to be more feasible than β=15°, because scour depth reduction is a little larger at piers that are inclined 15° than those inclined 10°. Considering the structural and economic parameters, designing and constructing of cylindrical bridge piers with an inclination angle of β=10° is more practical.
5. As the most downstream pier in a bridge pier group is inclined towards upstream, higher scour depth values are expected around it. But, the upstream piers reduce the negative effect of flow causing the scour and insignificant increase in scour depth is observed even though the most downstream pier has an inclination angle of 15°.
6. Pier spacing was constant (a=4D) throughout the experiments and separate but interfered scour holes were formed.

This study confirms that inclination of cylindrical piers directly affect the local scour in the laboratory setting. Moreover, flow intensity and relative flow depth are important variables that characterize the local scour. The following recommendations are made for further improvements in the study:

1. Experiments can be conducted using different configurations of pier groups.
2. Effect of inclination of bridge piers needs to be studied by varying sediment size and under different conditions of transport (live bed scour).
3. Additional experiments can be conducted over a larger range of velocities, pier spacing, pier diameter and channel sizes.

REFERENCES

Baker R.E., 1986. “Local scour at bridge piers in non-uniform sediment”, Thesis presented to the University of Auckland, at Auckland, New Zealand, in partial fulfillment of the requirements for the degree of Master of Engineering.

Başak V., Şentürk F., Aksoy Ş., Başlamışlı K. Y., Ergün Ö.,1975. “Bir Doğru Üzerinde Yeralan Kazık Grubu Etrafında Meydana Gelen Yerel Oyulmalar”, T.C. Enerji ve Tabii Kaynaklar Bakanlığı, DSI Genel Mudurlugu, Arastırma Dairesi Baskanlıgı,Ankara. Yayın No. HI-583.

Başak V., Başlamışlı Y., Ergün Ö., 1977. “Doğrusal Eksenli ve Dairesel Kesitli Kazık Grubu Etrafındaki Yerel Oyulma Derinlikleri”, D.S.I., T.A.K.K Dairesi Baskanlıgı, Yayın No. HI-641.

Bozkuş Z., Yıldız O., 2004. “Effects of Inclination of Bridge Piers on Scouring Depth”, ASCE Journal of Hydraulic Engineering, Vol.130, No. 8, 827-832, August 2004.

Bozkuş Z., Çeşme M.,2010. Reduction of Scouring Depth by Using Inclined Piers, Can. J. Civ. Eng. 37: 1621–1630 (2010)

Breusers H.N.C., Raudkivi A.J., 1991. “Scouring”. A.A. Balkema, Rotterdam, Brookfield.

Chang Wen-Yi, Lai Jihn-Sung, Yen Chin-Lien, 2004. “Evolution of Scour Depth at Circular Bridge Piers”, Journal of Hydraulic Engineering, Vol.130, No. 9, September 1, 2004.

Çeşme, Murat, 2005. “Experimental Investigation of Local Scour Around Inclined Dual Bridge Piers”. Master Thesis, Middle East Technical University.

Chiew Y.M., 1984. “Local scour at Bridge Piers”, Rep. No. 355, University of Auckland, School of Engineering, New Zealand.

Ettema R., 1976. “”Influence of material gradation on local scour”, Thesis presented to the University of Auckland, at Auckland, New Zealand, in partial fulfillment of the requirements for the degree of Master of Engineering.

Ettema R., 1980. “Scour at bridge piers”, University of Auckland, N.Z., School of Engineering, Rep. No.216.

Ettema R., Melville B.W., Barkdoll B., 1998. “Scale Effect in Pier-Scour Experiments”, Journal of Hydraulic Engineering, Vol. 124, No. 6, June, 1998. Technical Note No. 13837.

Hjorth P., 1975. “Studies on the nature of local scour”. Dept. Water Resources Engineering, Lund Institute of Technology, Bulletin Series A, No.46.

Laursen E.M., Toch A., 1956. “Scour around bridge piers and abutments”, Iowa Highway Res. Board Bulletin No. 4, 60 pp.

Md. Faruque Mia, Hiroshi Nago, 2003. “Design Method of Time-Dependent Local Scour at Circular Bridge Pier”, Journal of Hydraulic Engineering, Vol. 129, No. 6, June 1,2003. ASCE.

Melville B.W., 1975. “Local scour at bridge sites”, University of Auckland, N.Z., School of Engineering, Rep. No. 117.

Melville B.W., Raudkivi A.J., 1977. “Flow characteristics in local scour at bridge piers” , Journal of Hydraulic Research 15; 373-380.

Melville B.W., 1997. “Pier and Abutment Scour: Integrated Approach”, Journal of Hydraulic Engineering, Vol. 123, No. 2, February 1997. ASCE, Paper No. 10923.

Melville B.W., Chiew Y.M., 1999. “Time Scale for Local Scour at Bridge Piers”, Journal of Hydraulic Engineering, Vol. 125, No. 1, January 1999. ASCE, Paper No. 16274.

Melville B. W., Sutherland A.J., 1988. “Design Method for Local Scour at Bridge Piers”, Journal of Hydraulic Engineering, Vol. 114, No. 10, October 1988. ASCE, Paper No. 22830.

Neill C.R., 1964. “River-bed scour, a review for engineers”, Canadian Good Roads’ Assoc. Techn. Publ. No. 23, Ottawa.

Raudkivi A.J., Ettema R., 1977. “Effect of sediment gradation on clear-water scour”, Proc. ASCE 103(HY10); 1209-1213.

Raudkivi A.J., Ettema R., 1983. “Clear water scour at cylindrical piers”, Journal of Hydraulic Engineering, ASCE, 109(HY3), 338-350.

Yanmaz, A. Melih, 2002. “Kopru Hidroligi”, ODTU Gelistirme Vakfı Yayıncılık ve Iletisim A.S. Yayınları, METU Press, ISBN 975-7064- 55-6.

Yanmaz A.Melih, Altınbilek H.Doğan, 1991. “Study of Time-Dependent Local Scour Around Bridge Piers”, Journal of Hydraulic Engineering, Vol. 117, No. 10, October, 1991. ASCE, Paper No. 26220.
Yanmaz , A. Melih, 1989. “Time Dependent Analysis of Clear-water Scour Around Bridge Piers”, Ph. D. Thesis, Middle East Technical University, Science Code: 624.02.01.
Yıldız, Osman, 2001. “Experimental Investigation of Scouring Around Inclined Bridge Piers”, Master Thesis, Middle East Technical University.

APPENDIX A

EXPERIMENTAL RESULTS

In this section, time variation of local scour depth around cylindrical piers are shown graphically with an experimental order.

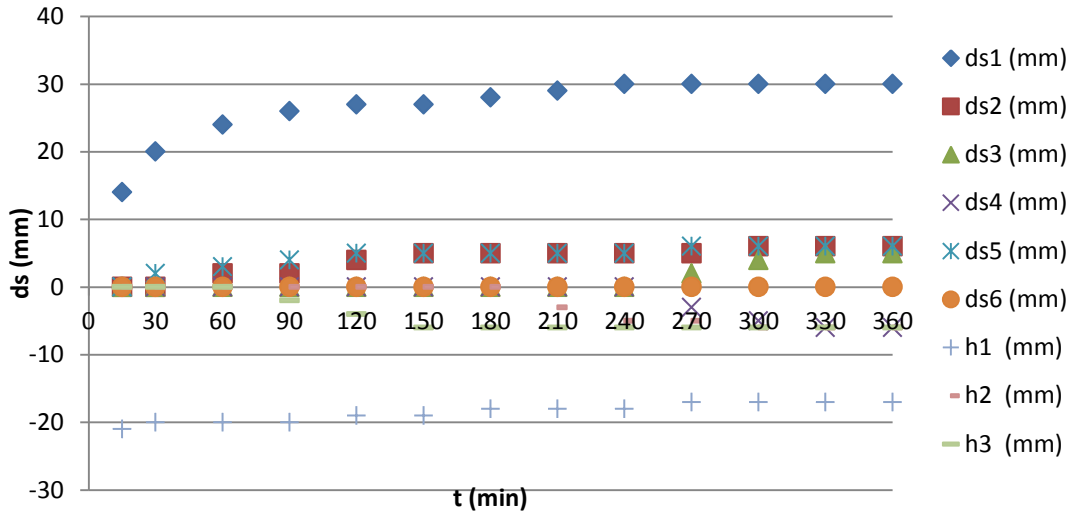

Figure A.1: Temporal development of local scour at all locations, Experiment #1 (d_0/D=0.740, β=0°)

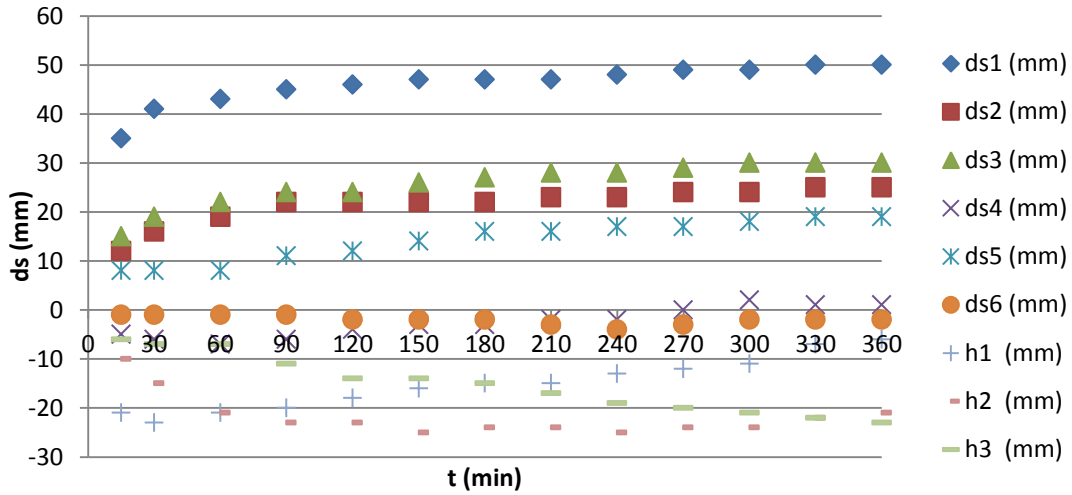

Figure A.2: Temporal development of local scour at all locations, Experiment #2 (d_0/D=0.940, β=0°)

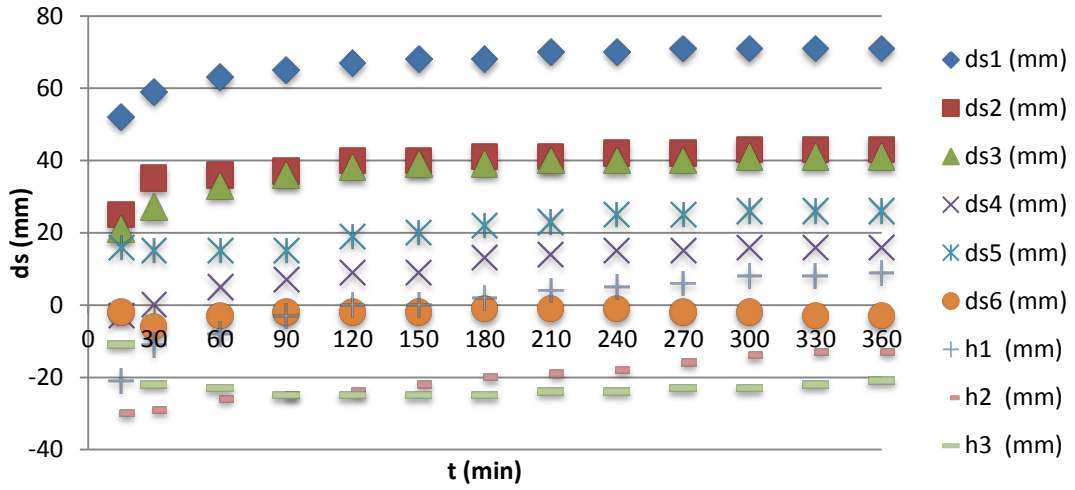

Figure A.3: Temporal development of local scour at all locations, Experiment #3 (d_0/D=1.080, β=0°)

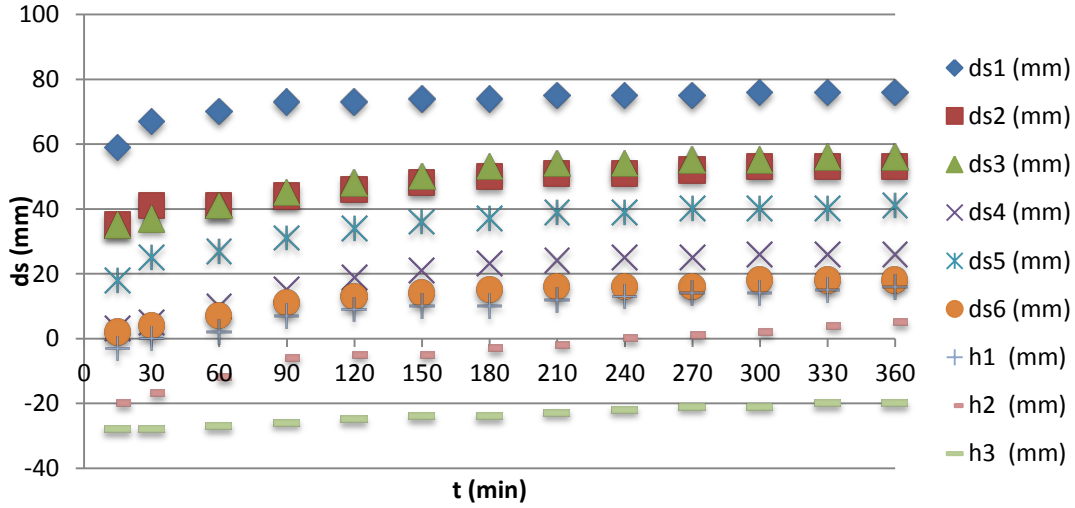

Figure A.4: Temporal development of local scour at all locations, Experiment #4 (d_0/D=1.280, β=0°)

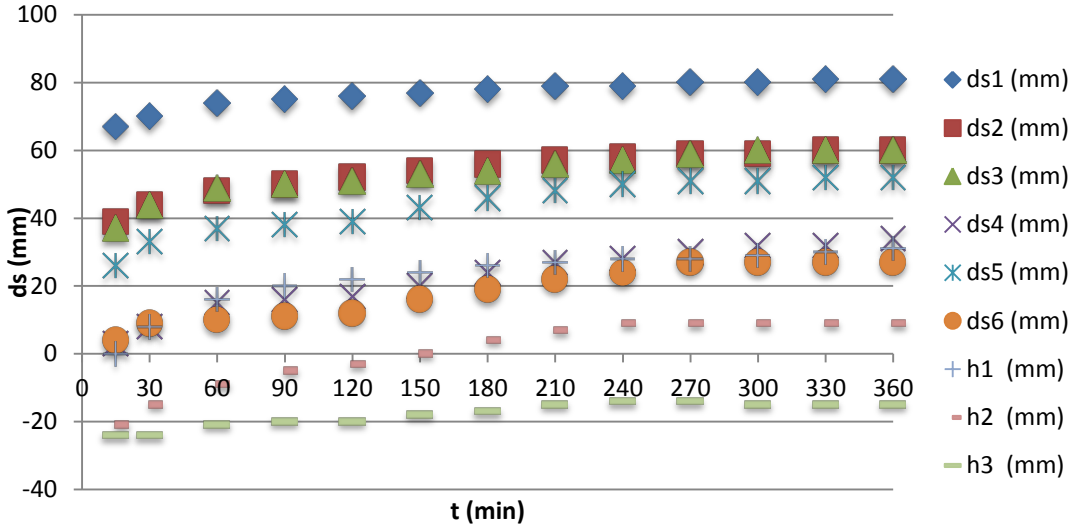

Figure A.5: Temporal development of local scour at all locations, Experiment #5 (d_0/D=1.380, β=0°)

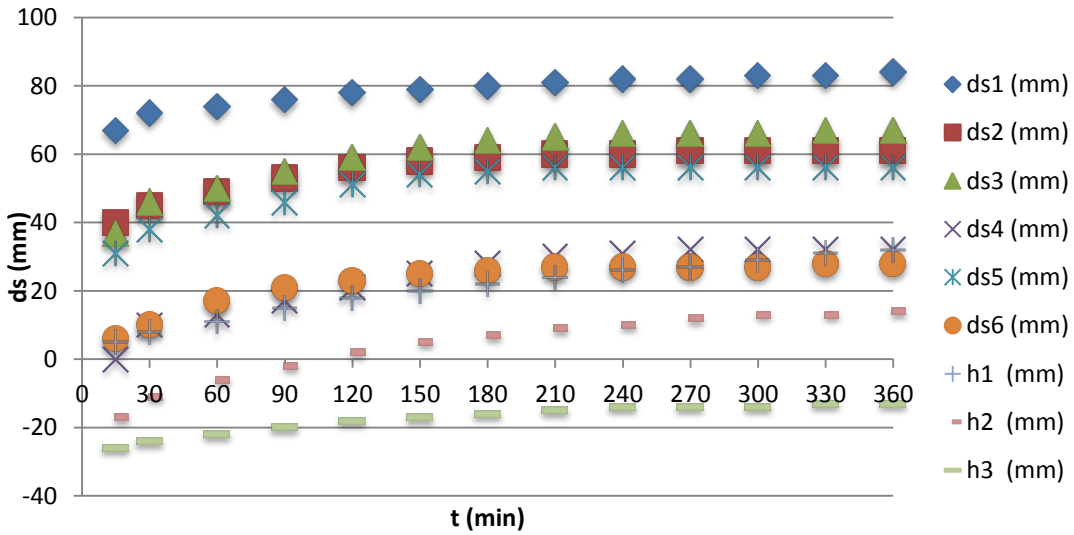

Figure A.6: Temporal development of local scour at all locations, Experiment #6 (d_0/D=1.480, β=0°)

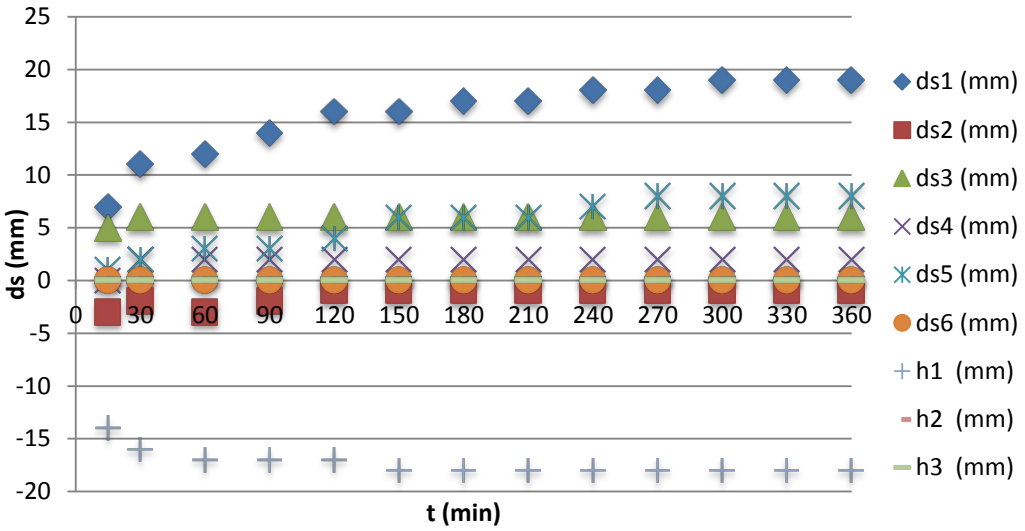

Figure A.7: Temporal development of local scour at all locations, Experiment #7 (d_0/D=0.740, β=10°)

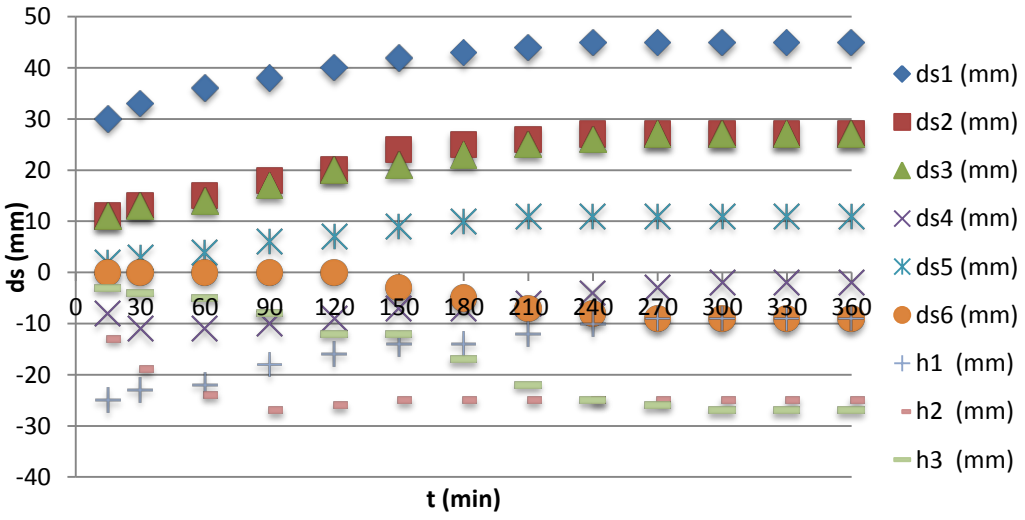

Figure A.8: Temporal development of local scour at all locations, Experiment #8 (d_0/D=0.940, β=10°)

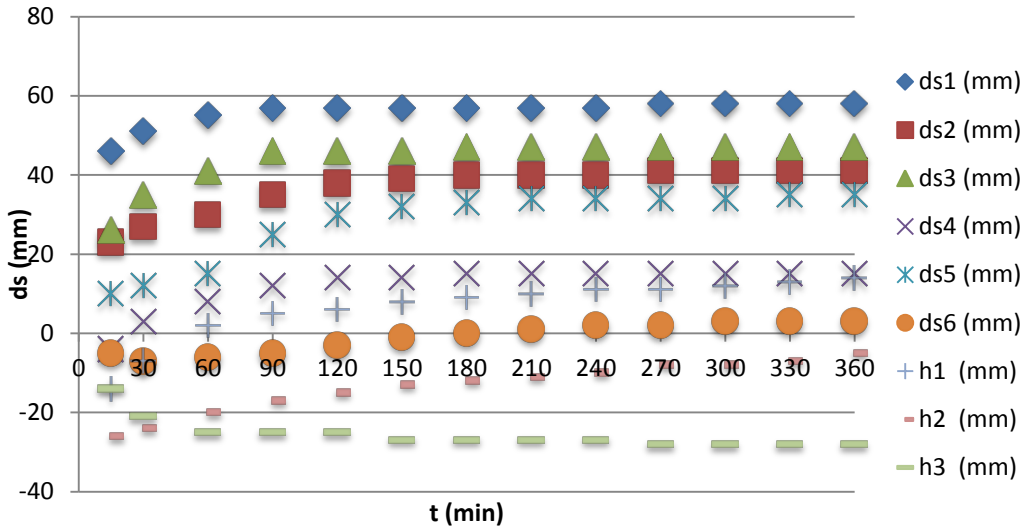

Figure A.9: Temporal development of local scour at all locations, Experiment #9 (d_0/D=1.080, β=10°)

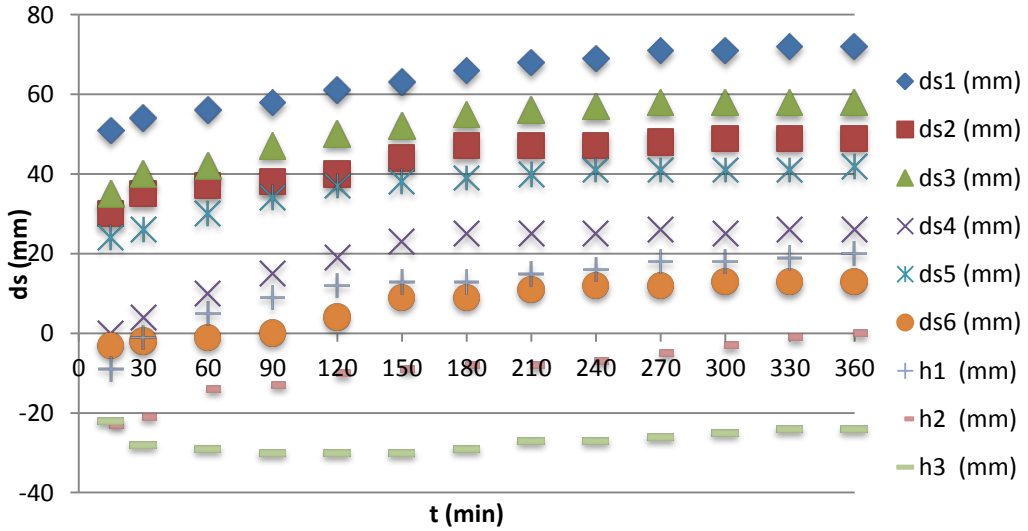

Figure A.10: Temporal development of local scour at all locations, Experiment #10 (d_0/D=1.280, β=10°)

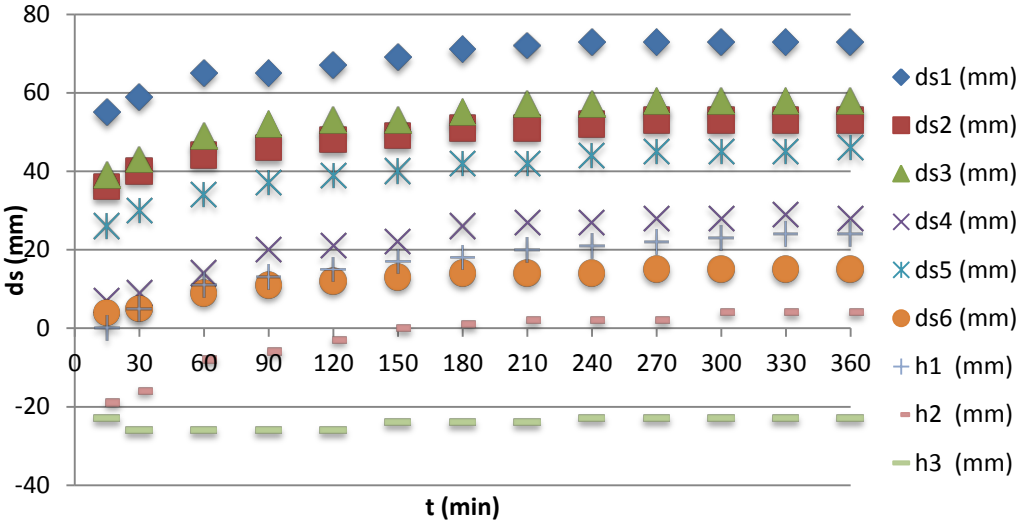

Figure A.11: Temporal development of local scour at all locations, Experiment #11 (d_0/D=1.380, β=10°)

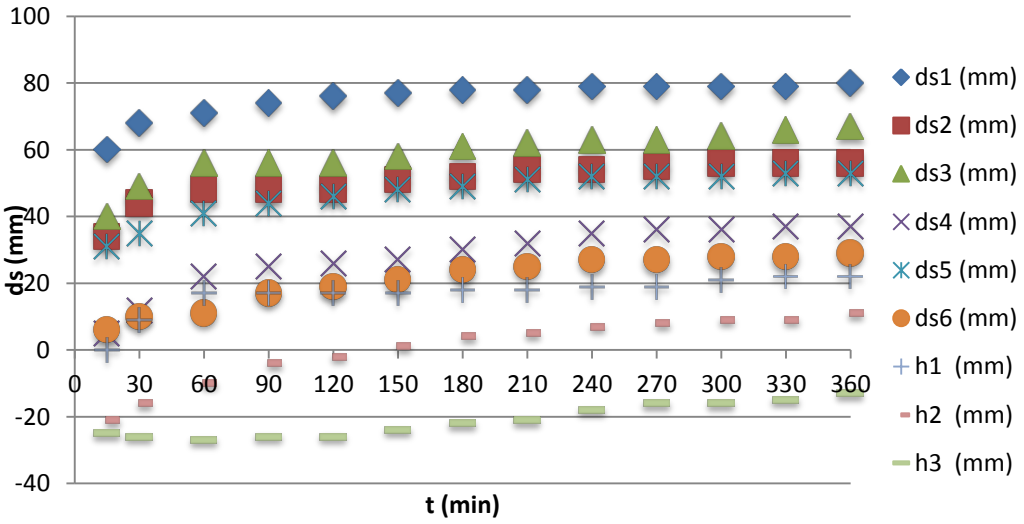

Figure A.12: Temporal development of local scour at all locations, Experiment #12 (d_0/D=1.480, β=10°)

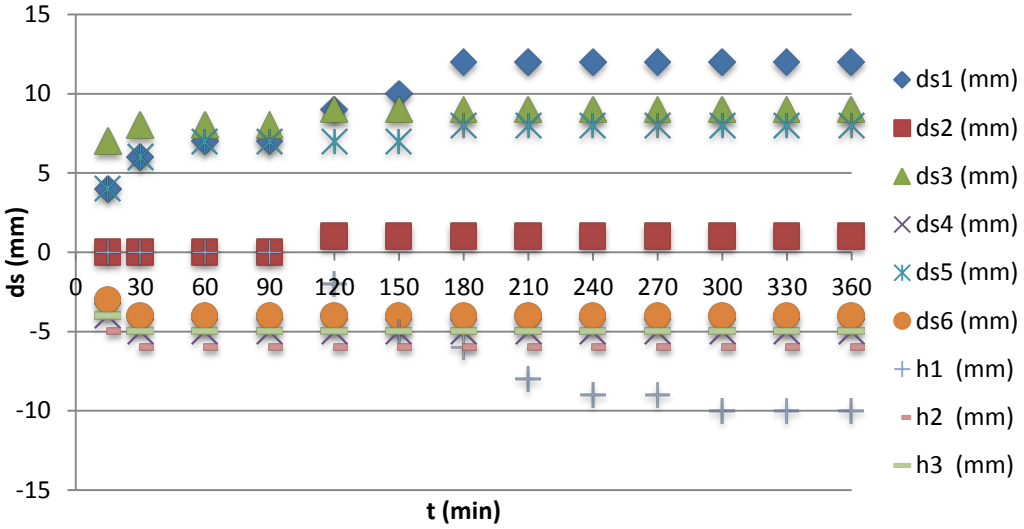

Figure A.13: Temporal development of local scour at all locations, Experiment #13 (d_0/D=0.740, β=15°)

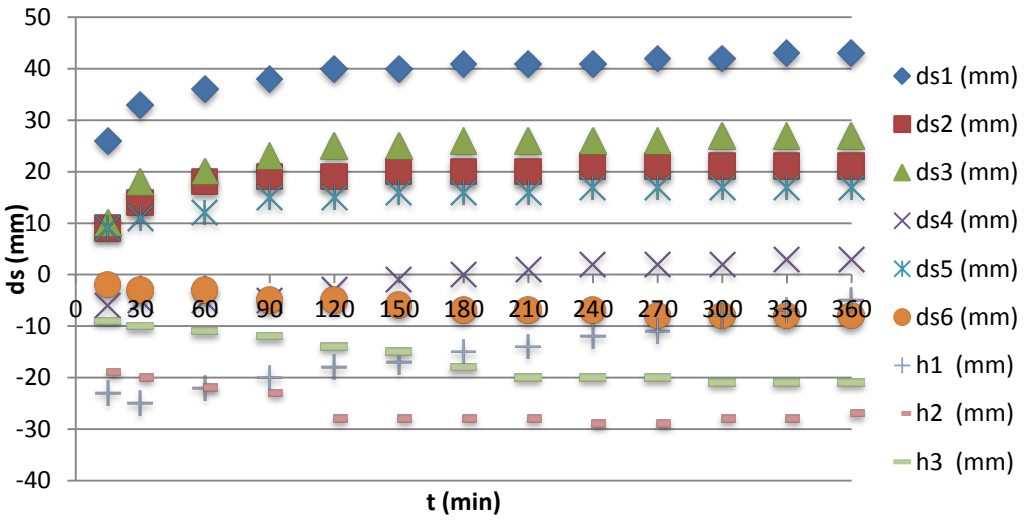

Figure A.14: Temporal development of local scour at all locations, Experiment #14 (d_0/D=0.940, β=15°)

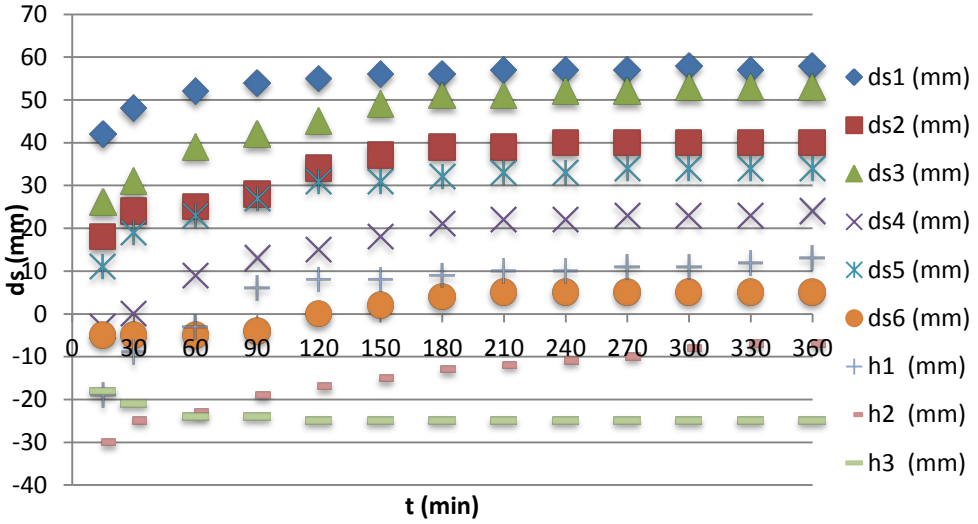

Figure A.15: Temporal development of local scour at all locations, Experiment #15 (d_0/D=1.080, β=15°)

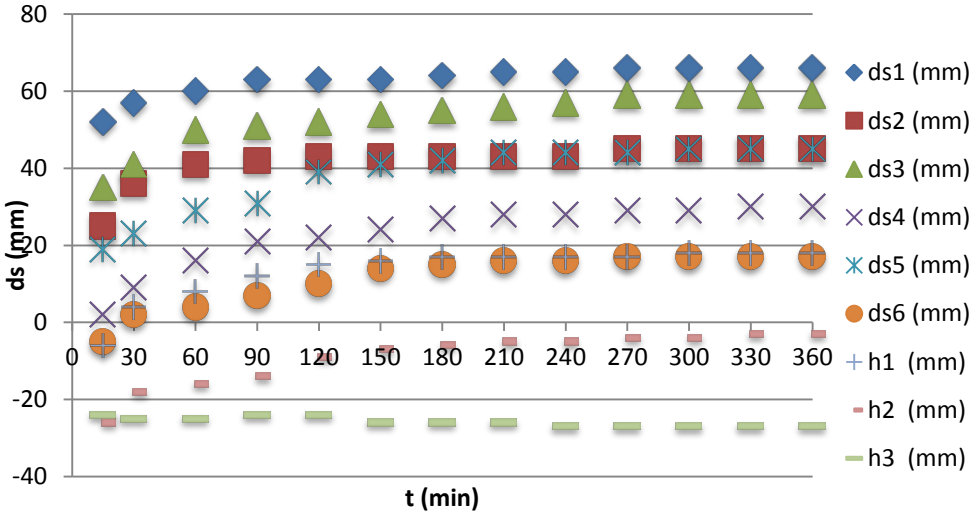

Figure A.16: Temporal development of local scour at all locations, Experiment #16 (d_0/D=1.280, β=15°)

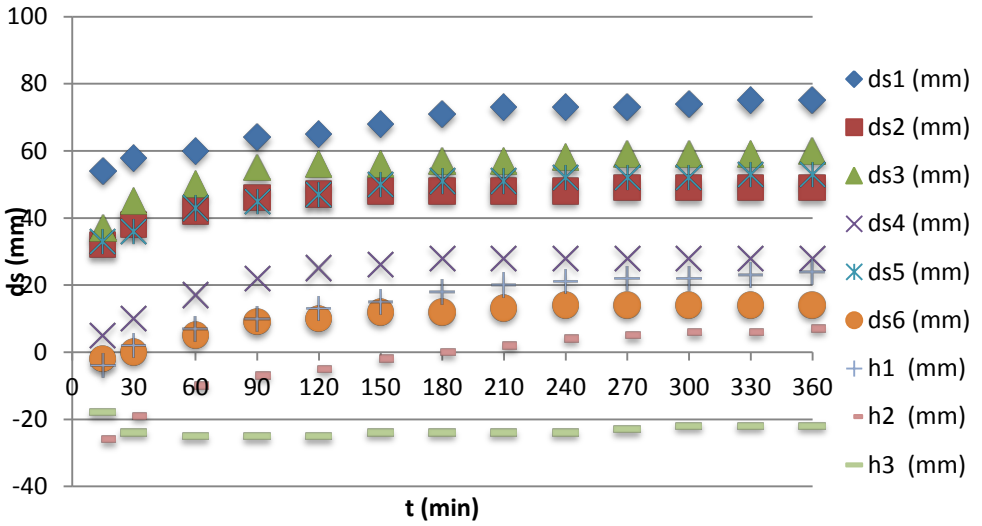

Figure A.17: Temporal development of local scour at all locations, Experiment #17 (d_0/D=1.380, β=15°)

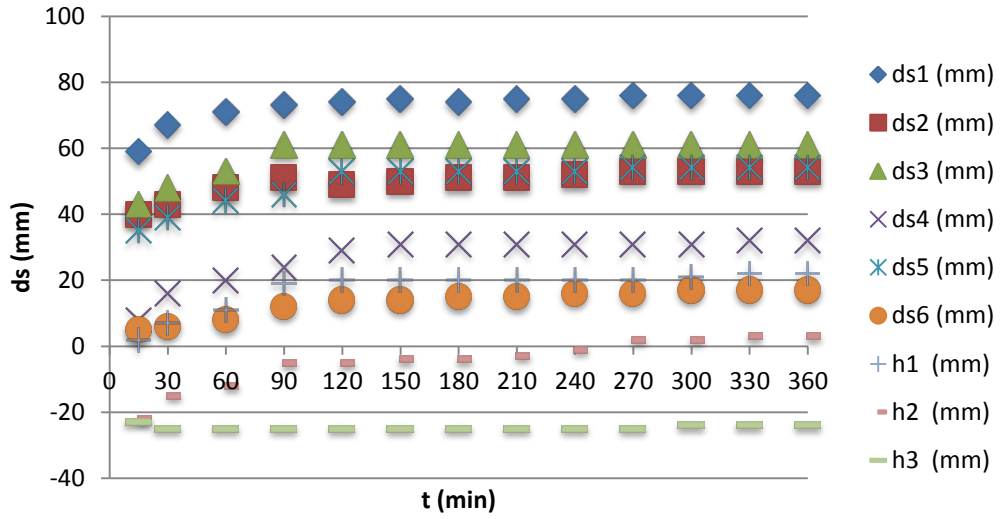

Figure A.18: Temporal development of local scour at all locations, Experiment #18 (d_0/D=1.480, β=15°)

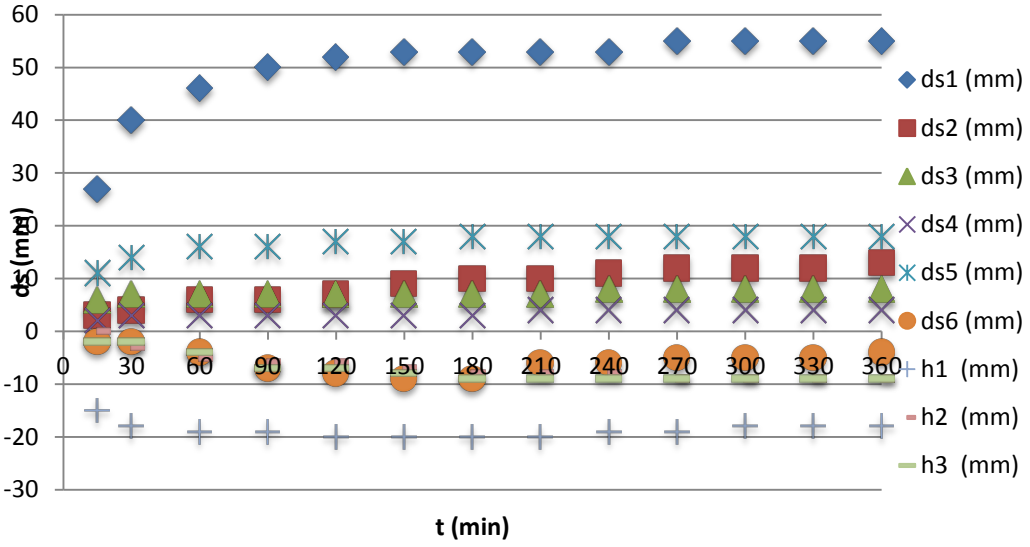

Figure A.19: Temporal development of local scour at all locations, Experiment #19 ($d_0/D=0.529$, $\beta=0°$)

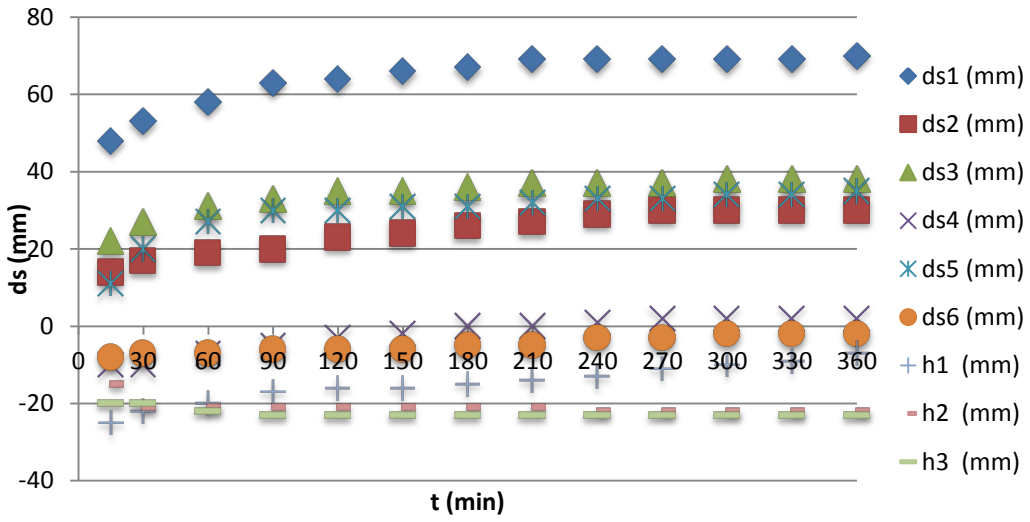

Figure A.20: Temporal development of local scour at all locations, Experiment #20 ($d_0/D=0.671$, $\beta=0°$)

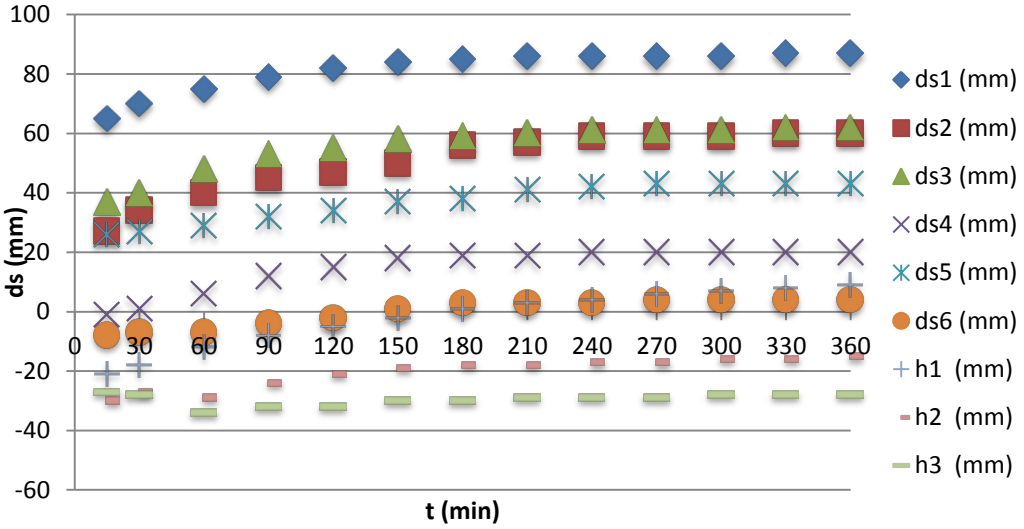

Figure A.21: Temporal development of local scour at all locations, Experiment #21 (d_0/D=0.771, β=0°)

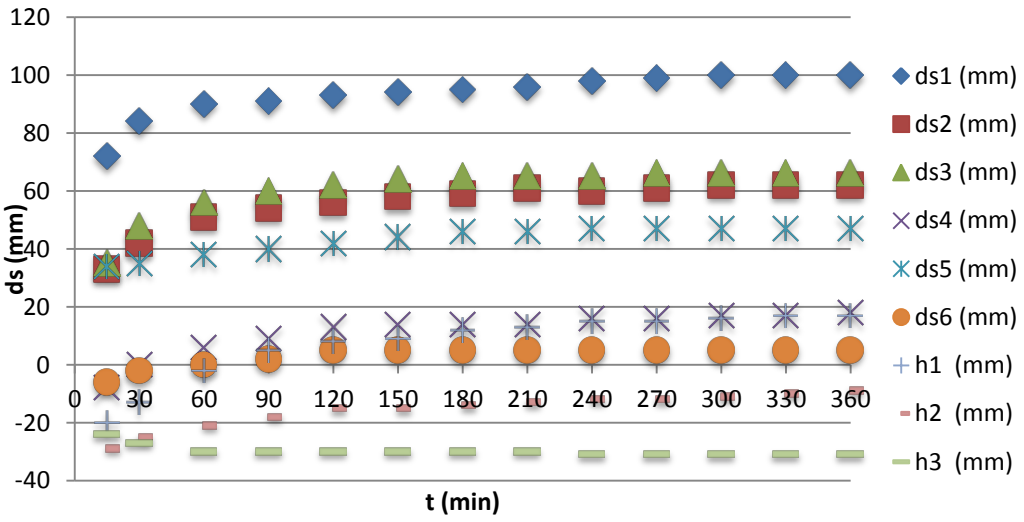

Figure A.22: Temporal development of local scour at all locations, Experiment #22 (d_0/D=0.914, β=0°)

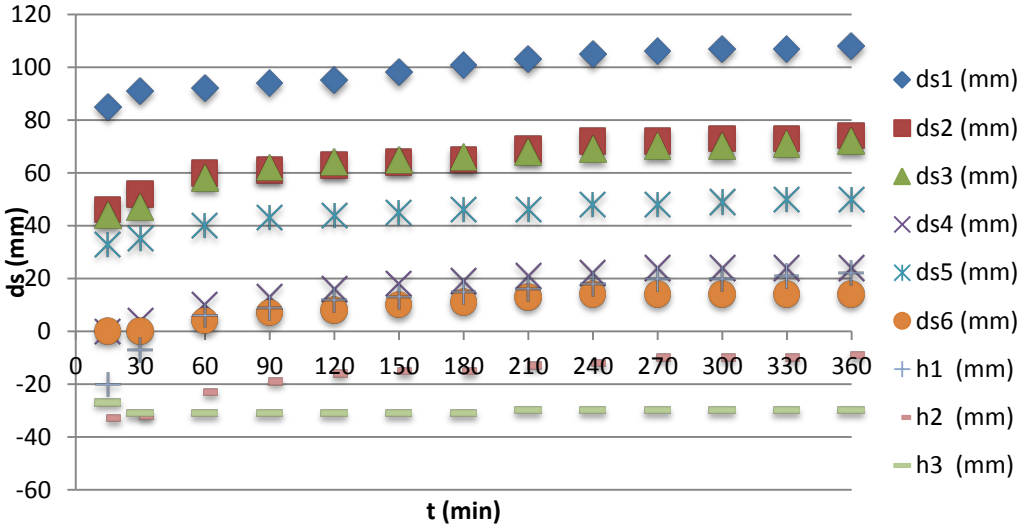

Figure A.23: Temporal development of local scour at all locations, Experiment #23 (d_0/D=0.986, β=0°)

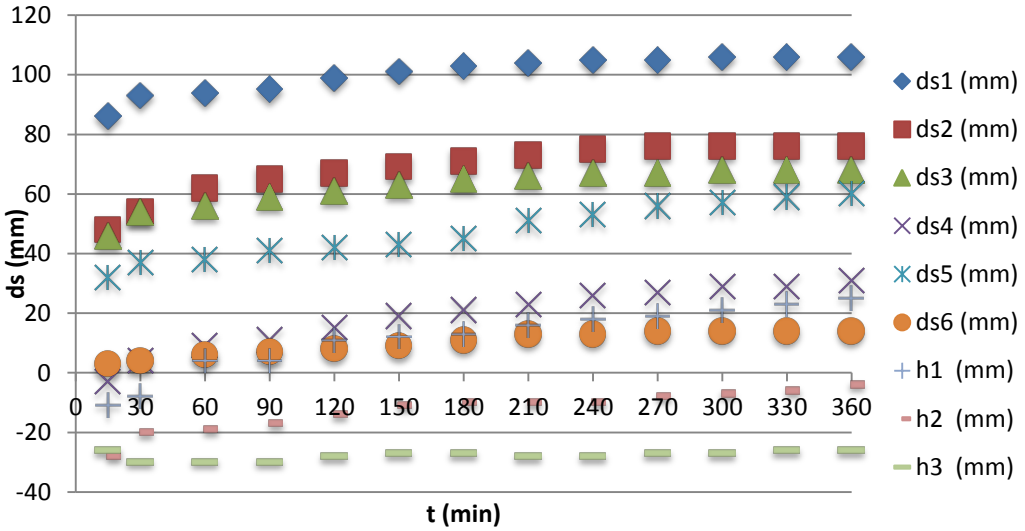

Figure A.24: Temporal development of local scour at all locations, Experiment #24 (d_0/D=1.480, β=0°)

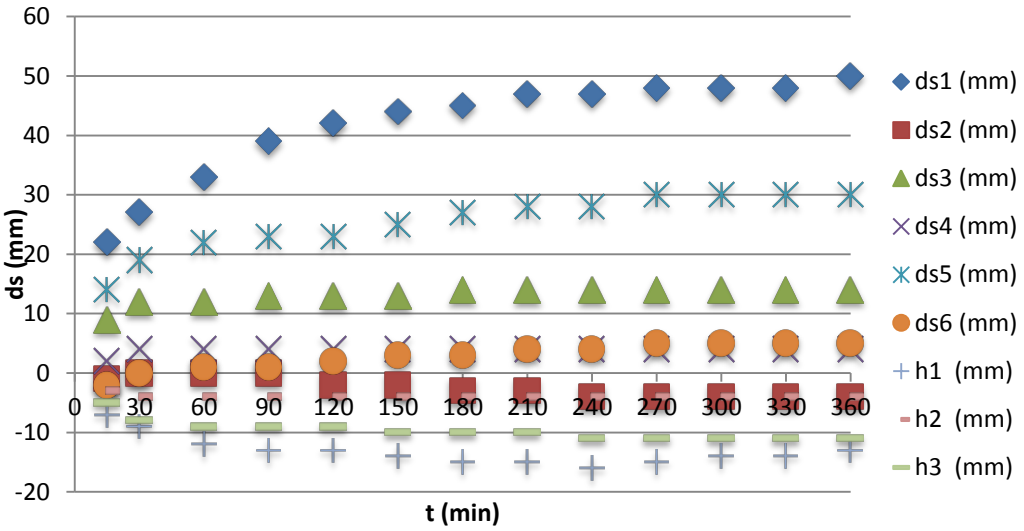

Figure A.25: Temporal development of local scour at all locations, Experiment #25 ($d_0/D=0.529$, $\beta=10°$)

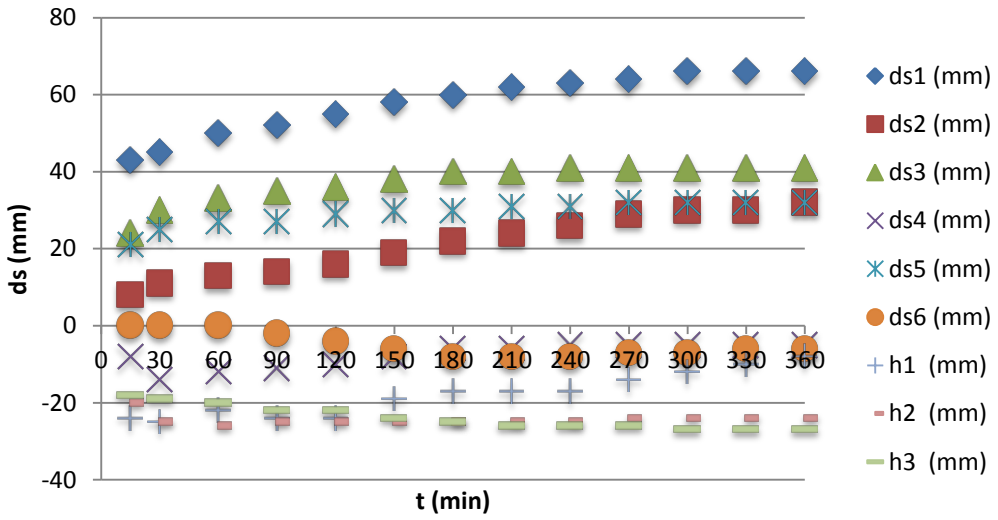

Figure A.26: Temporal development of local scour at all locations, Experiment #26 ($d_0/D=0.671$, $\beta=10°$)

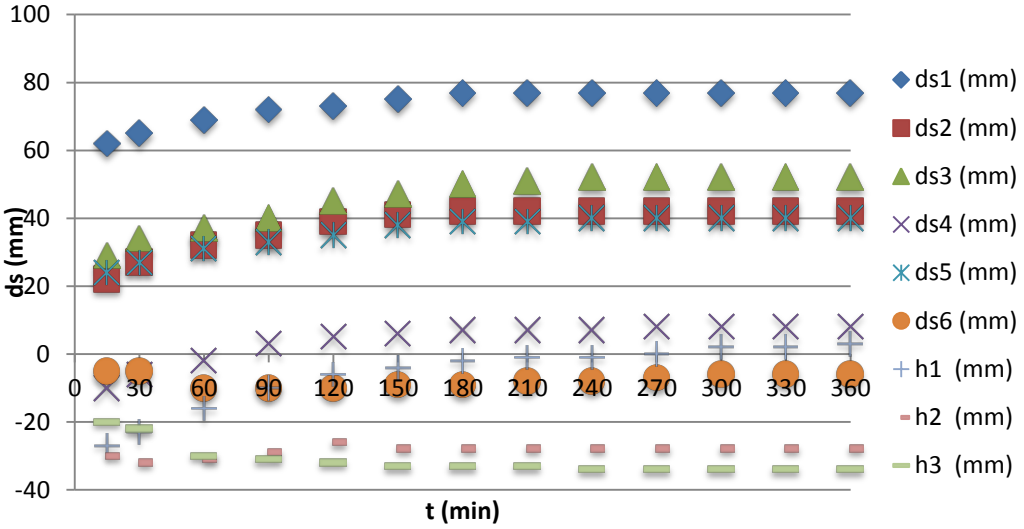

Figure A.27: Temporal development of local scour at all locations, Experiment #27 (d_0/D=0.771, β=10°)

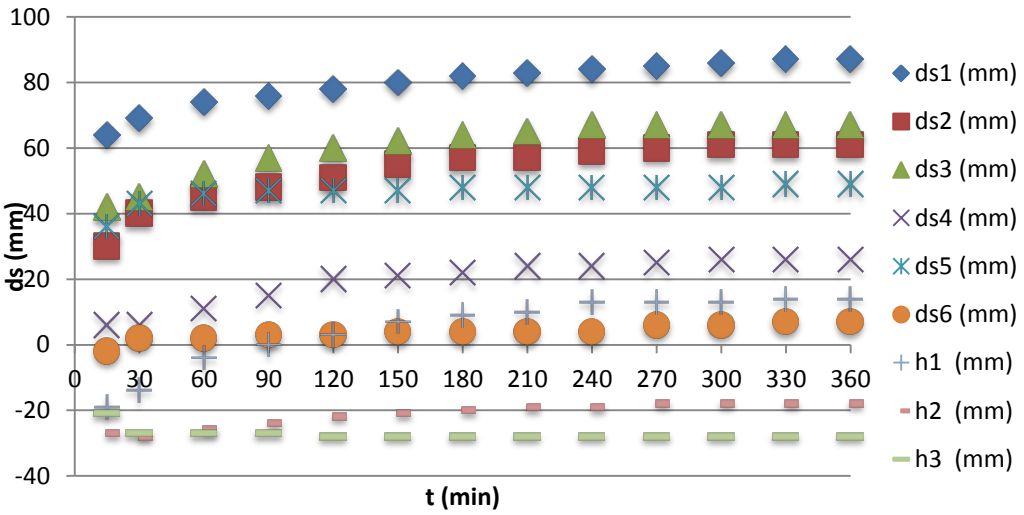

Figure A.28: Temporal development of local scour at all locations, Experiment #28 (d_0/D=0.914, β=10°)

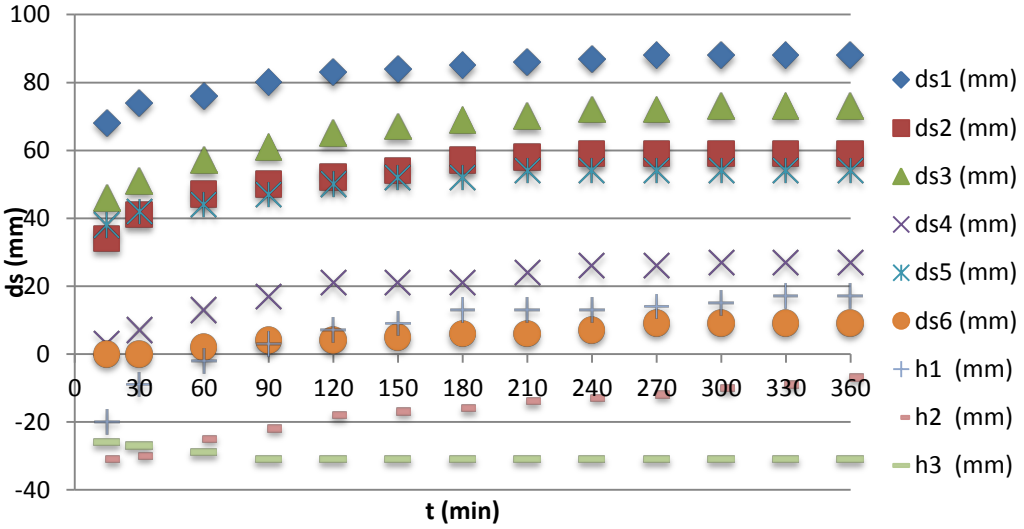

Figure A.29: Temporal development of local scour at all locations, Experiment #29 (d_0/D=0.986, β=10°)

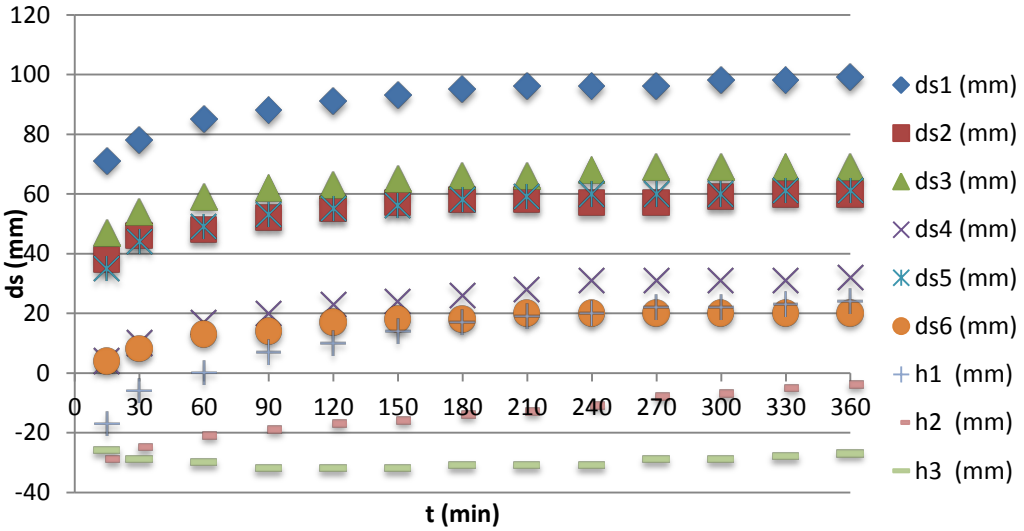

Figure A.30: Temporal development of local scour at all locations, Experiment #30 (d_0/D= 1.057, β=10°)

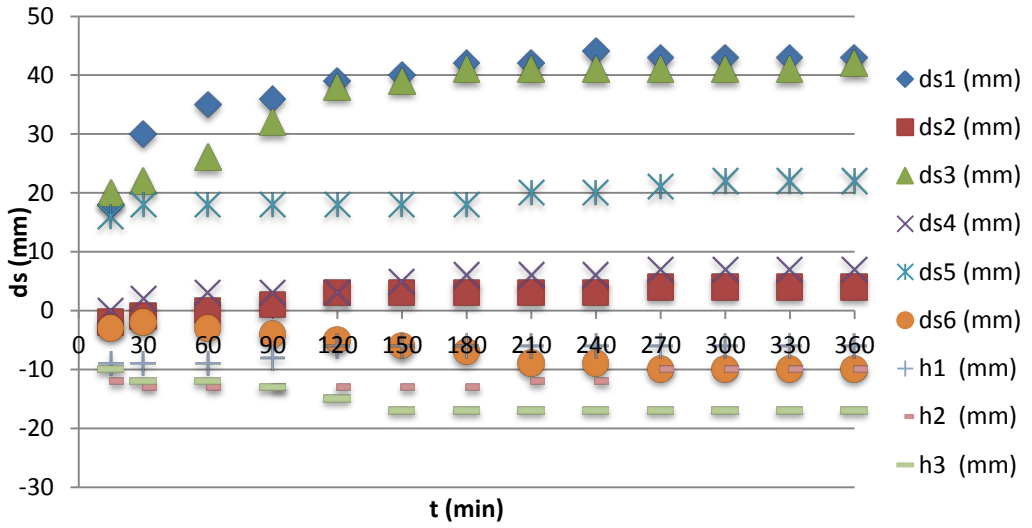

Figure A.31: Temporal development of local scour at all locations, Experiment #31 ($d_0/D=0.529$, $\beta=15°$)

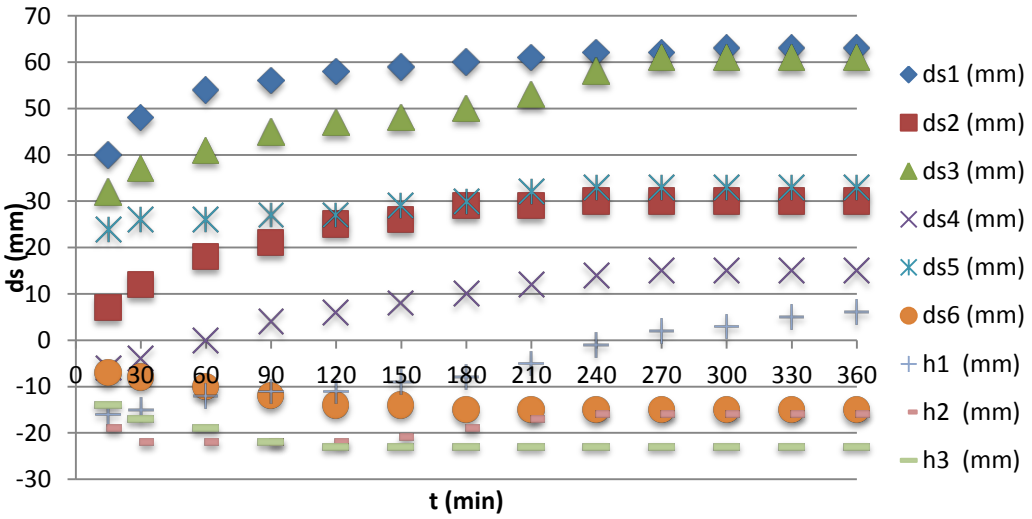

Figure A.32: Temporal development of local scour at all locations, Experiment #32 ($d_0/D=0.671$, $\beta=15°$)

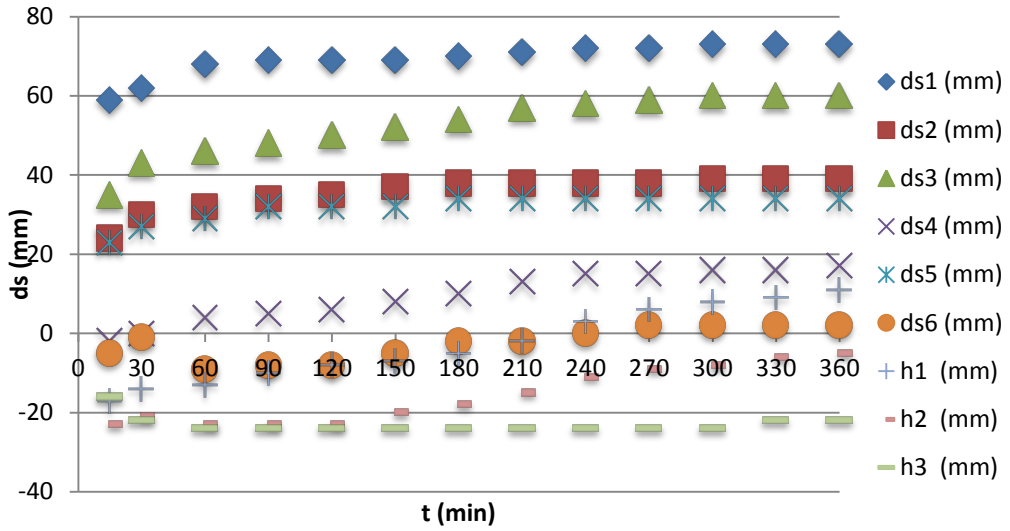

Figure A.33: Temporal development of local scour at all locations, Experiment #33 (d_0/D=0.771, β=15°)

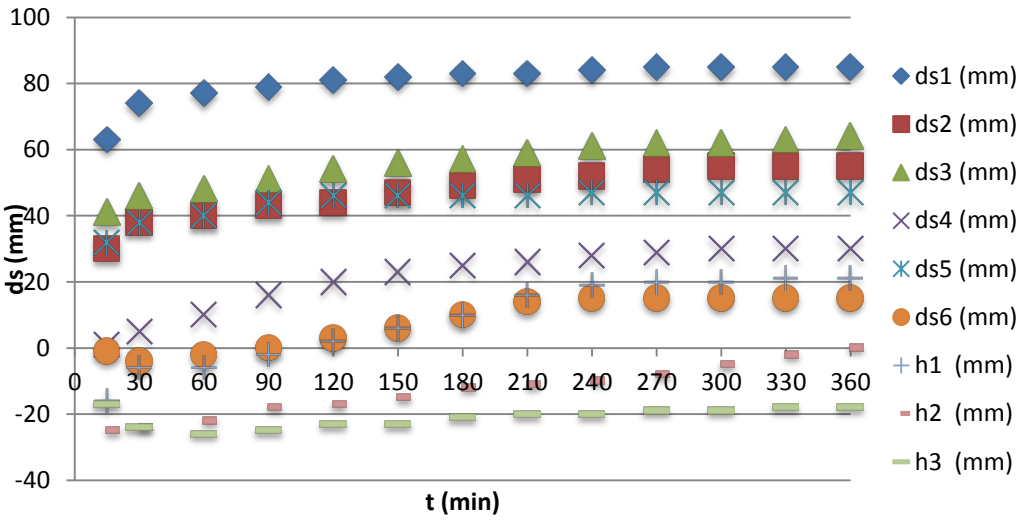

Figure A.34: Temporal development of local scour at all locations, Experiment #34 (d_0/D=0.914, β=15°)

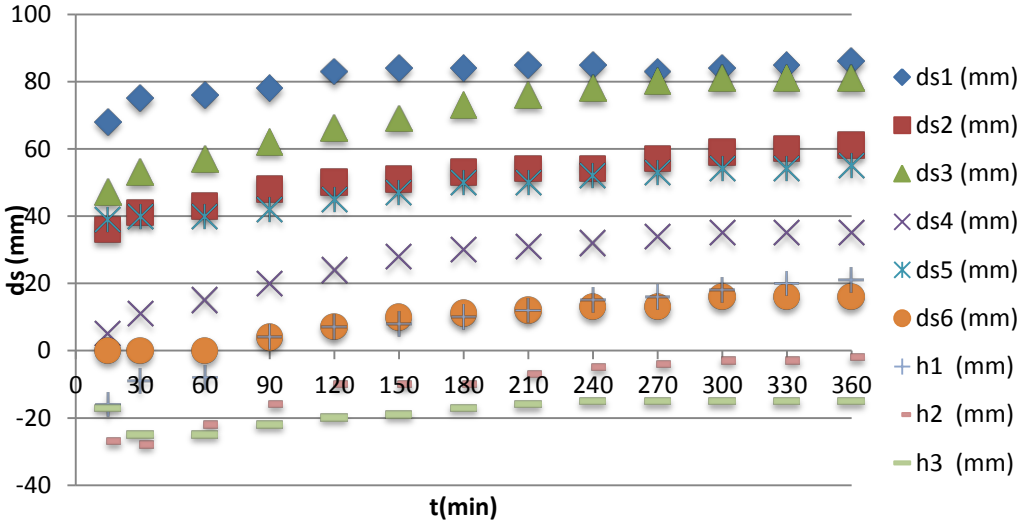

Figure A.35: Temporal development of local scour at all locations, Experiment #35 (d_0/D=0.986, β=15°)

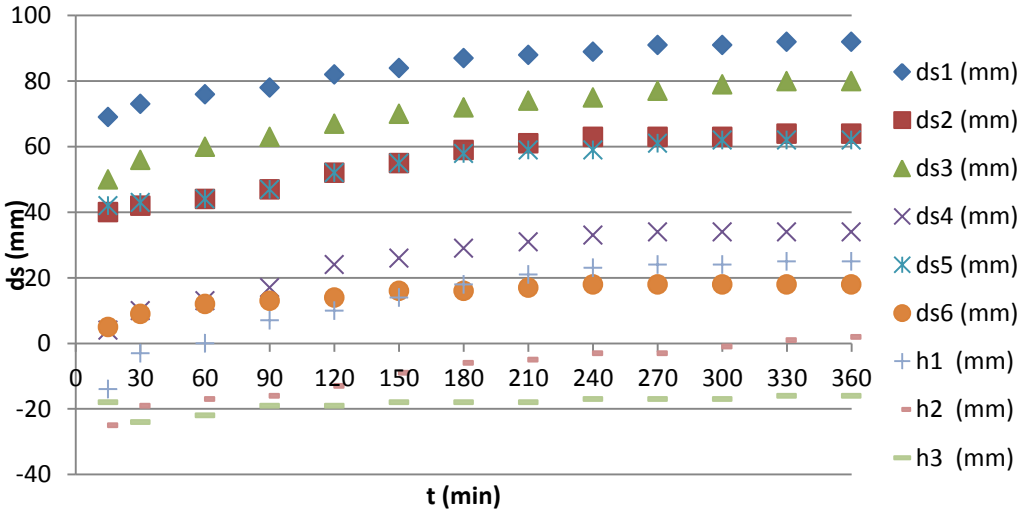

Figure A.36: Temporal development of local scour at all locations, Experiment #36 (d_0/D=1.057, β=15°)

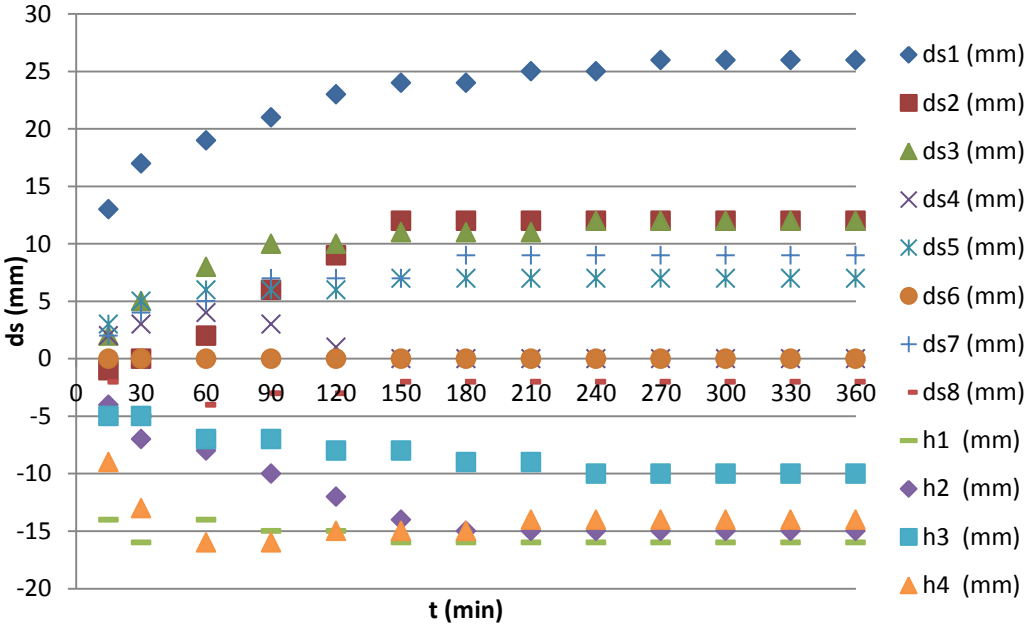

Figure A.37: Temporal development of local scour at all locations, Experiment #37 (d_0/D=0.740, β=0°)

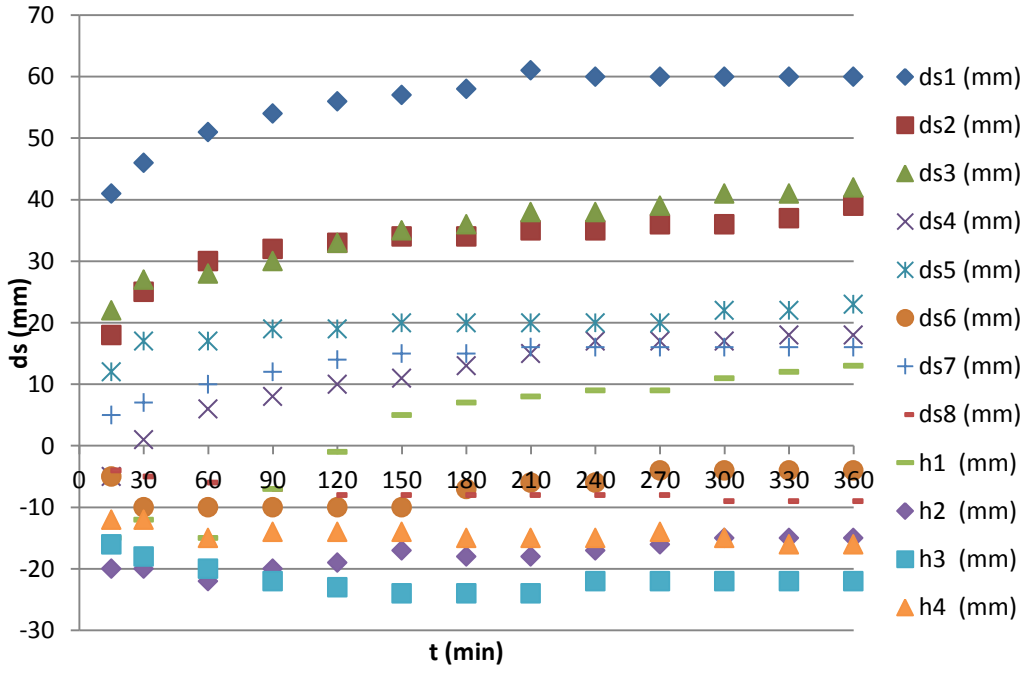

Figure A.38: Temporal development of local scour at all locations, Experiment #38 (d_0/D=0.940, β=0°)

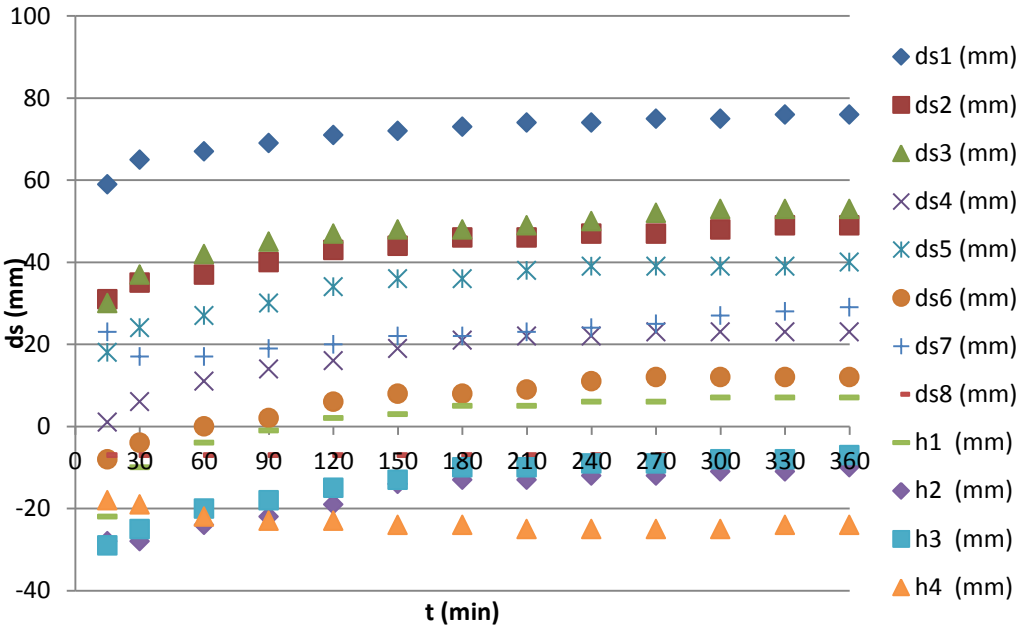

Figure A.39: Temporal development of local scour at all locations, Experiment #39 (d_0/D=1.080, β=0°)

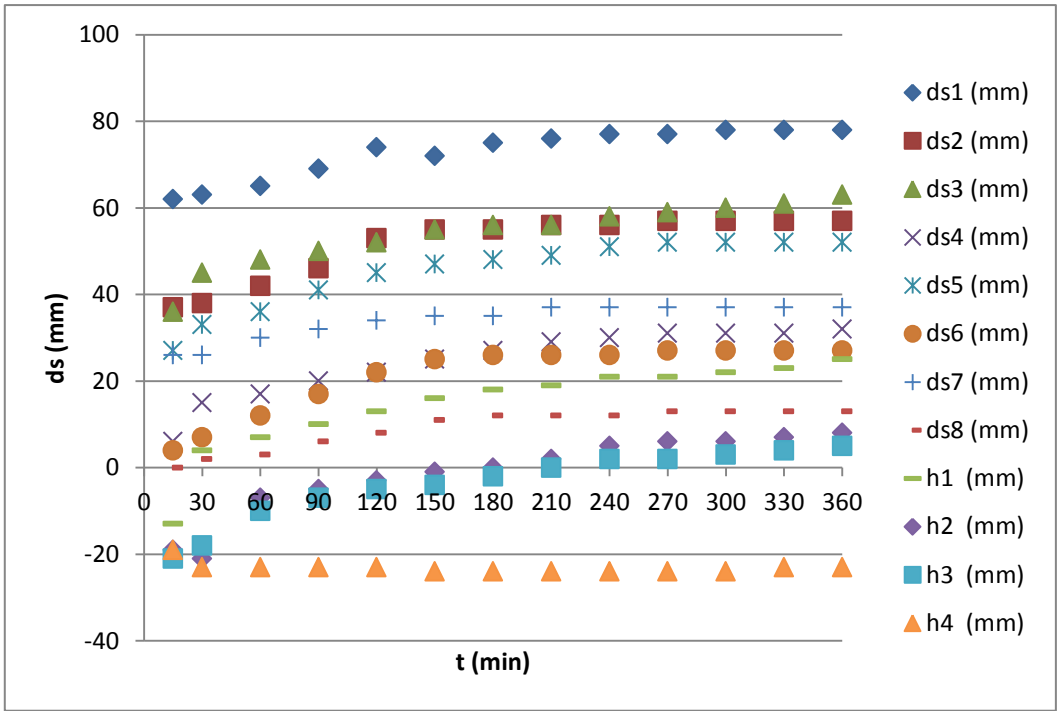

Figure A.40: Temporal development of local scour at all locations, Experiment #40 (d_0/D=1.280, β=0°)

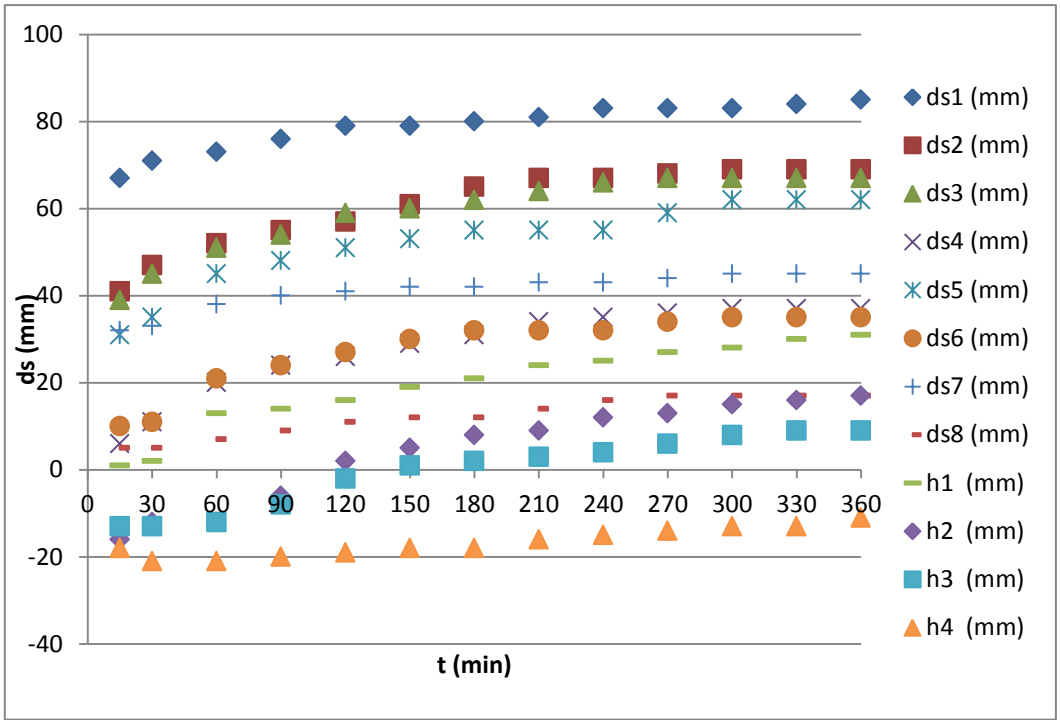

Figure A.41: Temporal development of local scour at all locations, Experiment #41 (d_0/D=1.380, β=0°)

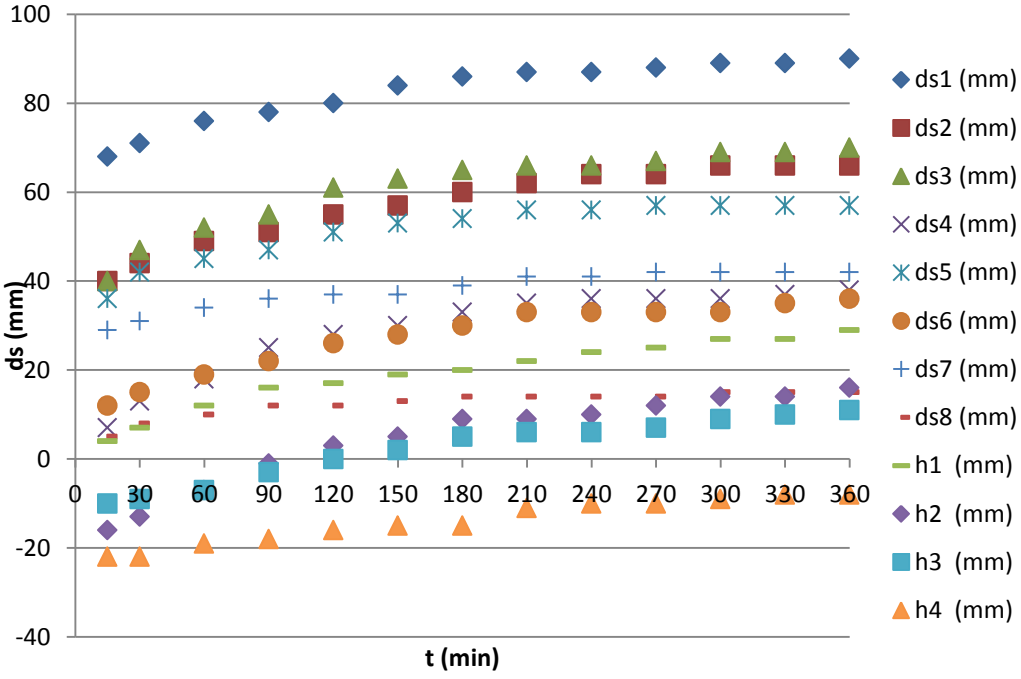

Figure A.42: Temporal development of local scour at all locations, Experiment #42 (d_0/D=1.480, β=0°)

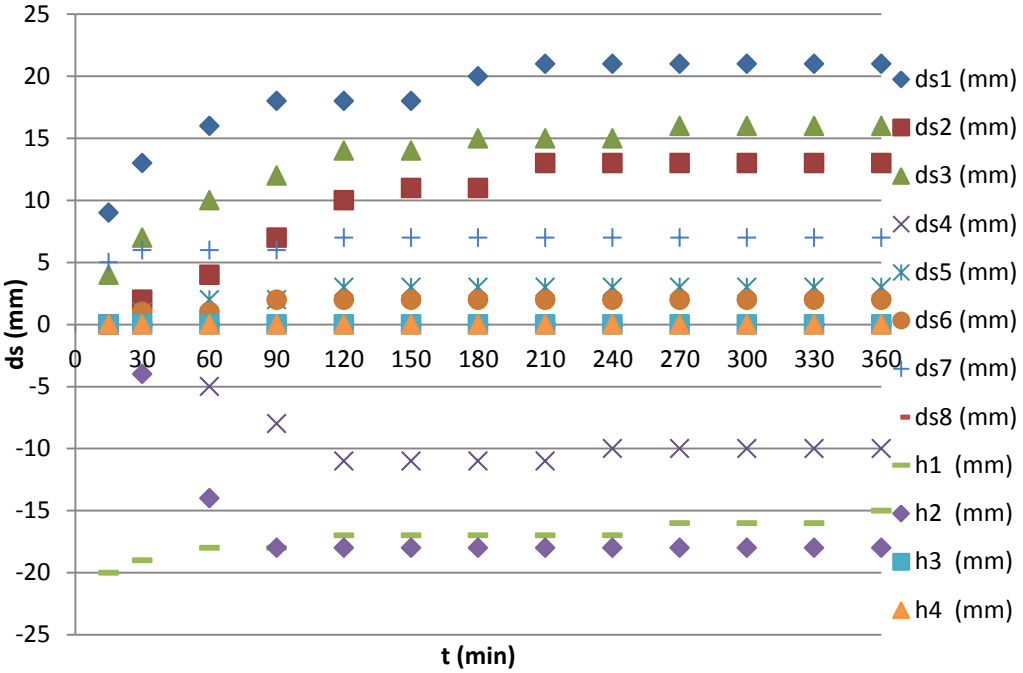

Figure A.43: Temporal development of local scour at all locations, Experiment #43 (d_0/D=0.740, β=10°)

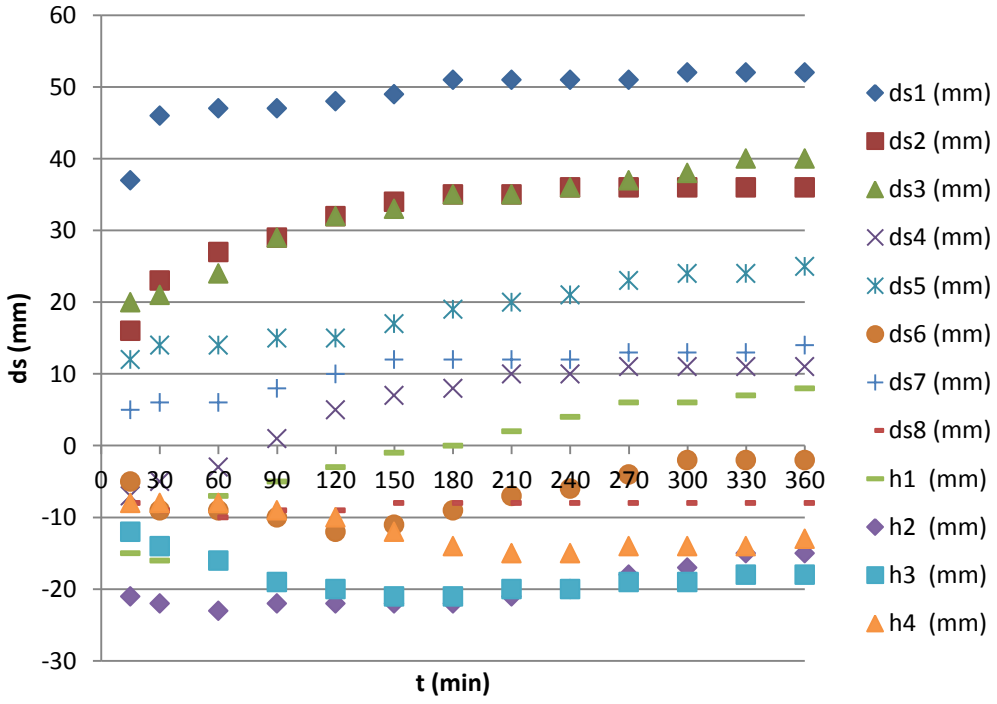

Figure A.44: Temporal development of local scour at all locations, Experiment #44 (d_0/D=0.940, β=10°)

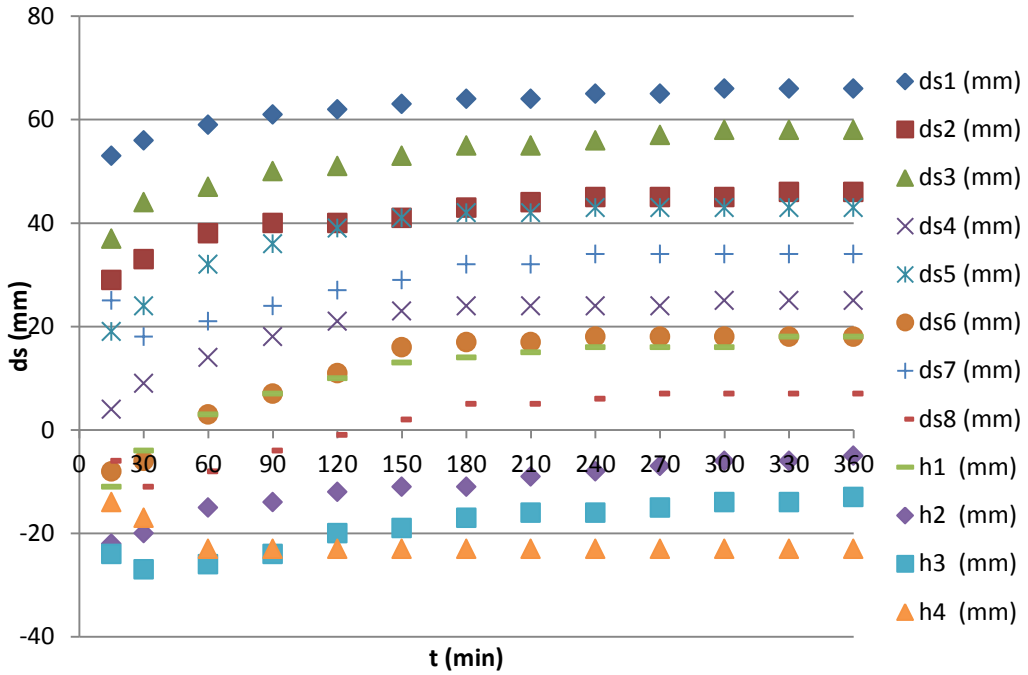

Figure A.45: Temporal development of local scour at all locations, Experiment #45 (d_0/D=1.080, β=10°)

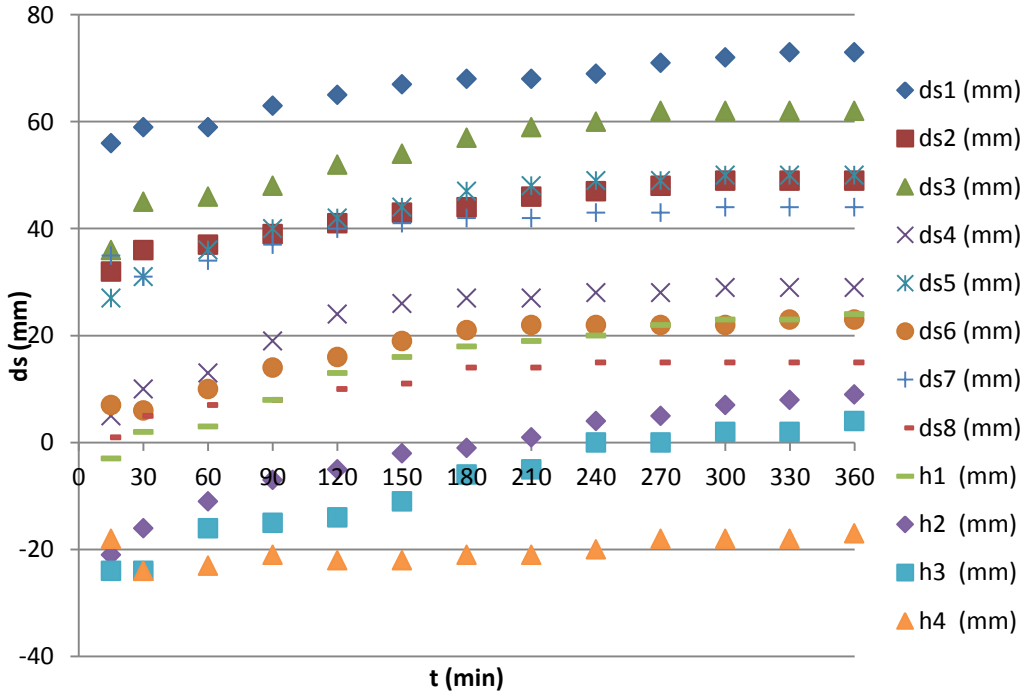

Figure A.46: Temporal development of local scour at all locations, Experiment #46 (d_0/D=1.280, β=10°)

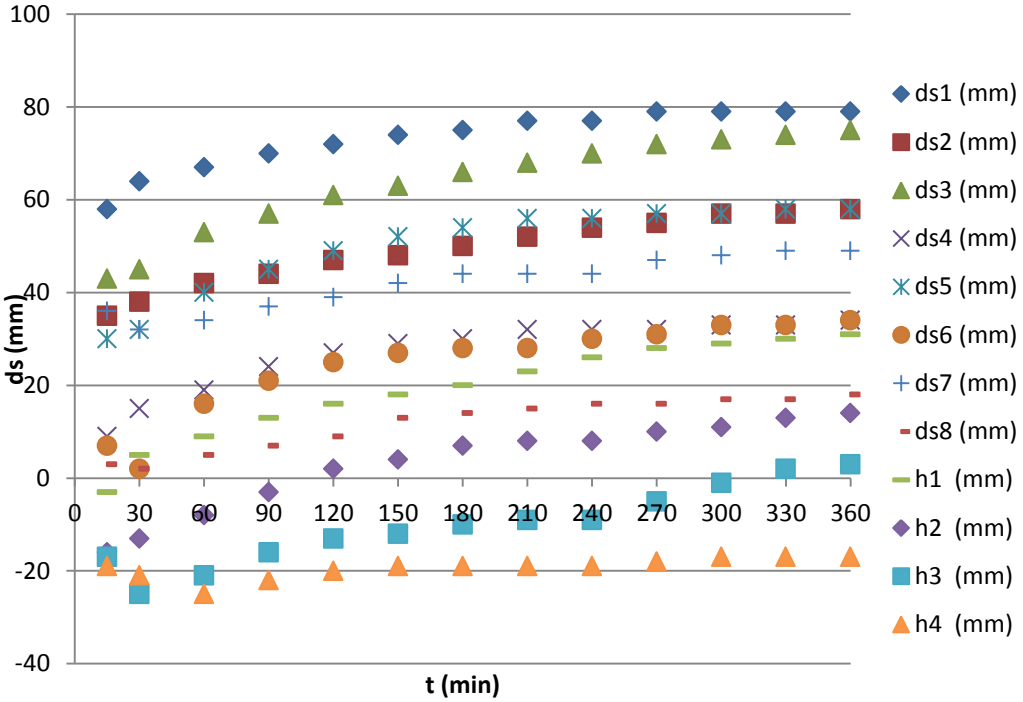

Figure A.47: Temporal development of local scour at all locations, Experiment #47 (d_0/D=1.380, β=10°)

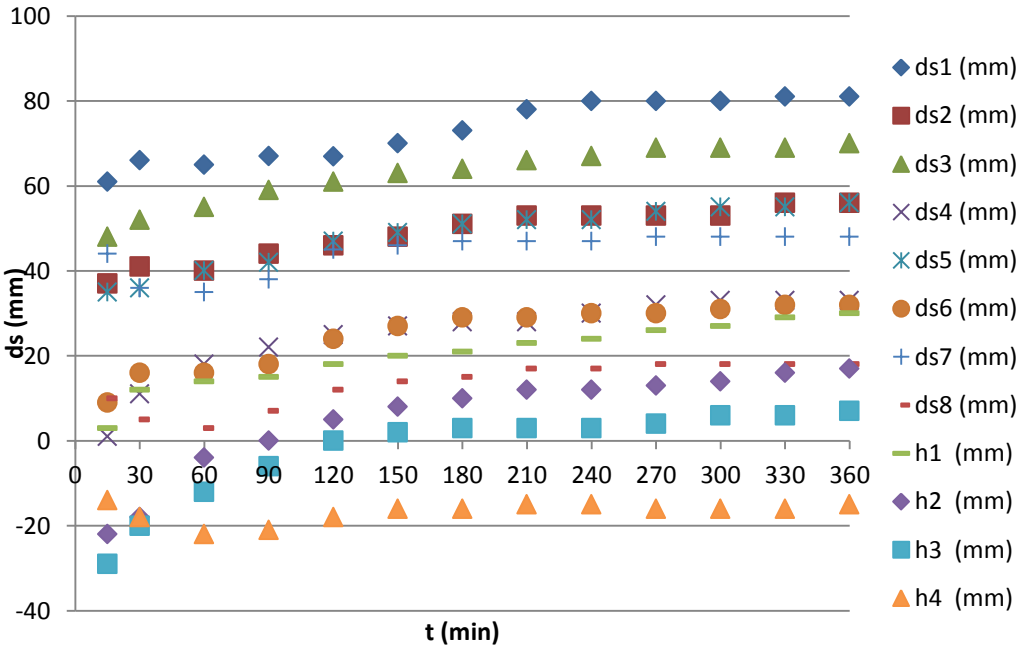

Figure A.48: Temporal development of local scour at all locations, Experiment #48 (d_0/D=1.480, β=10°)

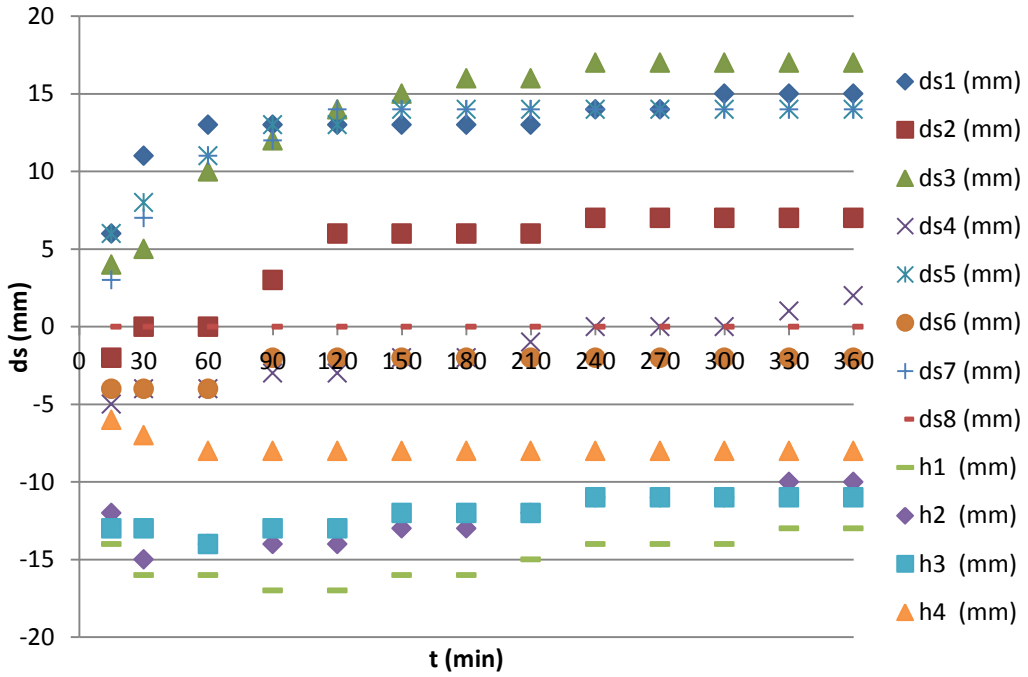

Figure A.49: Temporal development of local scour at all locations, Experiment #49 (d_0/D=0740, β=15°)

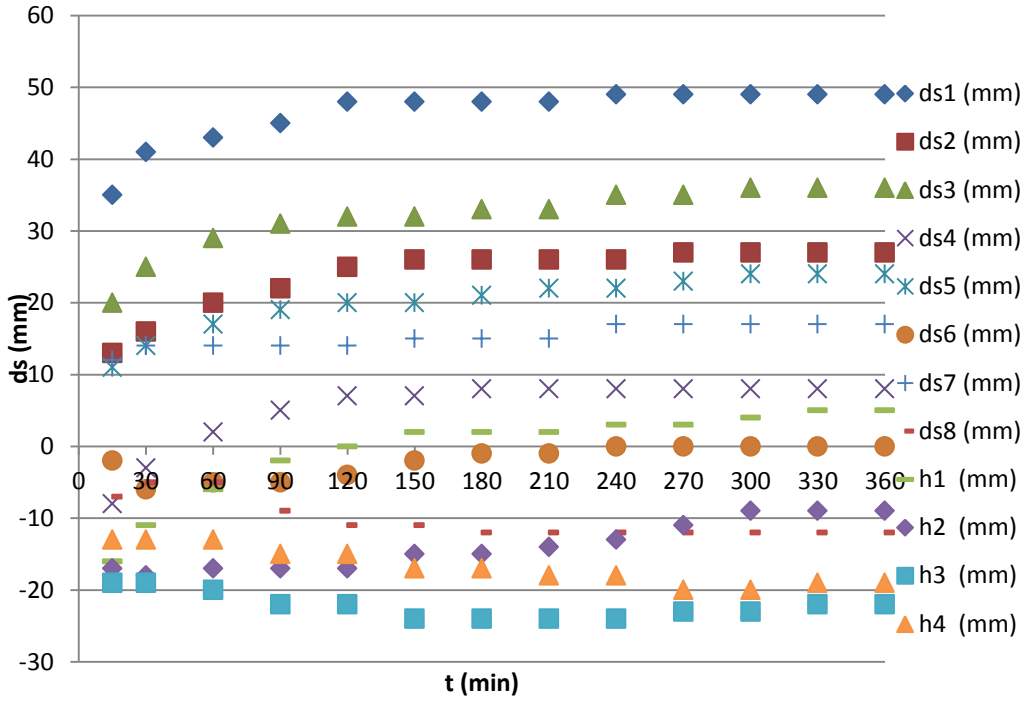

Figure A.50: Temporal development of local scour at all locations, Experiment #50 (d_0/D=0.940, β=15°)

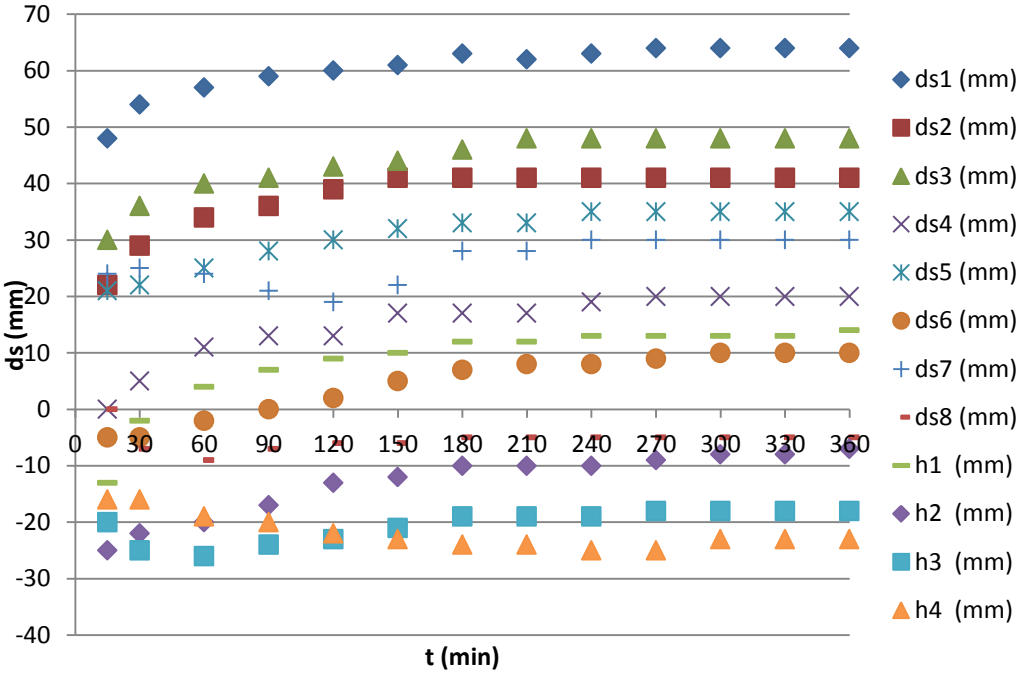

Figure A.51: Temporal development of local scour at all locations, Experiment #51 (d_0/D=1.080 , β=15°)

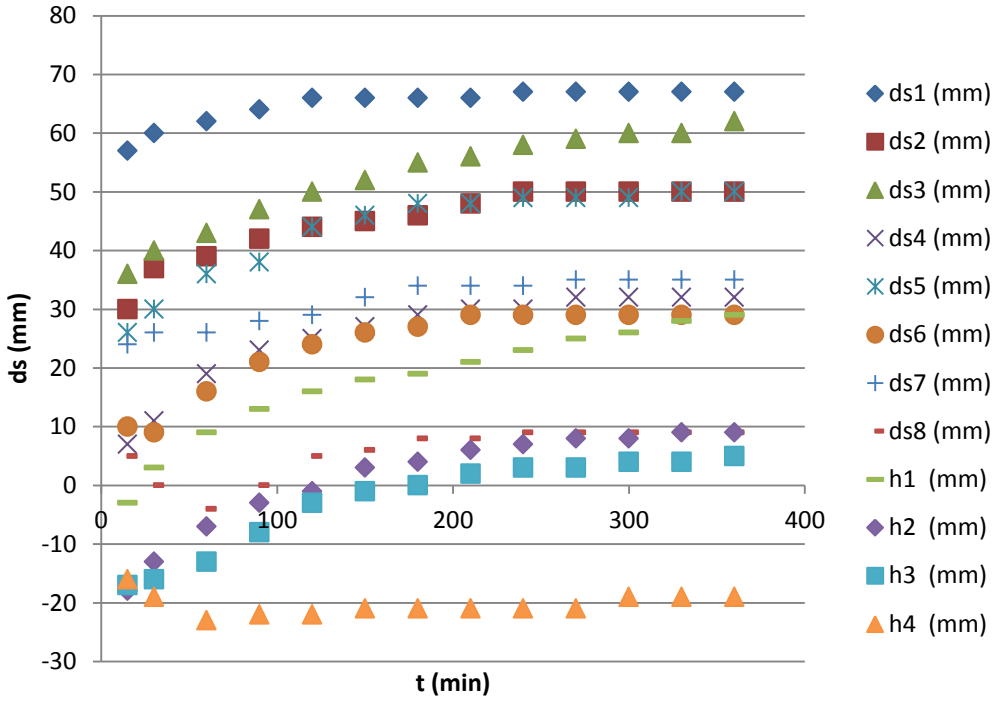

Figure A.52: Temporal development of local scour at all locations, Experiment #52 (d_0/D=1.280, β=15°)

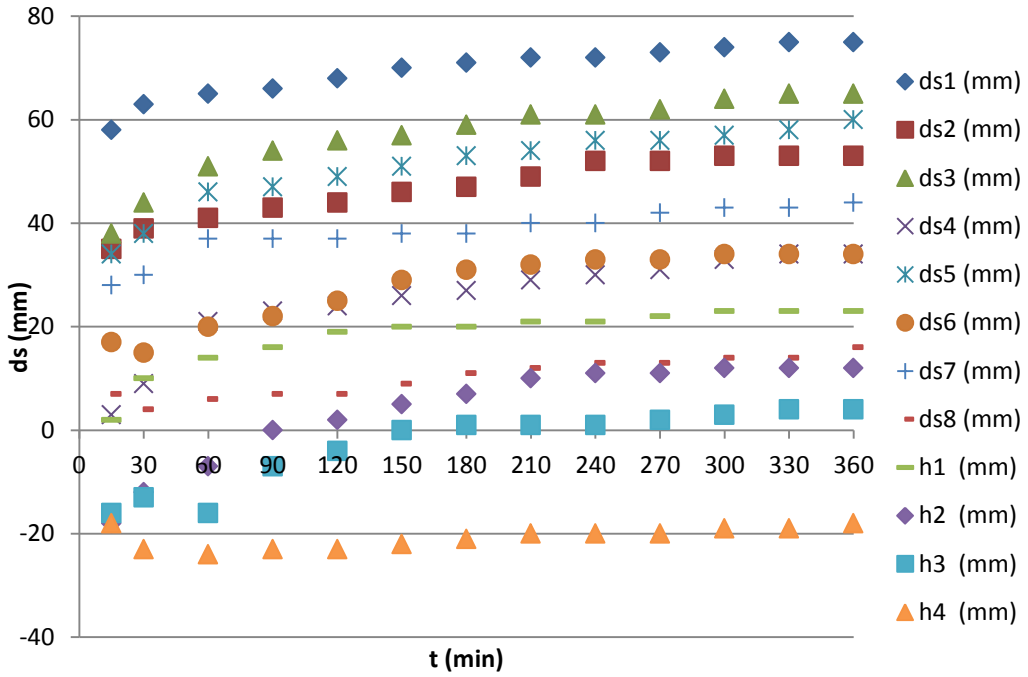

Figure A.53: Temporal development of local scour at all locations, Experiment #53 (d_0/D=1.380, β=15°)

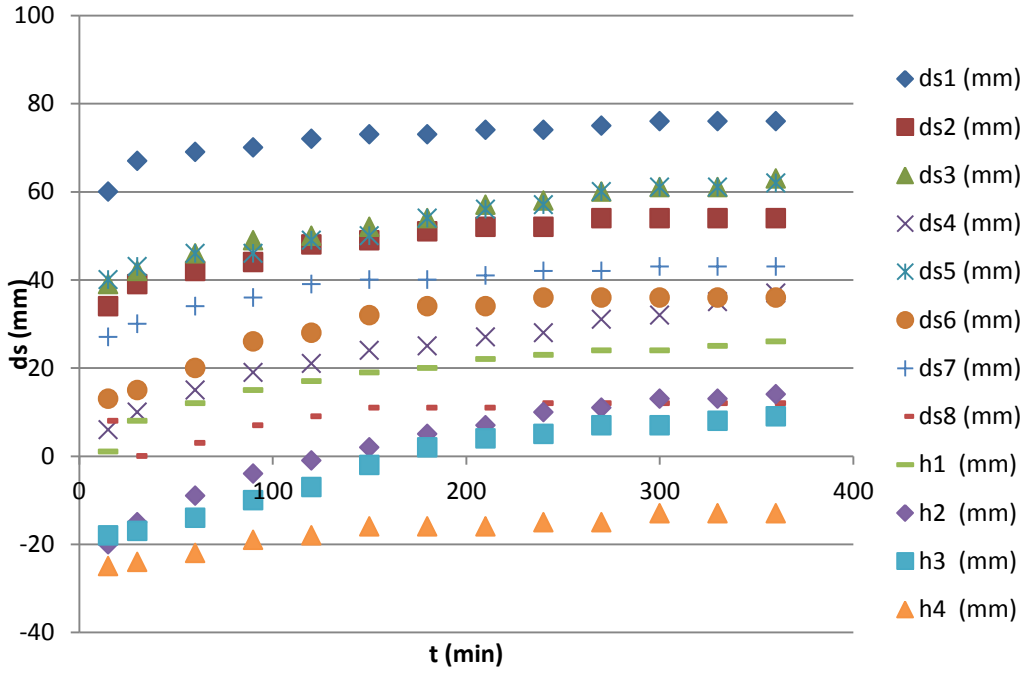

Figure A.54: Temporal development of local scour at all locations, Experiment #54 (d_0/D=1.480, β=15°)

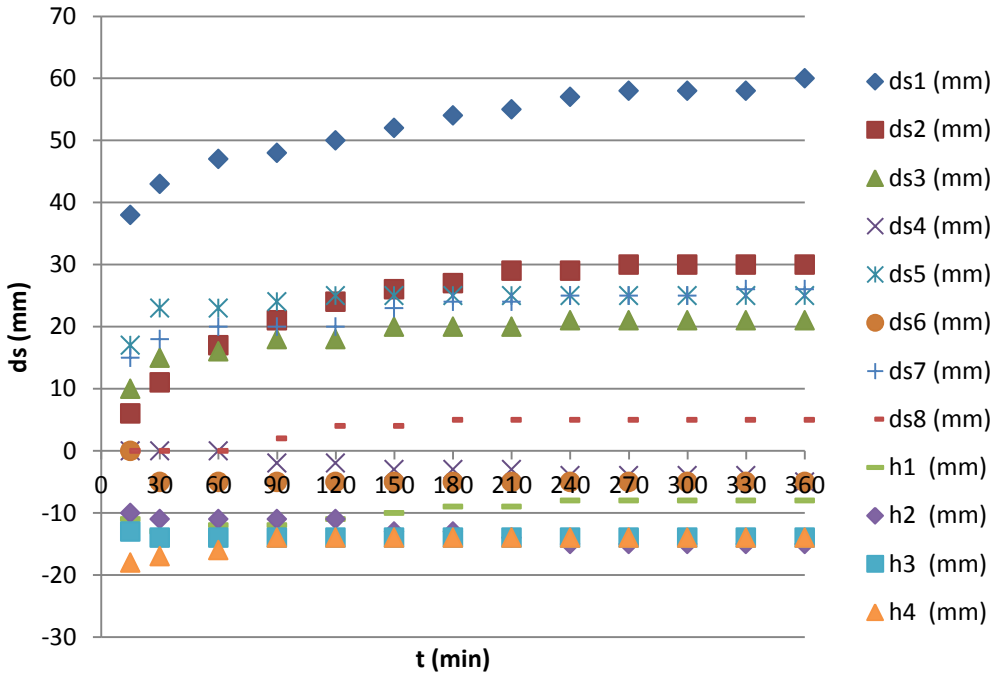

Figure A.55: Temporal development of local scour at all locations, Experiment #55 ($d_0/D=0.529$, $\beta=0°$)

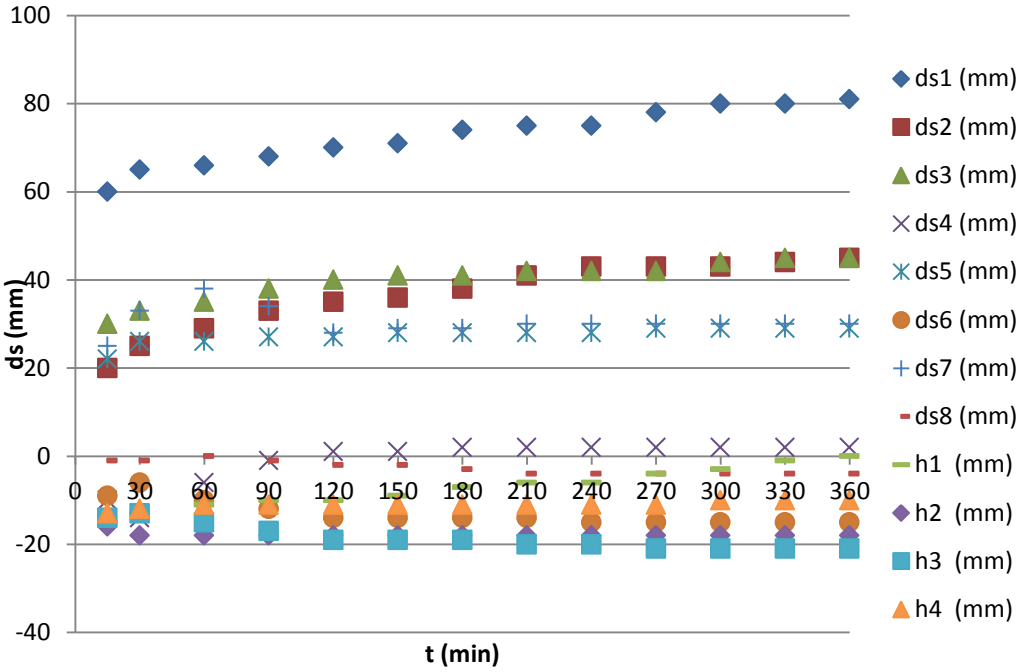

Figure A.56: Temporal development of local scour at all locations, Experiment #56 ($d_0/D=0.671$, $\beta=0°$)

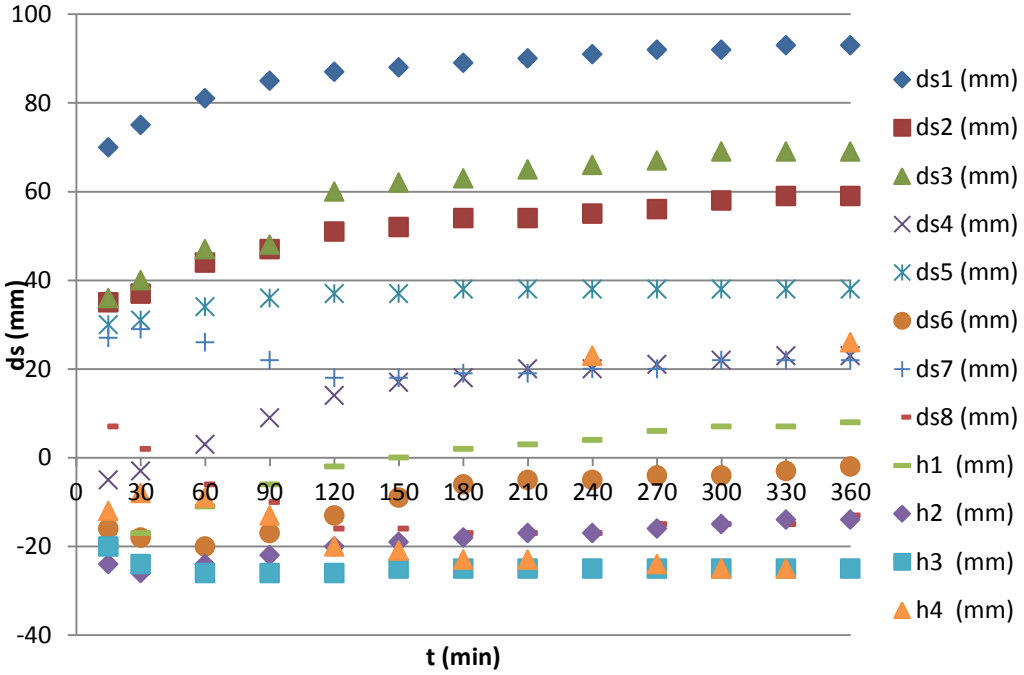

Figure A.57: Temporal development of local scour at all locations, Experiment #57 (d_0/D=0.771, β=0°)

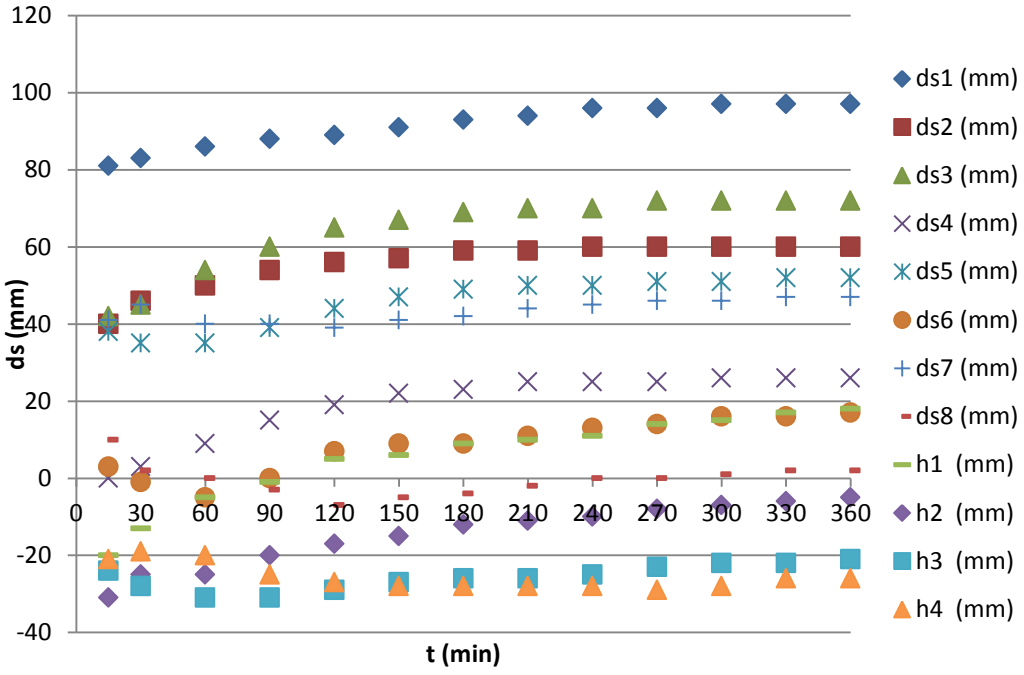

Figure A.58: Temporal development of local scour at all locations, Experiment #58 (d_0/D=0.914, β=0°)

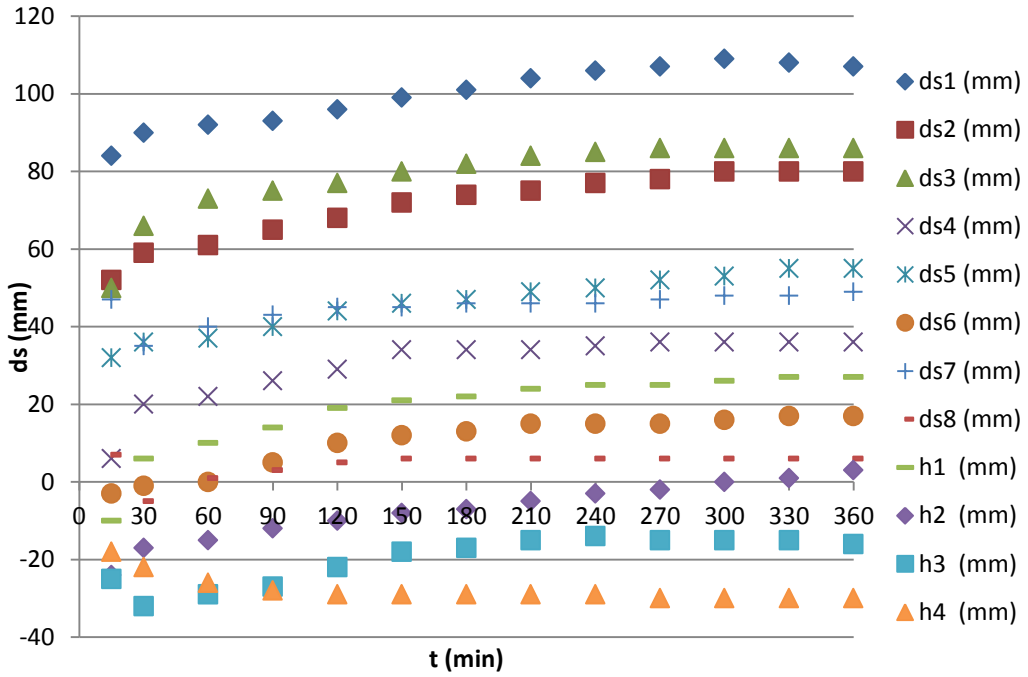

Figure A.59: Temporal development of local scour at all locations, Experiment #59 (d_0/D=0.986, β=0°)

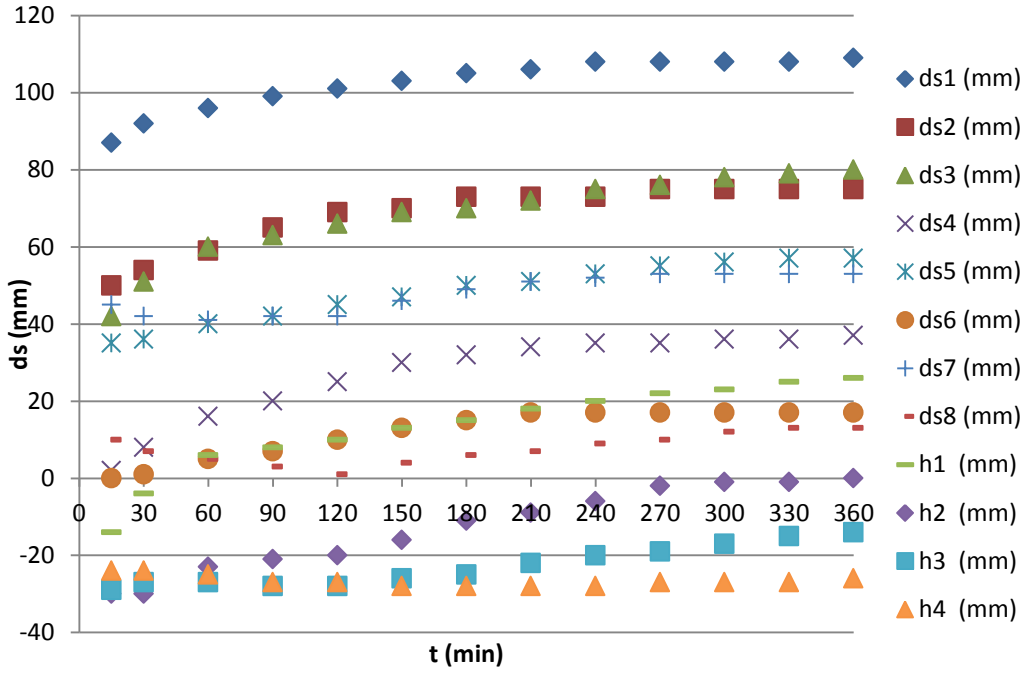

Figure A.60: Temporal development of local scour at all locations, Experiment #60 (d_0/D=1.057, β=0°)

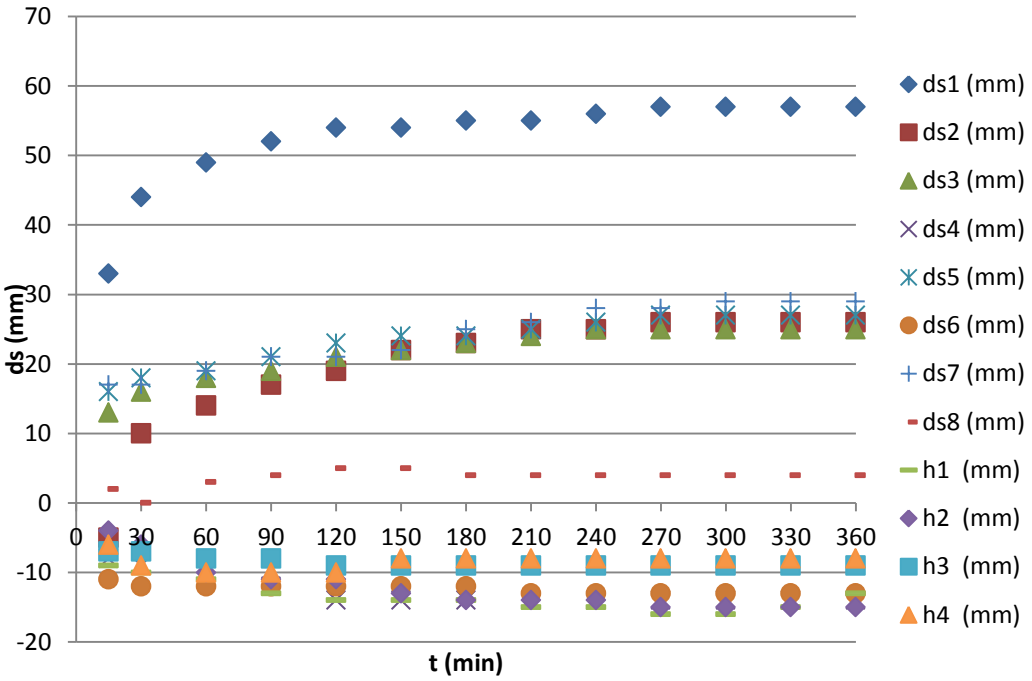

Figure A.61: Temporal development of local scour at all locations, Experiment #61 (d_0/D=0.529, β=10°)

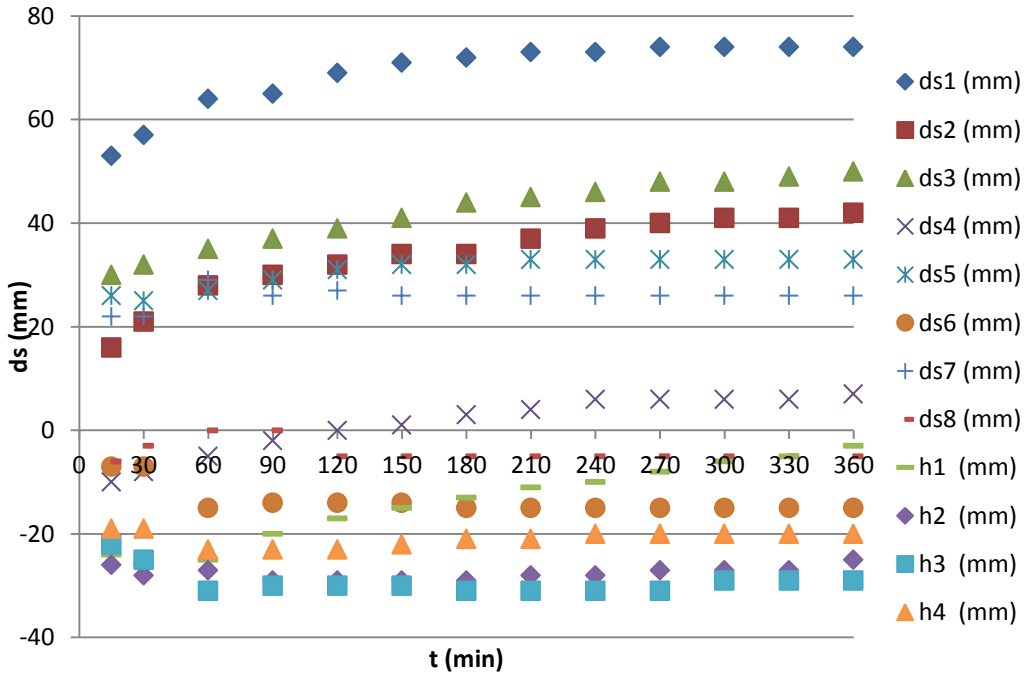

Figure A.62: Temporal development of local scour at all locations, Experiment #62 (d_0/D=0.671, β=10°)

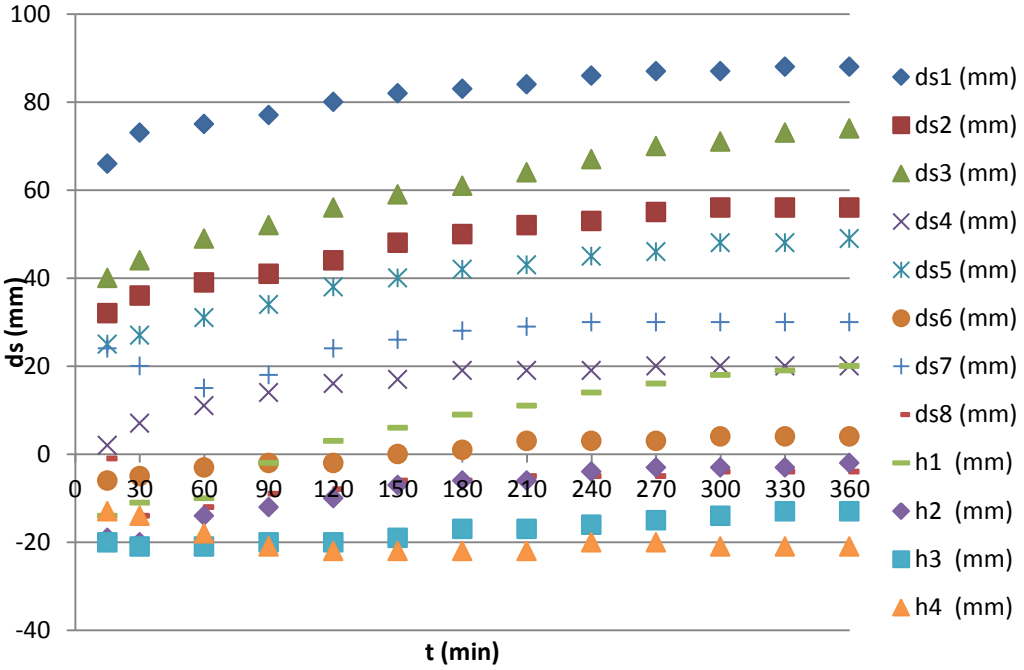

Figure A.63: Temporal development of local scour at all locations, Experiment #63 (d_0/D=0.771, β=10°)

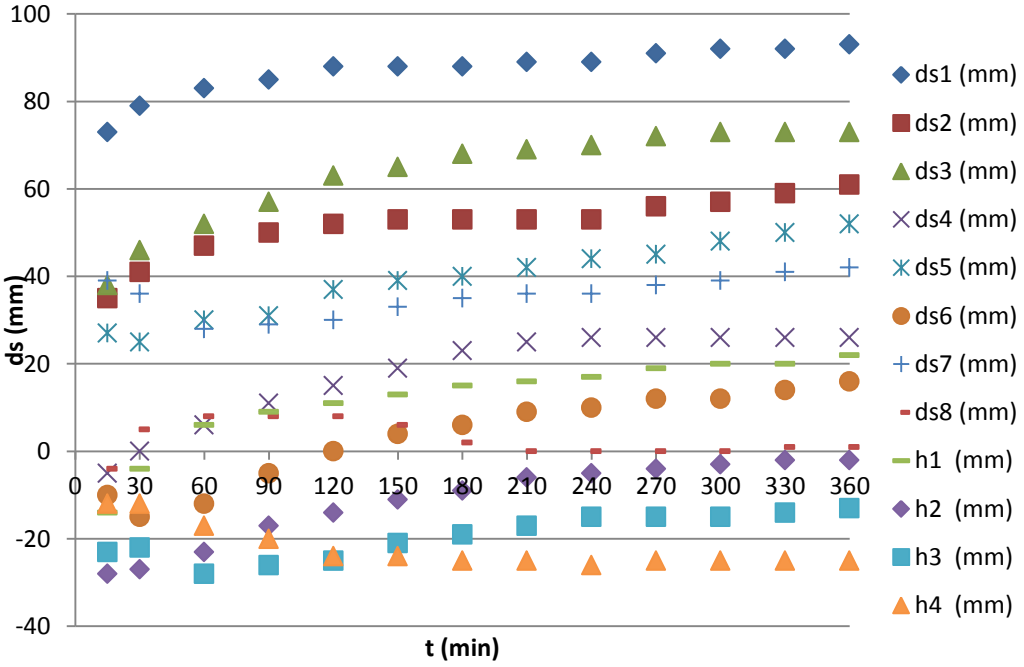

Figure A.64: Temporal development of local scour at all locations, Experiment #64 (d_0/D=0.914, β=10°)

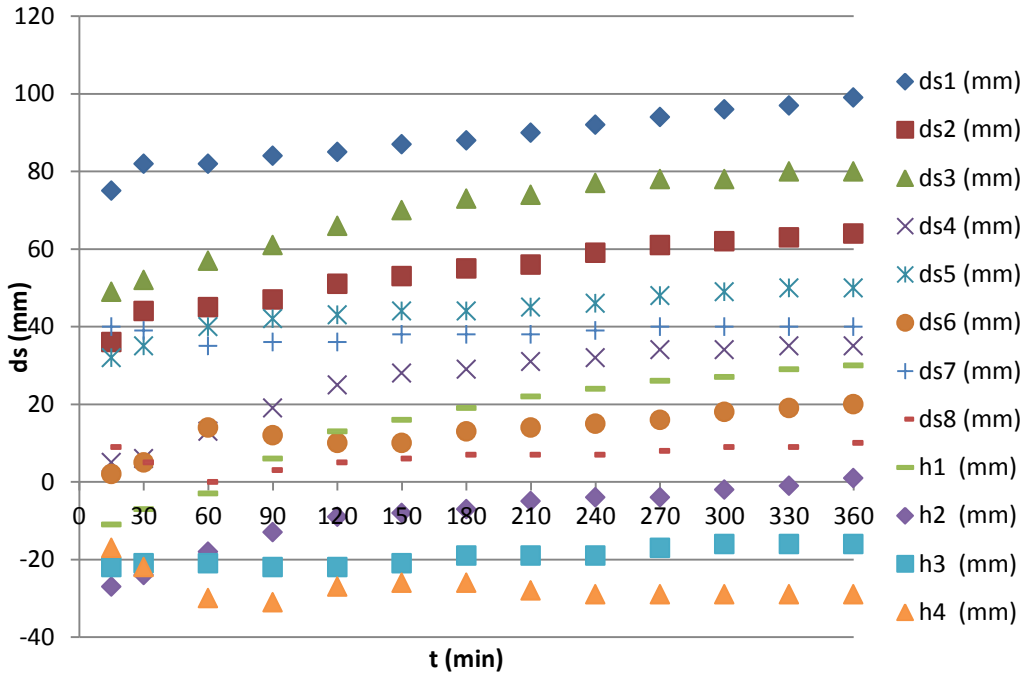

Figure A.65: Temporal development of local scour at all locations, Experiment #65 (d_0/D=0.986, β=10°)

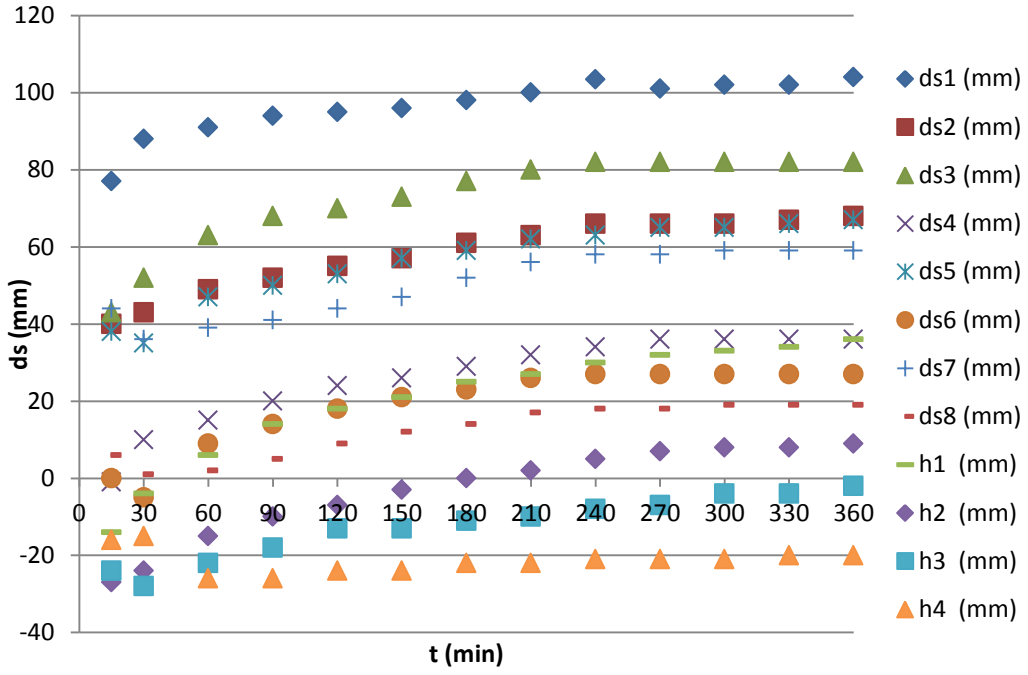

Figure A.66: Temporal development of local scour at all locations, Experiment #66 (d_0/D=1.057, β=10°)

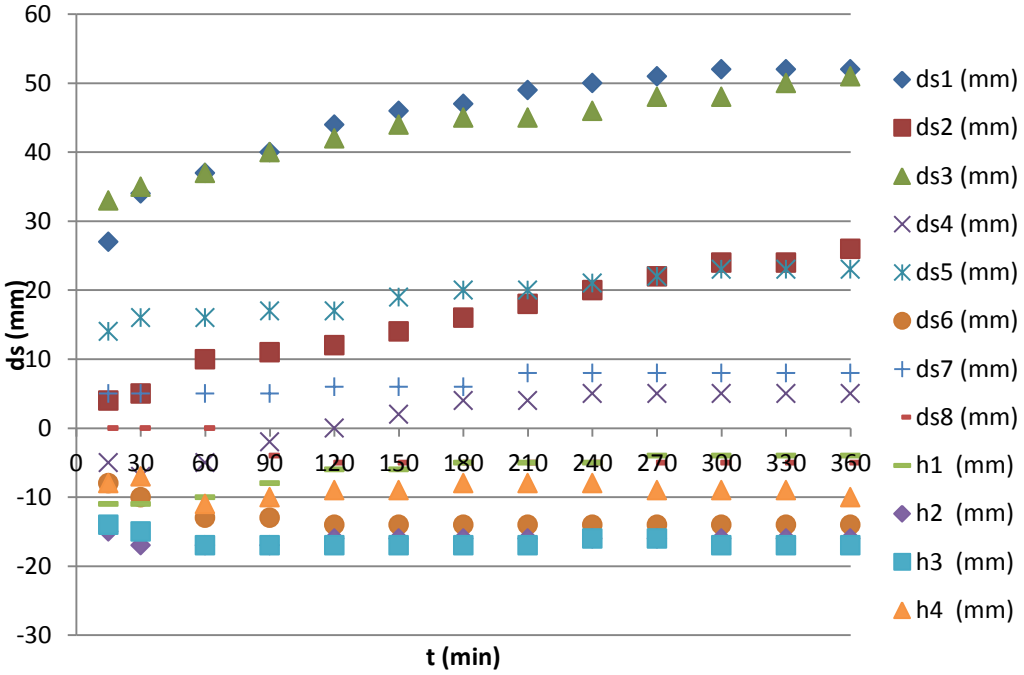

Figure A.67: Temporal development of local scour at all locations, Experiment #67 (d_0/D=0.529, β=15°)

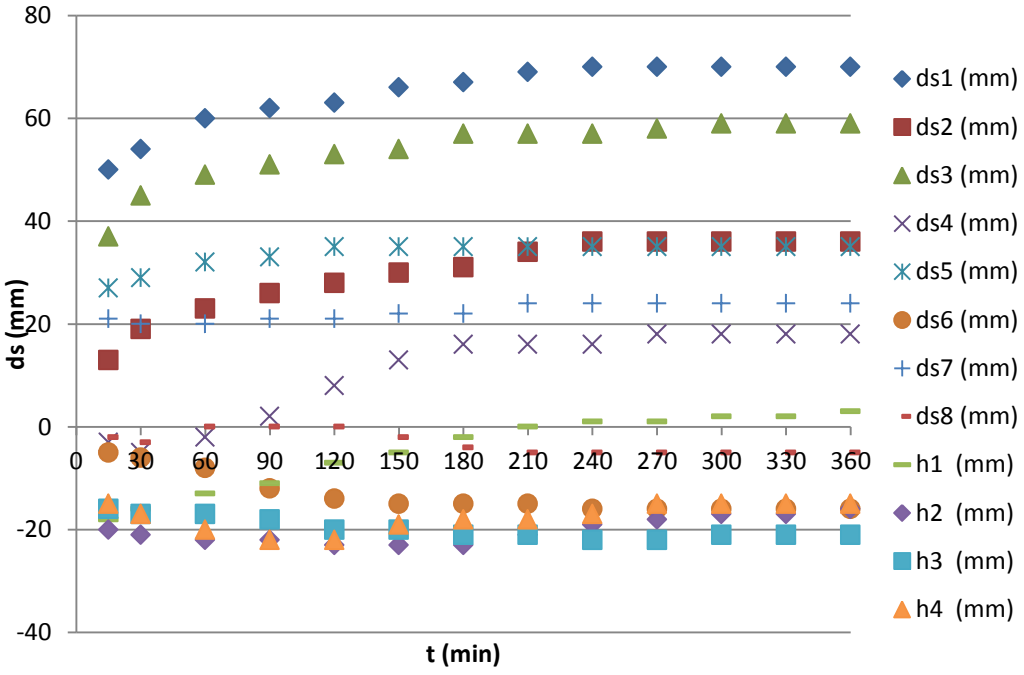

Figure A.68: Temporal development of local scour at all locations, Experiment #68 (d_0/D=0.671, β=15°)

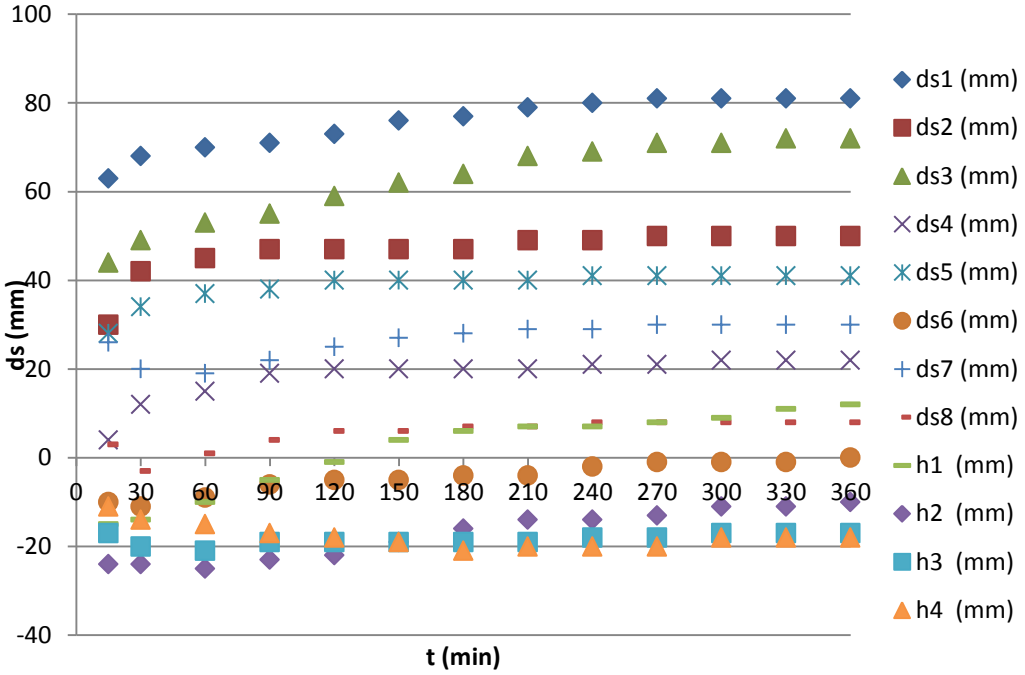

Figure A.69: Temporal development of local scour at all locations, Experiment #69 (d_0/D=0.771, β=15°)

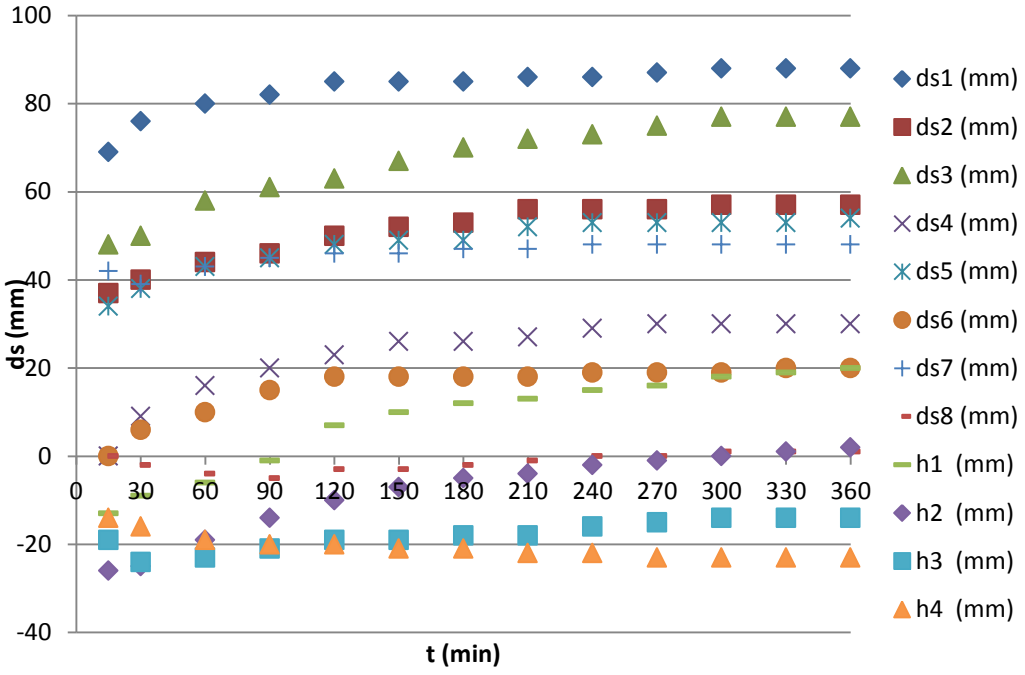

Figure A.70: Temporal development of local scour at all locations, Experiment #70 (d_0/D=0.914, β=15°)

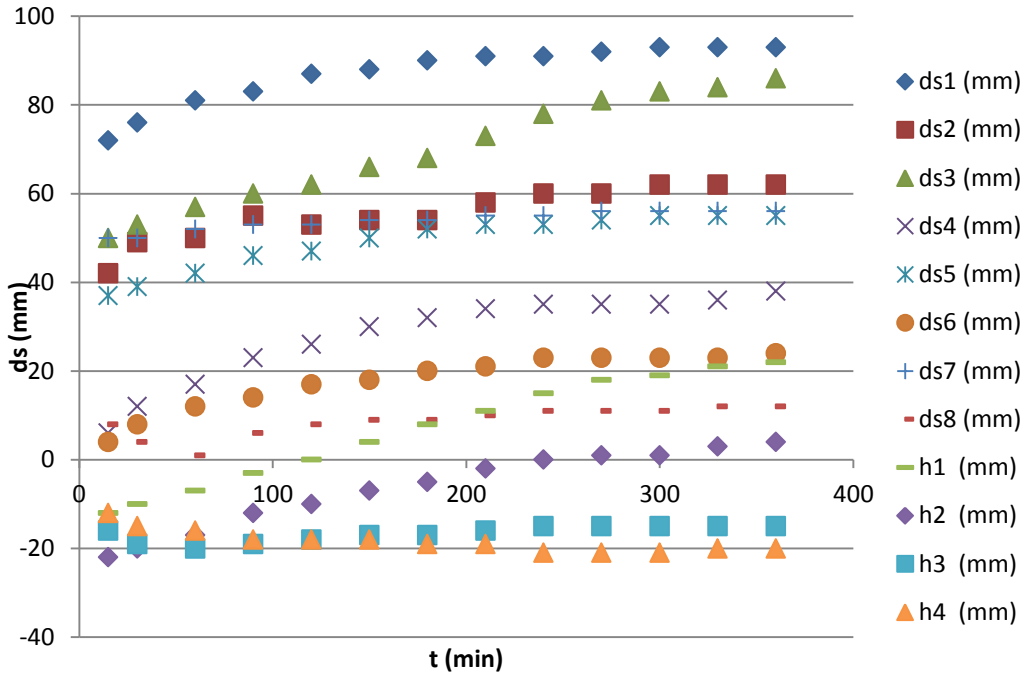

Figure A.71: Temporal development of local scour at all locations, Experiment #71 (d_0/D=0.986, β=15°)

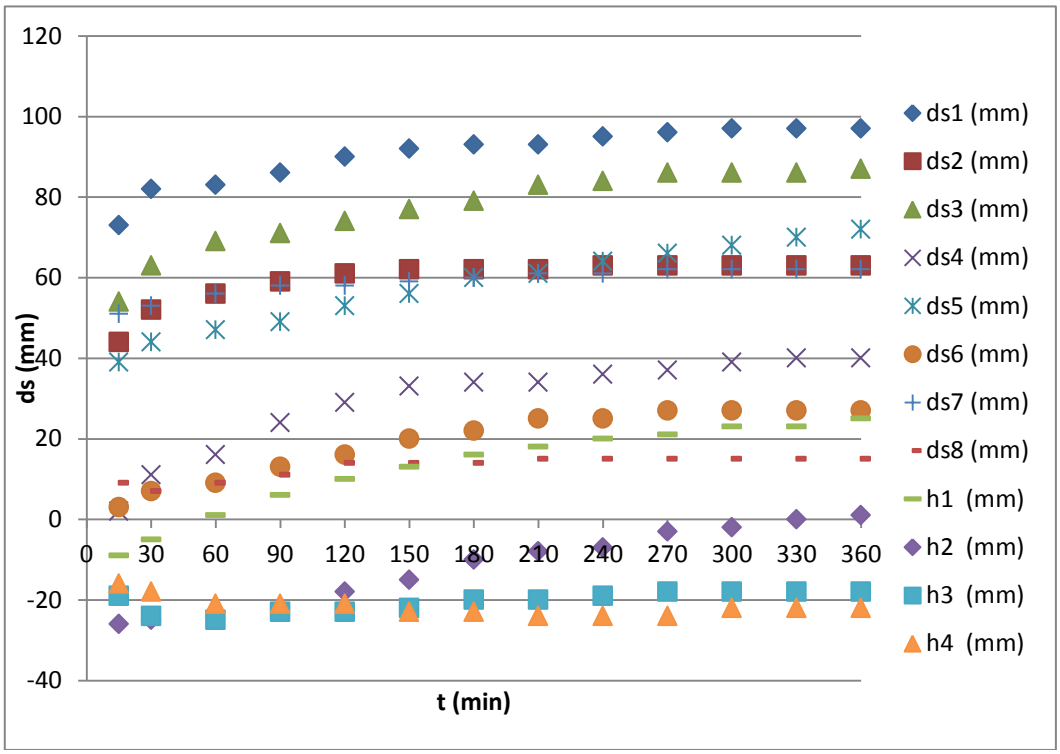

Figure A.72: Temporal development of local scour at all locations, Experiment #72 (d_0/D=1.057, β=15°)

APPENDIX B

Equations Proposed for Each Pier in the Configurations C1 and C2

In this section equations developed for each pier in the pier groups through the regression analysis are given in Table B.1 and computed values of relative scour depths for configurations C1 and C2 with respect to relative flow depth are shown graphically in Figures B.1 and B.2 respectively.

Table B.1: Equations proposed for each pier

Location	Configuration	r^2	Equation
d_{s1}	C1	0.97	$\frac{d_s}{D} = 1.136\left(\frac{d_0}{D}\right)^{0.250}\left(\frac{V}{V_c}\right)^{1.186}\alpha^{1.136}$
d_{s1}	C2	0.97	$\frac{d_s}{D} = 1.192\left(\frac{d_0}{D}\right)^{0.251}\left(\frac{V}{V_c}\right)^{0.909}\alpha^{0.785}$
d_{s2}	C1	0.72	$\frac{d_s}{D} = 1.303\left(\frac{D}{d_0}\right)^{0.844}\left(\frac{V}{V_c}\right)^{6.168}\alpha^{1.986}$
d_{s2}	C2	0.86	$\frac{d_s}{D} = 1.453\left(\frac{D}{d_0}\right)^{0.935}\left(\frac{V}{V_c}\right)^{4.027}\alpha^{1.128}$
d_{s3}	C1	0.72	$\frac{d_s}{D} = 4.239\left(\frac{D}{d_0}\right)^{1.034}\left(\frac{V}{V_c}\right)^{5.242}\alpha^{-1.284}$
d_{s3}	C2	0.86	$\frac{d_s}{D} = 3.076\left(\frac{D}{d_0}\right)^{0.891}\left(\frac{V}{V_c}\right)^{3.880}\alpha^{-0.584}$
d_{s4}	C1	0.76	$\frac{d_s}{D} = 2.616\left(\frac{D}{d_0}\right)^{0.646}\left(\frac{V}{V_c}\right)^{6.529}\alpha^{-2.331}$
d_{s4}	C2	0.87	$\frac{d_s}{D} = 1.321\left(\frac{d_0}{D}\right)^{0.138}\left(\frac{V}{V_c}\right)^{4.992}\alpha^{-0.499}$
d_{s5}	C1	0.79	$\frac{d_s}{D} = 2.058\left(\frac{D}{d_0}\right)^{1.105}\left(\frac{V}{V_c}\right)^{4.706}\alpha^{-0.255}$
d_{s5}	C2	0.80	$\frac{d_s}{D} = 2.265\left(\frac{D}{d_0}\right)^{0.800}\left(\frac{V}{V_c}\right)^{4.350}\alpha^{-0.403}$
d_{s6}	C1	0.60	$\frac{d_s}{D} = 0.183\left(\frac{d_0}{D}\right)^{1.572}\left(\frac{V}{V_c}\right)^{1.525}\alpha^{0.796}$
d_{s6}	C2	0.84	$\frac{d_s}{D} = 0.713\left(\frac{d_0}{D}\right)^{1.606}\left(\frac{V}{V_c}\right)^{4.352}\alpha^{-0.583}$
d_{s7}	C2	0.81	$\frac{d_s}{D} = 1.378\left(\frac{D}{d_0}\right)^{0.649}\left(\frac{V}{V_c}\right)^{3.814}\alpha^{0.099}$
d_{s8}	C2	0.36	$\frac{d_s}{D} = 0.092\left(\frac{d_0}{D}\right)^{2.673}\left(\frac{V_c}{V}\right)^{2.682}\alpha^{0.128}$

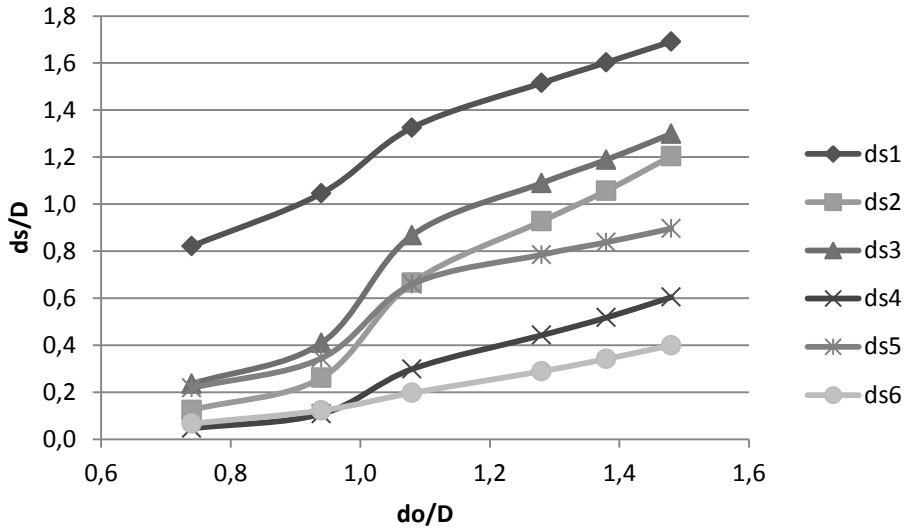

Figure B.1: Variation of relative scour depth at all locations with respect to relative flow depth (β=10°, C1)

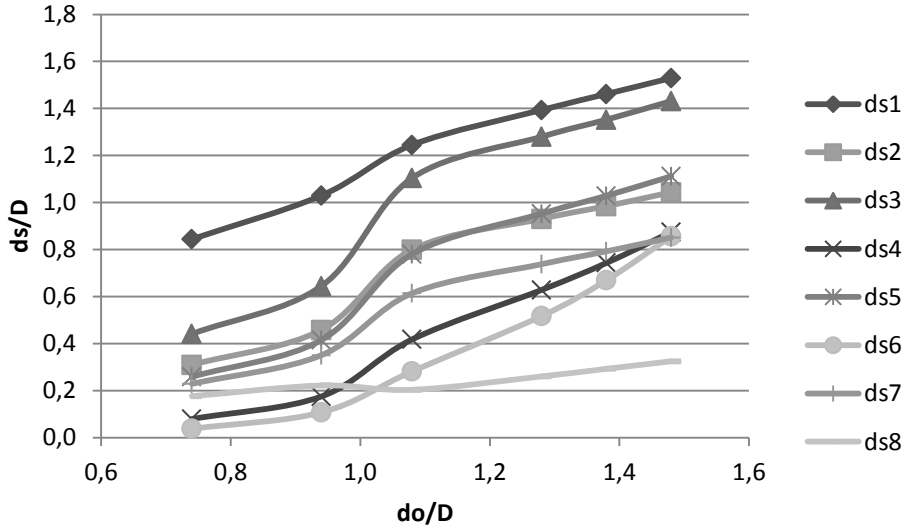

Figure B.2: Variation of relative scour depth at all locations with respect to relative flow depth (β=15°, C2)

APPENDIX C

Photos Taken During the Experiments

Figure C.1: 4 pier configuration (D=70mm, β=10°)

Figure C.2: 3 pier configuration (D=50mm, β=0°)

Figure C.3: Local scour formation after running the experiment (C2)

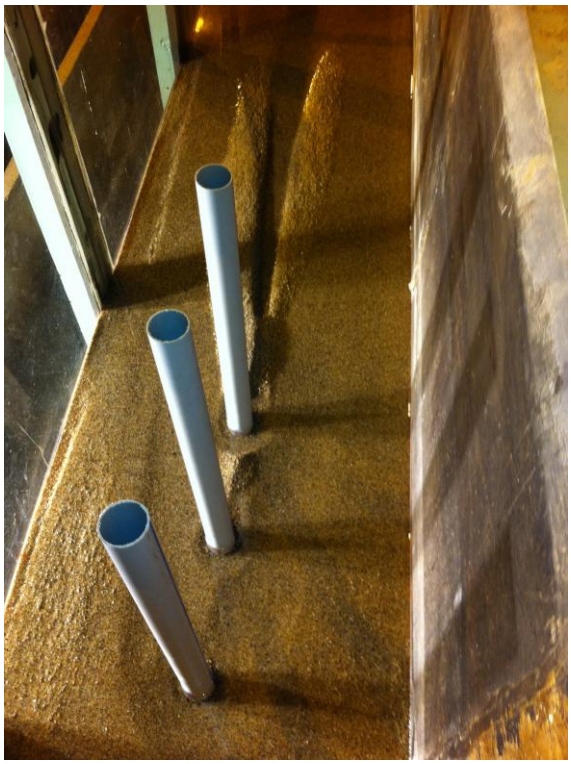

Figure C.4: Local scour formation after running the experiment (C1)

Figure C.5: Inflow pipe and steel meshes

Figure C.6: Small stones that are placed at a transition area

Figure C.7: Main channel

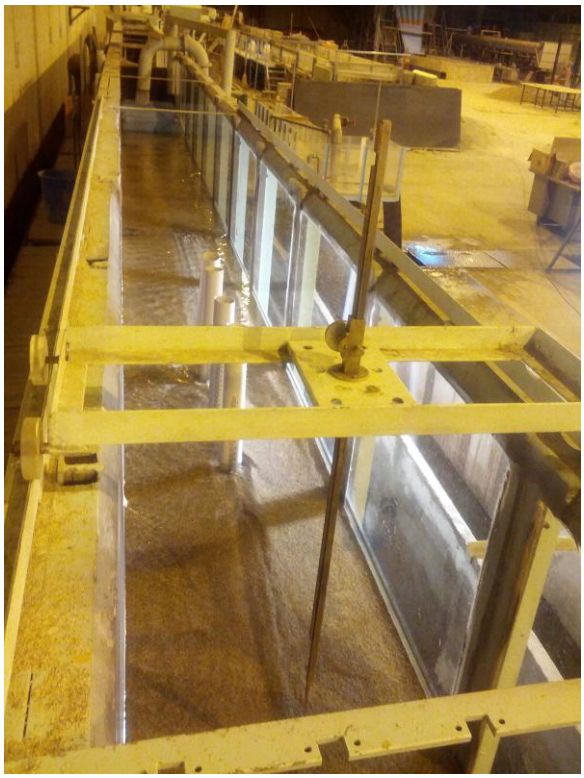

Figure C.8: Mobile point gauge

Figure C.9: Outflow pipe and settling pool

Figure C.10: Secondary channel and sharp crested weir

Figure C.11: The flowmeter that is installed on inflow pipe